Stony Brook University

Accelerating Amyloid Formation by Islet Amyloid Polypeptide

A Thesis Presented

by

Rehana Akter

to

The Graduate School

in Partial Fulfillment of the

Requirements

for the Degree of

Master of Science

in

Chemistry

Stony Brook University

December 2013

Stony Brook University

The Graduate School

Rehana Akter

We, the thesis committee for the above candidate for the Master of Science degree, hereby recommend acceptance of this thesis.

Daniel P. Raleigh, Ph.D., Research Advisor

Professor, Department of Chemistry

Isaac S. Carrico, Ph.D., Chairperson of Defense

Professor, Department of Chemistry

Lisa M. Miller, Ph.D., Third Member

Professor, Department of Chemistry

This thesis is accepted by the Graduate School

Charles Taber
Dean of the Graduate School

Abstract of the Thesis

Accelerating Amyloid Formation by Islet Amyloid Polypeptide

by

Rehana Akter

Master of Science

in

Chemistry

Stony Brook University

2013

Islet amyloid polypeptide (IAPP) is a 37 residues long polypeptide hormone. IAPP is co-secreted with insulin by the β-cells in the pancreas and is stored with insulin in secretory vesicles. IAPP helps to maintain glucose homeostasis in the body by regulating glucagon secretion. IAPP is one of the most amyloidogenic peptide known, and IAPP amyloid formation plays a role in type 2 diabetes. IAPP amyloid formation contributes to β-cells dysfunction and β-cells loss in islets. There is one known naturally found IAPP mutant; the serine 20 to glycine (S20G) mutant weakly increases the risk of early onset diabetes in Asian populations. *In vitro* studies provided the evidence that the S20G mutant accelerates amyloid formation. This thesis research is about the molecular mechanism of accelerating amyloid formation by the S20G mutant.

Studies with D-amino acid mutants at position 20 confirm that increased rate of amyloid formation by S20G mutant is not the result as of unusual backbone conformation adopted by serine 20 in the wild type peptide. Experiments using helical prone natural and unnatural amino acid substitution show that enhanced amyloid formation by the S20G mutant is not the result of a steric clash or the relief of unfavorable hydrogen bond interactions that slow amyloid formation in wild type IAPP. Analysis of a S19G mutant confirms the specific amyloidogenic profile of the S20G mutant. Seeding studies suggests that the single point mutations do not cause significant changes in final fibril structure.

Table of Contents

List of Figures

List of Abbreviations

2D-IR	Two-dimensional infrared spectroscopy
Aβ	The proteolytical fragment of the precursor protein that is responsible for amyloid formation in Alzheimer's disease
Abu	2-aminobutyric acid
CD	Circular dichroism
CGRP	Calcitonin gene-related peptide
DMSO	Dimethyl sulfoxide
EPR	Electron paramagnetic resonance
Fmoc	9-Fluorenylmethoxycarbonyl
HBTU	O-benzotriazole-N,N,N',N'-tetramethyluronium hexafluorophosphate
HFIP	Henxafluoroisopropanol
HPLC	High-performance liquid chromatography
HSPG	Heparan sulfate proteoglycan
hIAPP	Human Islet amyloid polypeptide
IAPP	Islet amyloid polypeptide
MALDI-TOF-MS	Matrix-assisted laser desorption ionization time-of-flight mass Spectrometry
NMR	Nuclear magnetic resonance
PAL-PEG-PS	Pegylated polystyrene support resin, 5-(4'-Fmoc-aminometyl-3', 5-dimethoxyphenol) valeric acid
PC1/3	Prohormone convertase 1/3

PC2	Prohormone convertase 2
preproIAPP	Precursor sequence of proIAPP and mature IAPP
proIAPP	Pro-islet amyloid Polypeptide
t_{50}	Time to 50% completion of fibril formation during a thioflavin-T kinetic assay
TEM	Transmission electron microscopy
TFA	Trifluoroacetic acid
Tris	Tris(hydroxymethyl)aminomethane
UV	Ultraviolet
v/v	Volume to volume
WT	Wild type

Acknowledgements

The whole work in the thesis is guided by my research advisor, Professor Daniel P. Raleigh. I would like to express my sincere gratitude to my advisor for his guidance, support, and encouragement.

I would like to thank to my committee members, Prof. Isaac Carrico and Prof. Lisa Miller for participating in my defense.

Thank you to all of the members of the Prof. Raleigh Lab. Thank you to the former members: Dr. Ping Cao, Dr. Peter Marek, Dr. Wenli Meng, Harris Noor, Dr. Vadim Patsalo, Dr. Shifeng Xiao; and present members: Yuan Chen, Bowu Luan, Ivan Peran, Natalie Stenzoski, Ling-Hsien Tu (Cynthia), Matthew Watson, Hui Wang, Amy Wong and Xiaoxue Zhang. It has been a great pleasure working, learning and interacting with these wonderful nice colleagues. I specially thank Cynthia for training me all the experimental techniques.

Thank you to Katherine Hughes, student affairs coordinator, for all the reminders and support.

I would like to thank to my parents, my siblings, and my family friends for their love, encouragement, and support.

And, most of all thank to my Allah (my God) for blessing and guiding me through this.

1. Introduction

1.1 Amyloid

Amyloid is a general term for self-assembled, insoluble fibrous protein aggregates *in vivo* where the protein is in a β-sheet rich conformation (1, 2). More than 25 proteins *in vivo* are known to form amyloid (3, 4). Amyloid deposits are related to the pathogenesis of many protein misfolding diseases including type II diabetes and neurodegenerative diseases such as Alzheimer's disease, Parkinson's disease, and Huntington's disease (5, 6). Amyloid deposits are often found in different tissues in human organs such as the kidneys, liver, and heart, which increase the risk of severe diseases (4, 7).

Amyloid forming proteins have some common features; they are small in size, have local occurrence at high concentration, and are rich in hydrophobic, β-sheet propensity amino acid, and lack in proline (8). Both compact, natively folded globular proteins and intrinsically disordered proteins are able to form amyloid. Amyloid fibrils are usually unbranched 5-15 mm thick, and 0.1-10 μm long fibrils. Two to eight protofilaments coil together in a left-handed rotation to form a fibril (9, 10). Protofilaments form cross β supramolecular structures where the β-strands within the protofilament are perpendicular to the fibril long axis and the intermolecular hydrogen bonds within the β-sheet are parallel to the fibril axis (11, 12) (Figure 1.1).

Amyloid formation can be affected by pH, temperature, pressure, solvent or ionic strength changes, as well as interaction with membrane or by mutations that cause the protein to unfold from the native state to an aggregation prone state. The mechanism of amyloid formation has not yet been well defined. It is assumed that peptides form amyloid fibrils in a nucleation

dependent mechanism (13). The process is normally made up of three phases. These are the lag phase, a growth phase and the final plateau phase (Figure 1.2). The lag phase is the rate-limiting phase. During this time, monomers aggregate to form fibril nuclei. The lag phase can be bypassed by adding pre-formed fibrils into the monomer solution as seeds (Figure 1.3). It is believed that seeds reduce the energy barrier for fibril formation. Seeds can act as a template for docking the monomer onto the fibril tips or as sites of secondary nucleation. Seeding specificity results can be used to probe structural differences between the two different amyloid fibril structures. This is done by cross-seeding experiments (14). Generally, seeding efficiency is higher for homologous seeding than heterologous or cross seeding. Part of my thesis project is comparing the structural difference between two different amyloid fibrils by seeding experiments. This will be discussed more in chapters 2 and 3.

The growth phase is the fibril elongation phase. This phase may be accelerated by secondary nucleation. Secondary nucleation causes the production of more fibril ends by breaking newly produced fibrils or by allowing growth on the sides of existing fibers. More fibril tips provide more sites to dock monomers on to it. The final phase is the plateau phase where fibrils are in equilibrium with soluble peptides (15) (Figure 1.2).

The kinetics of amyloid formation are usually followed by using fluorescence dye binding assays such Congo red, and Thioflavin-T (16, 17). Thioflavin–T is a small molecule dye that is somewhat specific for amyloid. Thioflavin-T has fluorescence excitation and emission maxima at wavelengths 342 nm and 430 nm respectively in solution. When Thioflavin-T binds to the amyloid fibril a red shift occurs, and its excitation maxima moves to 440 nm and emission maxima to 482 nm (18, 19). Rotation between the benzothiazole and aniline ring of Thioflavin–T

in solution causes a low fluorescence quantum yield (19) (Figure 1.4). Binding to amyloid fibril locks the movement of these two rings and increases quantum yield. It is unknown how Thioflavin bind to the amyloid fibrils, but it is assumed that it binds to the grooves of the β-sheets (20) (Figure 1.4).

1.2 Islet Amyloid Polypeptide (IAPP), Islet Amyloid and Type II Diabetes

1.2.1 Islet Amyloid Polypeptide (IAPP)

Islet amyloid deposits are common features for patients with type II diabetes. IAPP amyloid deposits are mostly found in the islets of the pancreas. IAPP amyloid deposits are also found in brain blood vessel, heart, kidney tissues (21-24). They contribute to the dysfunction, cell death, and loss of the β-cells in islets (25-27). The major component protein of islet amyloid deposit in islets is islet amyloid polypeptide (IAPP) which is also known as amylin (28-30). IAPP is co-secreted with insulin by β-cells in the pancreas and is co-stored with insulin in secretory vesicles (31, 32). IAPP helps to maintain glucose homeostasis in the body by regulating insulin and glucagon secretion. It has inhibitory effects on gastric emptying (33, 34). IAPP has binding sites in the brain, and possibly contributes to regulation of satiety (35, 36). It has been found that IAPP null mice exhibited a reduced pain response in the Formalin Paw test (37). IAPP has also been reported to inhibit osteoclastic activity (38).

IAPP is a 37-residue long polypeptide hormone with an intramolecular disulfide bond between Cys-2 and Cys-7 (Figure1.5). The N-terminus is free and the C-terminus is amidated. IAPP is a normally soluble and intrinsically disordered protein, although NMR studies have shown the evidence of a transient helical structure in its N-terminal region (39-41). This helical

structure may be involved in binding to amylin specific receptors. NMR data obtained with SDS micelle environment and other model of cell membranes have provided evidence that this transient α-helical structure might be stabilized in the cell membrane (42, 43).

Though IAPP is partially identical to the neuropeptide calcitonin gene related peptide (CGRP), it is encoded by one single copy gene chromosome 12 while CGRP is encoded by chromosome 11 (44). Initially, IAPP is expressed as an 89 amino acid pre-proprotein. The 22 amino acid long signal peptide is removed from the pre-proprotein in the endoplasmic reticulum to produce proIAPP. The pH dependent conversion of the proIAPP to IAPP occurs in the Golgi and secretory granules by two endoproteases; prohormone convertase 2 and prohormone convertase 1/3, and by carboxy peptidase E. Mature IAPP is formed by the conversion of a C-terminal glycine residue to an amide bond by the peptidyl amidating mono-oxygenase (PAM) complex and by disulfide bond formation between residue 2 and 7 (45). IAPP is stored in the halo region of β-cell secretory granules at pH 5-6 with other components such as insulin, proinsulin, proinsulin C peptide, and their processing intermediate (46, 47). Insulin is localized in the dense core. IAPP expression in β-cells is stimulated by glucose response similar to insulin (48). IAPP is also expressed in the delta cells of islets in rat as well as the gastrointestinal tract of mice, cats, rats, and humans. IAPP is also expressed in the brain and in the intestine of chickens (49, 50).

1.2.2 Islet Amyloid and Type II Diabetes

Islet amyloid plays a role in type II diabetes. About 347 million peoples in the world are suffering with diabetes and among 90% of them with type II diabetes (51, 52). Islet amyloid formation is related to the type II diabetes. β-cell dysfunction, β-cell loss in type II diabetes is

related to IAPP amyloid formation. IAPP is the main protein component of islet amyloid deposits found in up to 90% of type II diabetes patients (29). Rat IAPP which differs in 6 residues in primary sequence with human IAPP does not form amyloid and rats do not develop type II diabetes (53).

Transgenic rats expressing human IAPP have developed islet amyloid with β-cell loss (54). β-cell dysfunction, β-cell loss in type II diabetes are related, in part to IAPP aggregation and toxicity (55, 56). Islet amyloid deposit plays important roles in islets transplantation failure in type II diabetes. Rapid amyloid formation by IAPP is related to islet graft failure. It has been reported that significant amount of amyloid deposit is found only after two weeks in human islet transplantation in nude mice while transgenic mice islets expressing human IAPP contain very less amount of amyloid deposit (57). Transplantation of transgenic mice islets expressing human IAPP in diabetic mice developed hyperglycemia again and increased rates β-cell death and decreased β-cell replication while non-transgenic mice did not do that over the 6 weeks of islets transplantation (58). Porcine islets (pig peptides are less amyloidogenic) showed increased the graft longevity compare to islets of human (59).

The missense S20G (AGC Ser to GGC Gly) IAPP mutant has been found at low levels in the Asian populations as 2.6 % in Japanese, 1.92 % in Korean and 2.8 % in Chinese type II diabetes patient and is the only reported mutation in the coding region of the human IAPP gene (60-64). S20G mutation found in patients with type II diabetes in young age and had severe diabetes and strong family diabetes history (60). Therefore, this mutation has been proposed to increase the risk early onset (age < or equal 40 years) type II diabetes in Asian populations (60, 61, 62). Long-term observation of S20G mutant patients showed greater decline of insulin

secretion compare to other type II diabetes patients in Japanese population (65). This has been proposed that enhanced β-cell dysfunction in type II diabetes caused by S20G mutation. Insulin can inhibit amyloid formation. However, for the case of the S20G mutant, it has been reported that insulin is a less effective inhibitor (66). Other reports have been reported that S20G mutation is not related to the risk of type II diabetes (64, 67, 68).

In vitro studies have shown that the S20G mutant can form amyloid much faster than wild type IAPP (66, 69,70). *In vitro* studies have also shown that the S20G mutant is similarly toxic as wild type hIAPP (69, 70). The main focus of my research is to find out the reasons that cause the S20G mutant to aggregate faster than wild type hIAPP. This work will be described in chapters 2 and 3.

Typically, islet deposits are found in the extracellular region of β-cells. Cultured islet models have shown that IAPP amyloid formation increases with the increase of IAPP secretion, which suggests the extracellular amyloid formation (71). However, both *in vivo* and *in vitro* studies showed the evidence of intracellular amyloid deposits and their growth sites were mainly found in the endoplasmic reticulum (ER), golgi and secretory granules (72, 73) (Figure 1.6). Although this work has been questioned since at lease some of the studies involved levels of IAPP expression.

In early studies, it was suggested that amyloid fibrils penetrated β-cells and disrupted the cell function (72). *In vitro* cytotoxicity studies using cultured pancreatic cell lines also found that intermediate products formed during fibrillogenesis were more toxic whereas amyloid fibrils were inert to the cell (69, 74). However, the size and conformation of the oligomeric intermediates are unknown.

Multiple factors are believed to be important for IAPP amyloid initiation. NMR studies shows that IAPP adopts transient α helical conformation and *in vitro* studies suggests that the helical intermediate is on the pathway of IAPP amyloid formation (75, 76). Helix-helix association may initiate IAPP aggregation (77). The Maltose binding protein IAPP fusion crystal structure also shows helix-helix dimerization (78). Intracellular IAPP amyloid formation may be initiated by inappropriate prohormone (ProIAPP) processing (79). There is evidence of ProIAPP with the N-terminal flanking region in islet amyloid deposits (80). *In vitro*, studies show that ProIAPP is amyloidogenic (81). Incomplete processing may play role in extracellular amyloid formation. The sulfate proteoglycan perlecan is found in IAPP amyloid deposit. *In vitro* studies show that Heparan sulfate proteoglycan (HSPG) can bind with ProIAPP and accelerates amyloid formation (82, 83). Another important hypothesis is that IAPP aggregation may be the result of interaction of IAPP with lipid membranes (84-86). IAPP is positively charged peptide and *in vitro* studies show that IAPP highly interacts with model membranes that have high fraction of anionic lipid. Recent studies have shown that cholesterol and gangliosides of the membrane may important for membrane interactions (87, 88). Fibril formation at the membrane surface disrupts model membrane. It has also pointed out from recent studies that amyloid fibrils interacting with cell membranes disturb might Ca^{2+} flux into the cell which ultimately affect the cell function (89). However, it is not known if there is a direct correlation between *in vitro* studies with model membrane and *in vivo* toxicity.

1.3 Structural Models of IAPP Amyloid

The general features of the IAPP amyloid fibril are a cross β- structure where the β-strands are perpendicular to the fibril long axis. The hydrogen bonds within the β-strands of two adjacent

chains are parallel to the fibril axis. The first seven residues likely do not participate in β-sheet formation because of the structural constraint raised by the disulfide bond between the two cysteine residues at position 2 and 7.

There are several models proposed for hIAPP amyloid fibrils. One of the hIAPP amyloid fibril models was proposed by the Tycko group at the NIH which was based on one dimensional and two dimensional solid state nuclear magnetic resonance (NMR) spectroscopy experiments together with scanning transmission emission microscopy (STEM) and atomic force microscopy (AFM) (Figure 1.7) (90). Using this data, Tycko et al. proposed a model in which hIAPP fibrils form a cross-β structure. Each layer of protofilaments, which they called a striated ribbon, is made up of two hIAPP monomers. Two monomers in each layer show C_2 symmetry about the axis. Each monomer within the fibril is U-shaped with two β-strands consisting of residue 8-17 and 28-37 connected by a hairpin loop segment 18-27 and each layer of the protofilaments consists of four β-strands, which are parallel in layers. The β-strands formed by residue 8-17 are located exterior of the protofilament and the one formed by the residues 23-37 are in the amyloidogenic core. According to this model, the protofilament core contains both polar and nonpolar residues. Nonpolar residues 23-27 interact with non-polar residues 15-17 and 32 while polar residues 28-31 interact with the same residues of the other molecular layers. This model has good agreement with fluorescence resonance emission transmission (FRET) studies of Tyr 37 and Phe23, but disagreement with studies of FRET between Tyr 37 and Phe15. This proposed structure has close similarity with forty residues Aβ amyloid of Alzheimer's disease (91). They proposed two structures. The main difference between the two structures is side chain orientation. For example, in one structure Arg11 is solvent exposed and in the other one, Arg11 is buried within the hydrophobic core, which is expected to be unfavorable.

The Eisenberg group at UCLA proposes another hIAPP amyloid fibrils model. This model is based on x-ray crystallography structures of small segments, NNFGAIL (residues 21-27) and SSTNV (residues 28-33) (Figure: 1.8) (92). The crystal structure of SSTNVG segment is closer to the fiber diffraction pattern. Therefore, they chose the SSTNV is in the centerpiece of the model that is called "Steric zipper" interface. The fibril is 6.4 nm width and 0.48 nm space between the intermolecular layers and serine 29 in the monomer interface form hydrogen bond interaction with each other. Like the Tycko proposed model, each layer consists of four parallel β-strands with two U-shaped monomer. β strands consist of residues 8-17 and 24-37 connected by a hairpin turn segment of residues 18-23. Residues 23-37 constitute the dry steric zipper interface of the fibrils. The Eisenberg proposed model is somewhat similar to the previously described structure based on NMR study (Tycko et al. proposed model) and they differ mainly in side-chain packing, the residues in the β-sheets and interspace between β- sheets. According to this model, the β-sheets are more closely interdigitated than the NMR derived structure.

There is another recently proposed hIAPP amyloid fiber model. This model is considerably different from the previously described models. This model is based on structure constraints from spin labeling with continuous wave and pulse EPR (Figure 1.9) (93). The proposed model, each hIAPP fibril consists of a horseshoe U-shaped hIAPP monomers and each monomer stacks to form cross-β structure fibrils. Each monomer consists of two β-strands of residue 12-19 and 31-36 and the β-strands are connected by a long β-hairpin loop. Each monomer in the fibrils is staggered by three peptide layers, which are about 15Å. Therefore, one of the β-strands of peptide i opposes another β-strand of peptide i+3. This model exhibits a left handed helical twist of fibril with 440 Å average pitch. One possible reason for differences between the proposed model and the other two model is the lack of disulfide bonds. Because

EPR studies requires a spin labeled cysteine mutant, which causes larger effect to use a variant without the disulfide bond between Cys2 and Cys7. In addition, the spin label is a large perturbing substitution.

1.4 The Relationship between the Primary Sequence of IAPP and Amyloid Formation

The amino acid sequences of IAPP found in mammalian species are highly conserved in nature. They mainly vary in the 20-29 region of the IAPP sequence (94). Differences in the primary sequence in this region have been proposed to cause the variation in amyloid formation (Figure 1.10). Human, non-human primates and cats IAPP are amyloidogenic. Cows, dogs, rats, and pigs, which have one or more proline residues in this region, are non-amyloidogenic (94, 95). Proline substitution in each position of a truncated 20-29 segment of IAPP has shown that proline substitution inhibits amyloid formation and residues Asn22, Gly24 and residues 26-28 had the largest effect (96). Proline is a well known as a β-sheet disrupter and a cyclic proline side chain imposes steric constraint in the structure (96, 97). However, substitution of rat IAPP residues, Arg18, Leu23 and Val26 by their human counterparts showed weak amyloidogenicity which suggests that proline residues are not the only factor for non-amyloidogenicity (98). However, a human IAPP variant (Pramlintide), which contains proline residues at the same position of rat IAPP, is non-amyloidogenic at least at moderate concentration. Pramlintide is an FDA approved drug for diabetes treatment (99, 100). Another important non-amyloidogenic human IAPP variant is I26P, which is a potent inhibitor of amyloid formation (101). IAPP of degu is non- amyloidogenic, insulin causes islet amyloid deposits in degu (102). The naturally found human IAPP mutant S20G, which shows accelerated amyloid formation and weakly increases the risk of diabetes in Asian populations (60-63).

There are a number of mutational studies on IAPP. However, it is difficult to compare them, because different methods are used in *in vitro* studies. Amyloid formation studies are very sensitive to pH, concentration of added co-solvent, concentration of added salt in buffer and component in the buffer (75, 103, 104). Despite of all these difficulties, mutational studies on IAPP show the importance of different regions in amyloid formation. Aromatic–aromatic and aromatic-hydrophobic interaction were thought to be very important amyloid formation. However, mutating all three aromatic residues of human IAPP with leucine (3XL IAPP) showed that 3XL IAPP can form amyloid fibril. This result indicates that aromatic-aromatic interaction are not crucial for amyloid formation (105-107). Mutational studies have also shown that not only the 20-29 region but also N-terminal transient helical region is also important for amyloid formation. Mutational studies of human IAPP at residues Asn14, Phe15, Leu16, Val17, and His18 suggests the significant importance of those residues on amyloid formation (75, 94, 108-110).

Mutational studies provide the evidence that different residues have different contribution in amyloid formation. Multiple factors may be play roles in amyloid formation. Single residue mutant at position 20 can accelerate amyloid formation, but the reason is not understood. The goal of this thesis is to understand the role of position 20 in amyloid formation.

1.5 Figures

(A) **(B)**

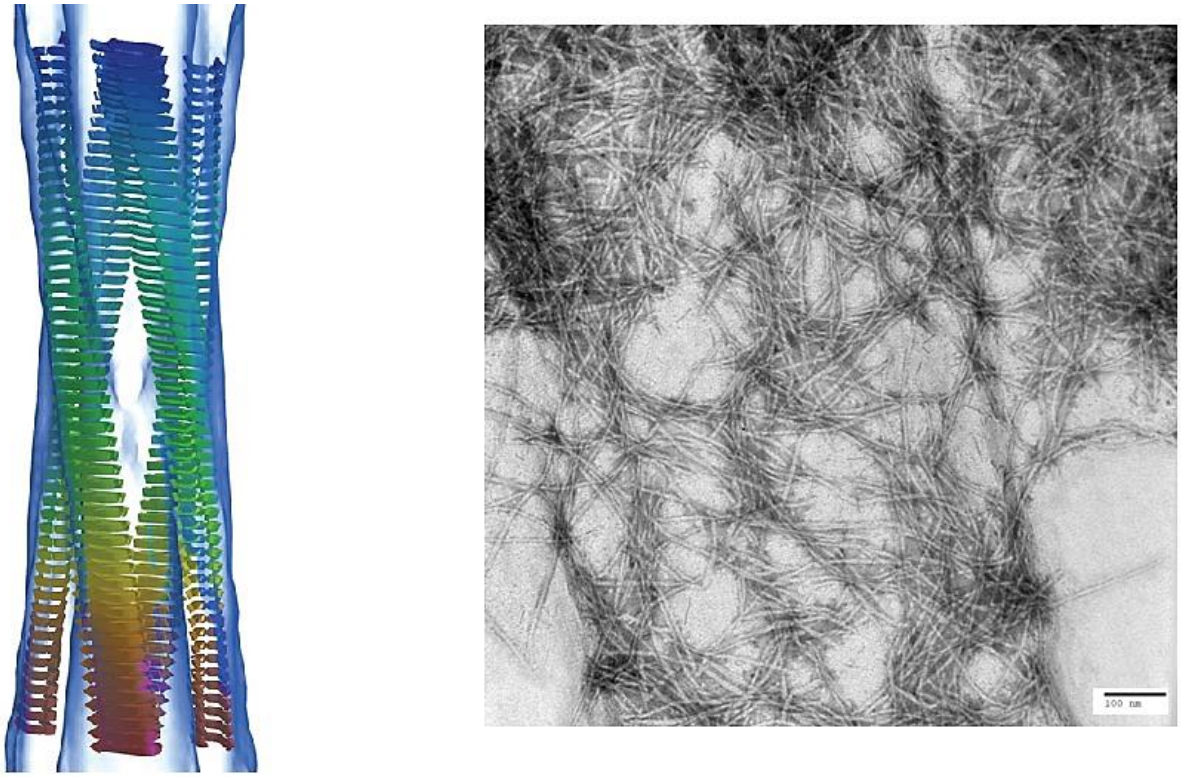

Figure 1.1: (A) Cross-β structure of amyloid fibrils; modeled into the electron density map of amyloid fibril image obtained by cyro-electron microscopy where protofilaments coil together with left-handed twist. Peptide chains are perpendicular to the fibril long axis (Figure is taken from Johnston, N. (2005) Scientist 19, 24-25) (12), (B) Transmission electron microscopy (TEM) image of hIAPP Amyloid fibrils. The scale bar in the image is 100 nm.

(A)

(B)

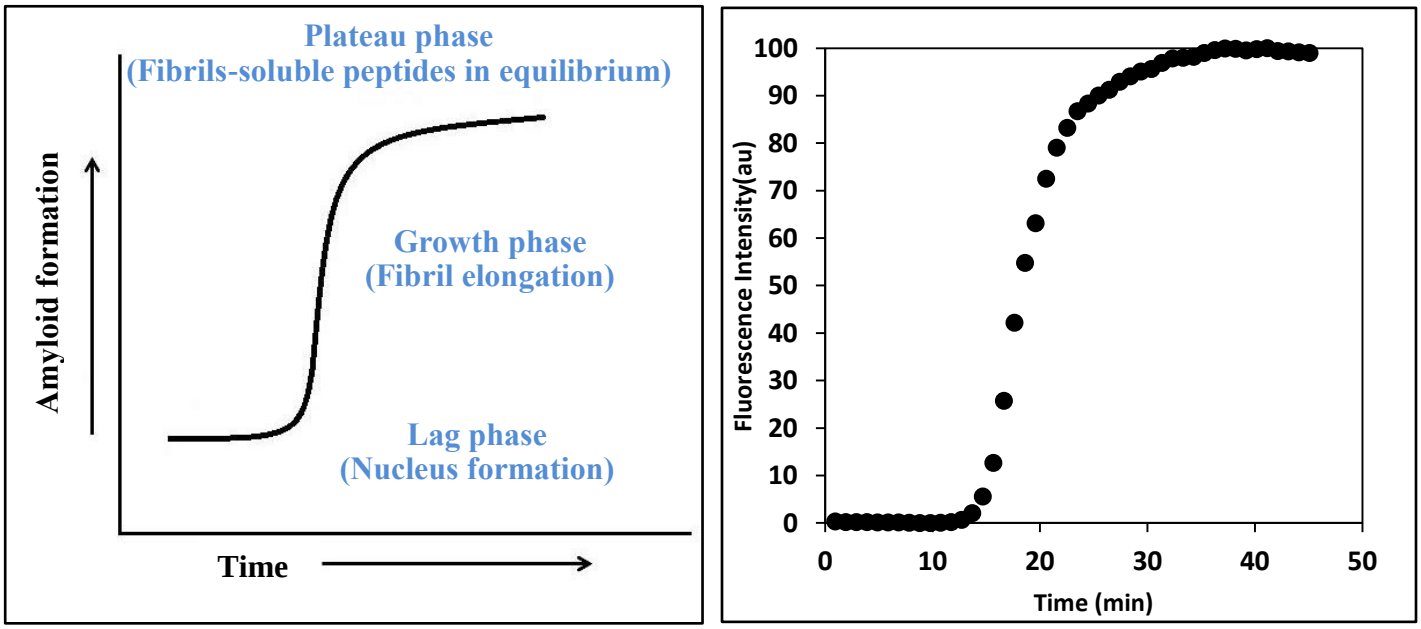

Figure 1.2: (A) A schematic representation of the kinetics of amyloid formation. Nucleation dependent amyloid formation process can be divided into three phase; lag phase, growth phase and plateau phase, (B) Kinetic curve of amyloid formation by hIAPP obtained from Thioflavin-T fluorescence dye binding assay.

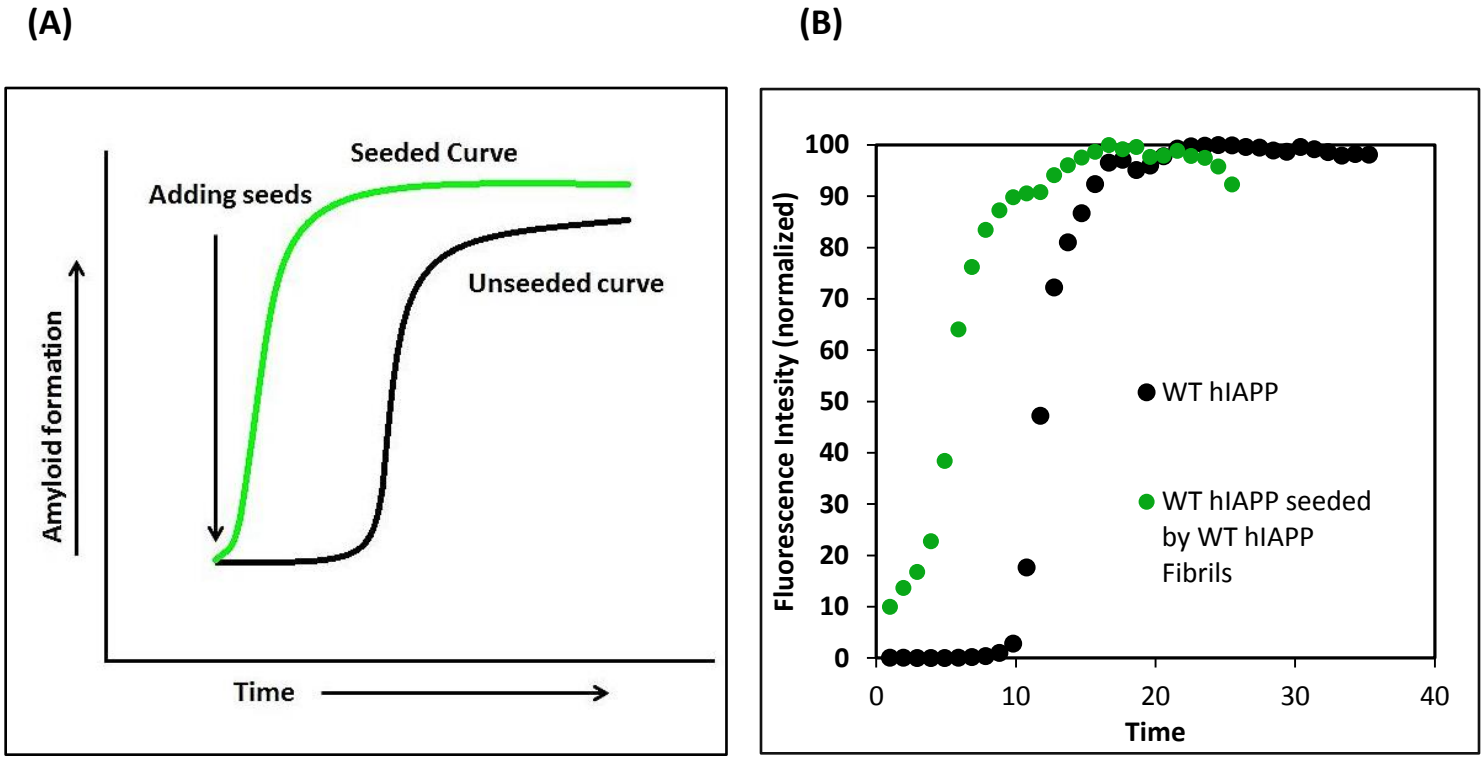

Figure 1.3: (A) A schematic representation of the kinetics of amyloid formation with addition of seeds. Black curve is the typical sigmoidal kinetic curve of amyloid formation and the green curve is the seeded kinetics curve when preformed fibrils are added to monomer solution. (B) Kinetics curve obtained from Thioflavin-T binding assay for wild type hIAPP (black) and seeded kinetics curve (green) when wild type hIAPP fibrils are added to the monomer solution at the beginning of the assay.

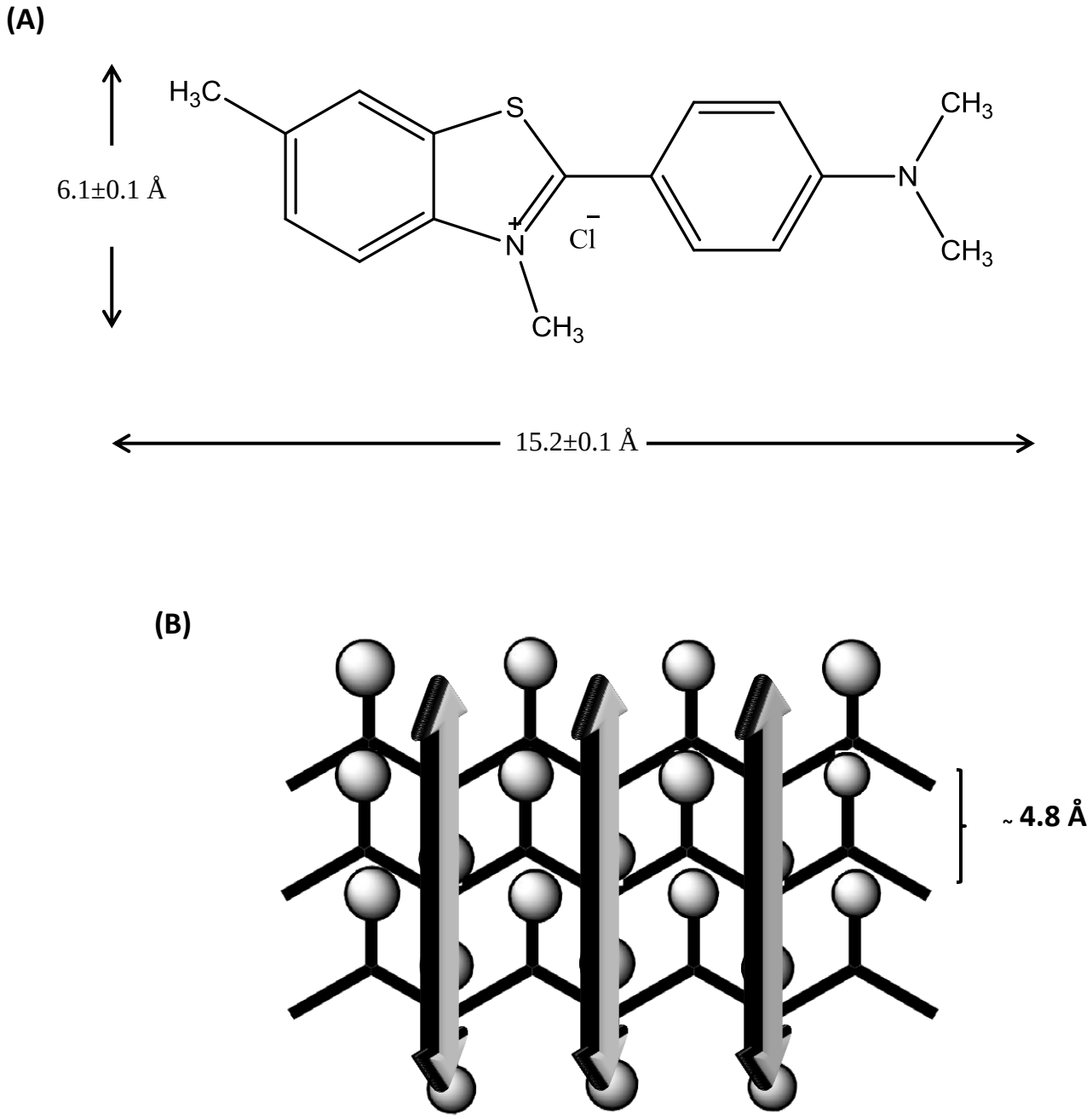

Figure 1.4: (A) Molecular structure of Thioflavin-T, Thioflavin-T is 15.2±0.1 Å long and 6.1±0.1 Å high, (B) Model of Thioflavin-T binding within a β-sheet where double-headed arrows indicate that axis of its binding parallel to long axis of fibrils.

(A)

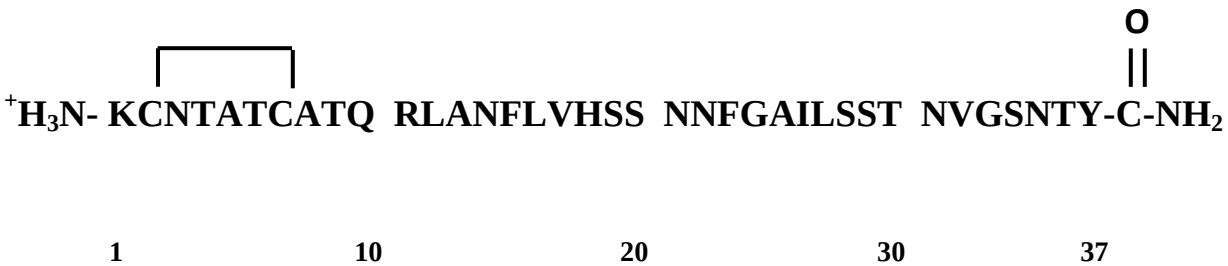

(B)

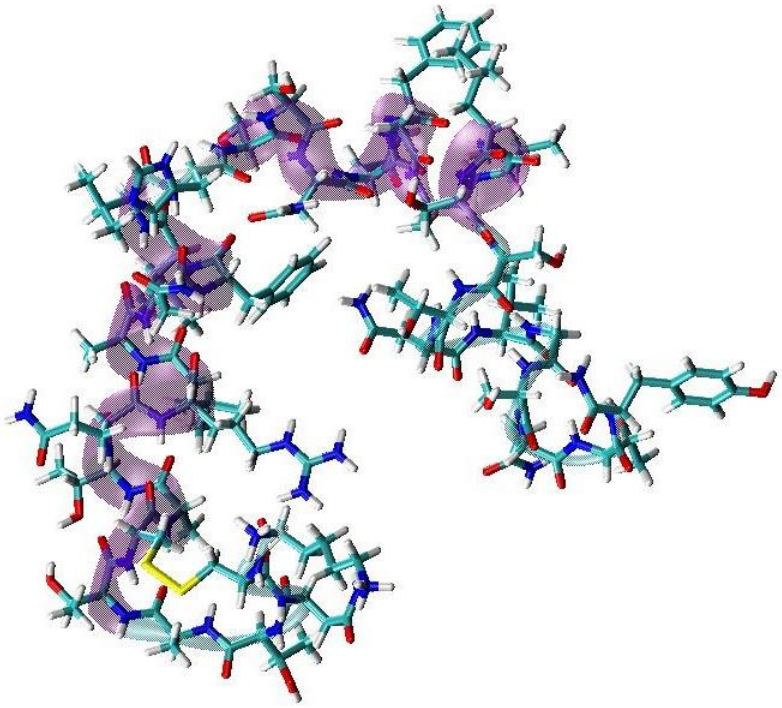

C-Terminus

N-Terminus

Figure 1.5: (A) Primary sequence of human Islet amyloid polypeptide (IAPP) with amidated C-terminal and free N-terminal and a disulfide bond in N-terminal between residues 2 and 7, (B) All atom representation of human Islet amyloid polypeptide molecule with intrapeptide disulfide bond (yellow colored) between Cys-2 and Cys-7 (NMR structure of human IAPP in SDS micelle, PDB: 2L86) (42) . The figure was prepared using VMD (111).

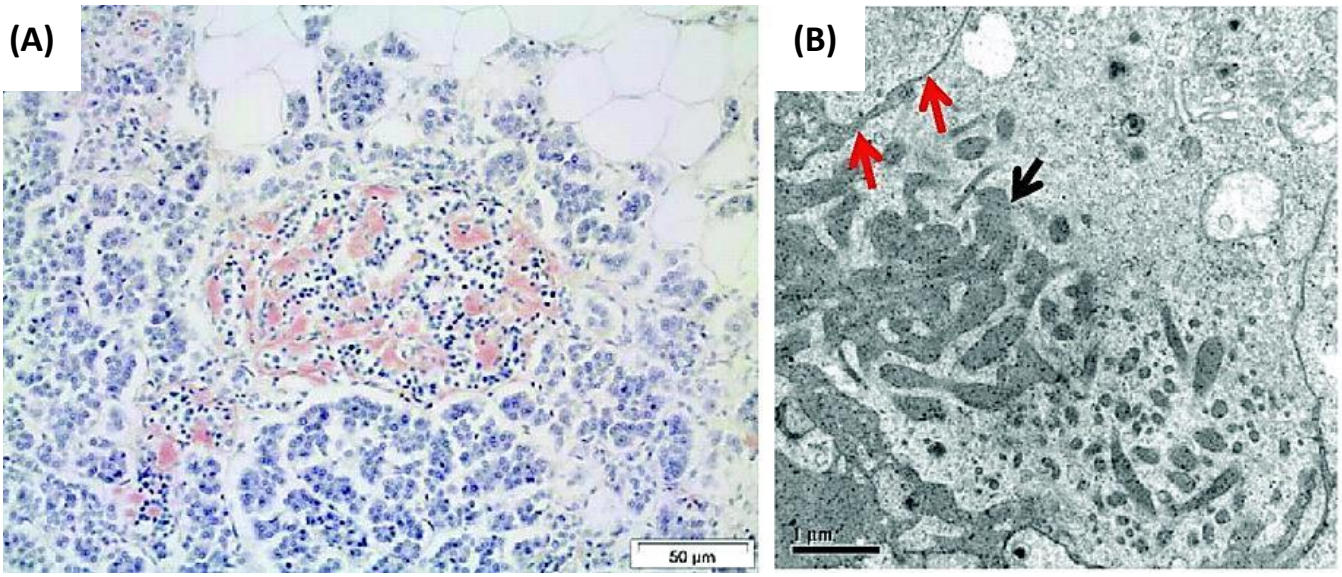

Figure 1.6: (A) Human pancreatic islet from a type II diabetic subject with extracellular amyloid deposits, visualized with Congo red, (B) A part of a β-cell with intracellular amyloid. Red arrows show amyloid fibrils between the two cells and black arrows indicate thin amyloid fibrils within the membrane-enriched compartments (Figure is taken from Westermark et al. (2011) Physiological reviews 91, 795-826) (30).

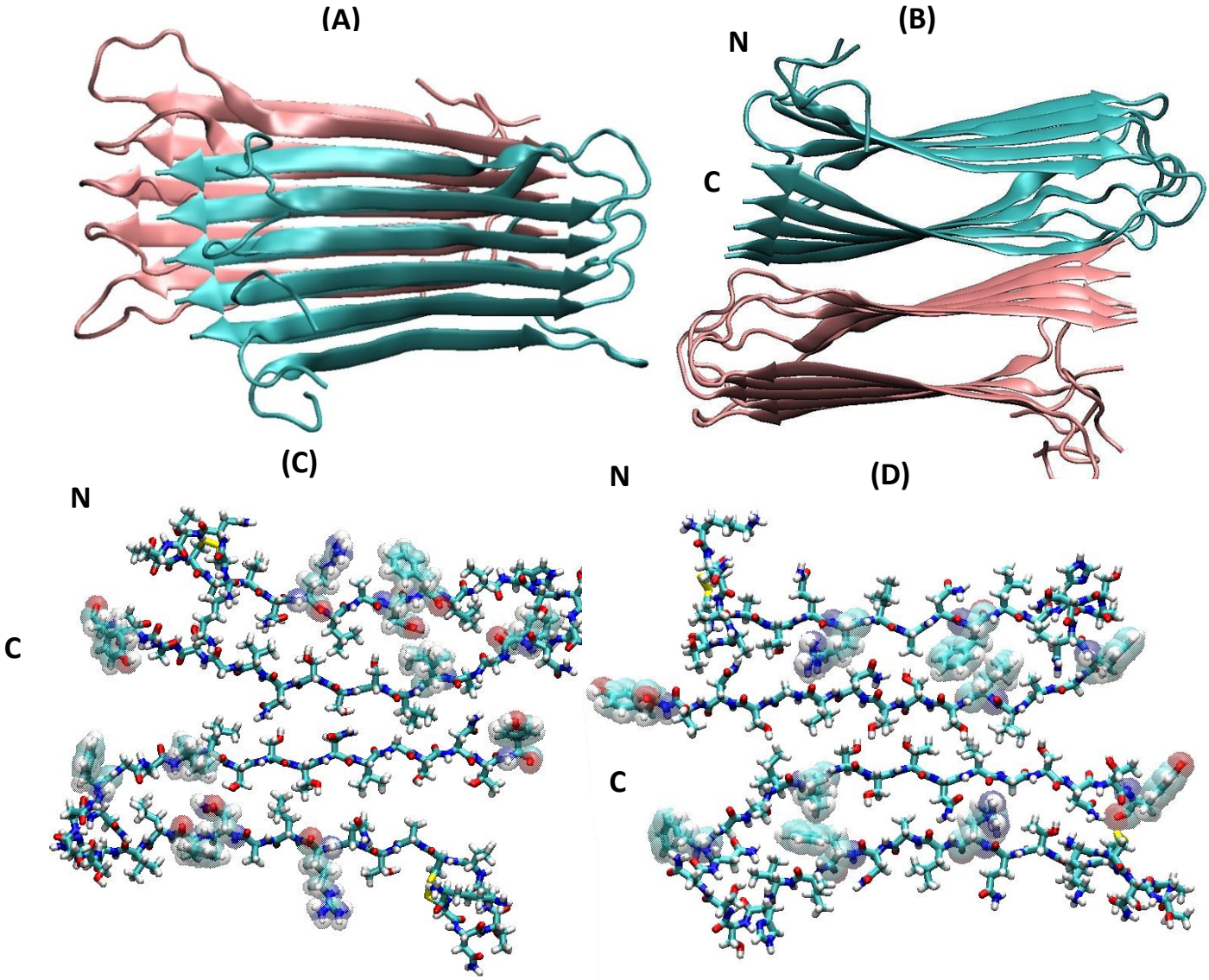

Figure 1.7: Human IAPP fibril (protofilament) model based on constraints obtained from solid state NMR data. (A) Perpendicular view of the fibrils where β-strands in each molecule are perpendicular to fibril long axis, (B) Cross sectional view of two IAPP monomer layers in protofilament which indicates C_2 symmetry of monomer along the fibril axis, (C, D) Cross sectional view (all-atom representations) of the monomers in the fibril. Figures show different orientation of different side chain. For example, in figure C, charge residues arginine are solvent exposed and in figure D, inside the amyloidogenic core (90). The figure was prepared using VMD (111).

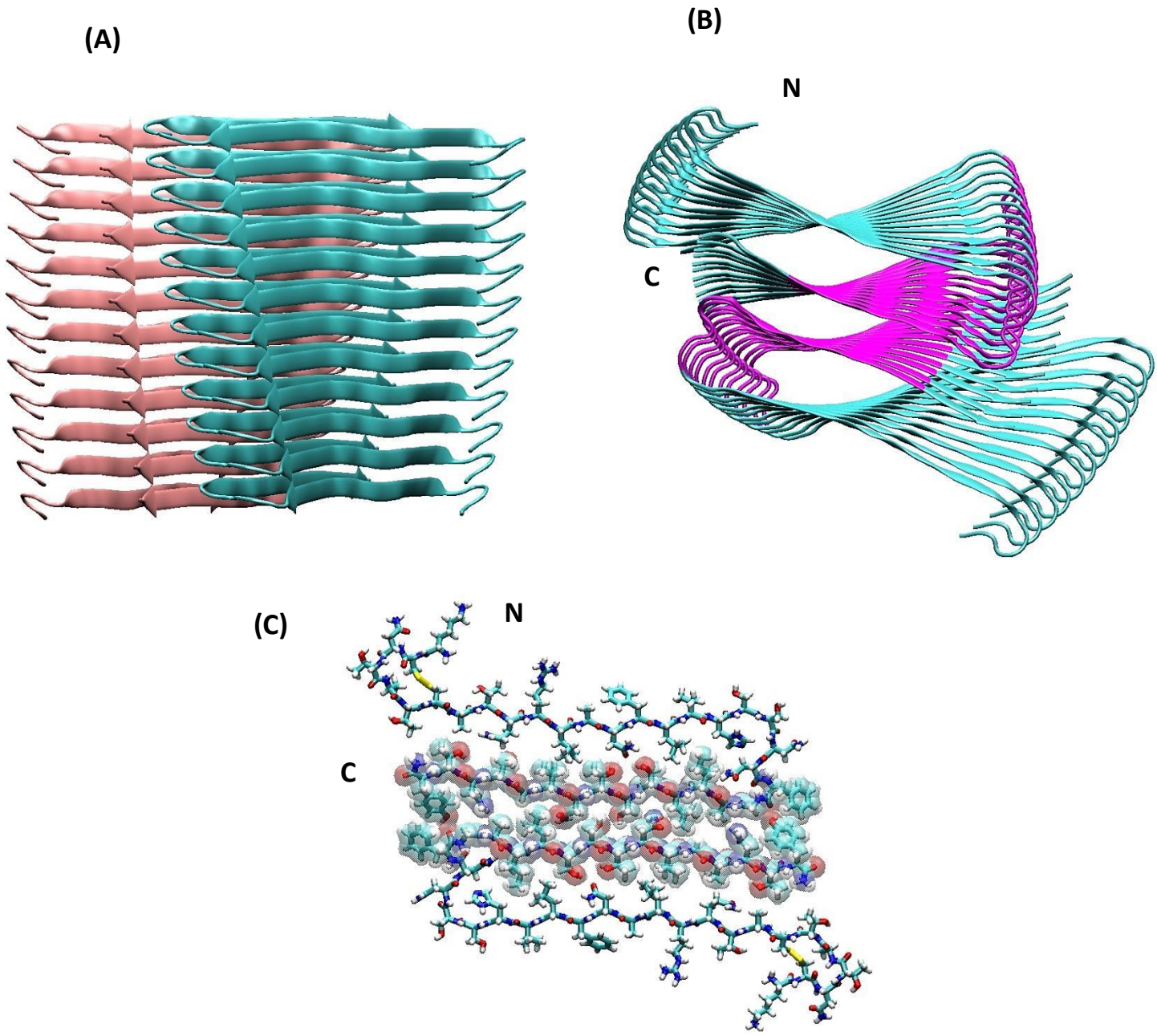

Figure 1.8: Model of human IAPP amyloid fibrils based on the x-ray crystal structure of two small fragments corresponding to residues 21-27 (NNFGAIL) and 28-33 (SSTNVG). (A) Perpendicular view of the fibril, (B) Cross sectional view of IAPP fibrils (residues 21-27 and 28-33 purple colored) (C) Cross sectional view of two IAPP molecules in the fibril, space filling presentation exhibits the "steric zipper" interaction between residues 23 and 37 of two molecules, (92). The figure was prepared using VMD (111).

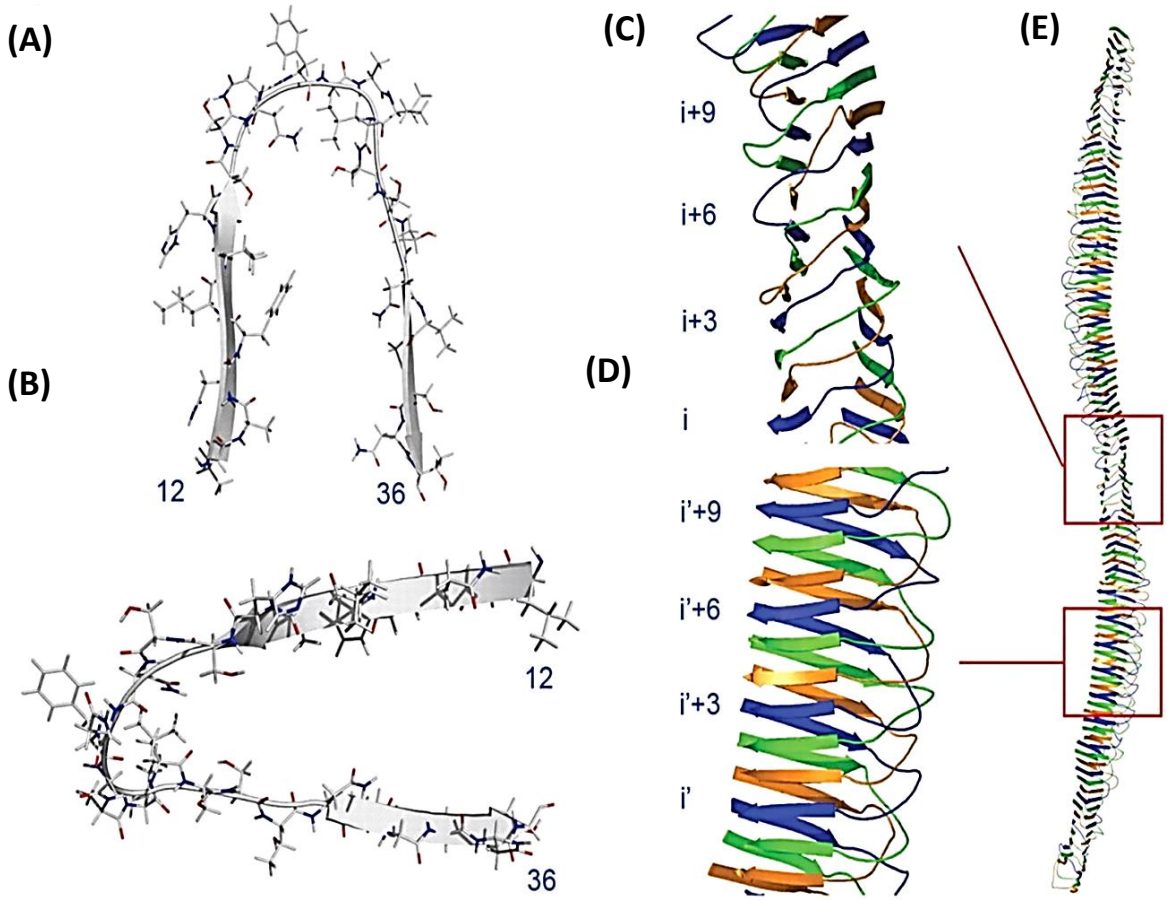

Figure 1.9: Model of human IAPP amyloid fibril based on EPR data. (A, B) IAPP monomer in fibrils showing two staggered β-strand (C,D) enlarged view two sections of IAPP fibril with 90° rotation of β-strands about the axis (E) Structural model of fibrils indicating left handed helix (Figure is taken from Langen et al. (2012), *J Biol Chem 287*, 5235-5241.) (93).

(A)

	1	10	20	30	37
Human	$^{+}H_3N$- KCNTATCAT	QRLANFLVHS	SNNFGAILSS	TNVGSNTY-$CONH_2$	
Baboon	$^{+}H_3N$- ICNTATCAT	QRLANFLVRS	SNNFGTILSS	TNVGSDTY-$CONH_2$	
Cat	$^{+}H_3N$- KCNTATCAT	QRLANFLIRS	SNNLGAILSP	TNVGSNTY-$CONH_2$	

(B)

Cow	$^{+}H_3N$- KCNGATCET	QRLANFLAPS	SNKLGAIFSP	TKMGSNTY-$CONH_2$
Dog	$^{+}H_3N$- KCNTATCAT	QRLANFLVRT	SNNLGAILSP	TNVGSNTY-$CONH_2$
Rat	$^{+}H_3N$- KCNTATCAT	QRLANFLVRS	SNNLGPVLPP	TNVGSNTY-$CONH_2$
Mouse	$^{+}H_3N$- KCNTATCAT	QRLANFLVRS	SNNLGPVLPP	TNVGSNTY-$CONH_2$
Degu	$^{+}H_3N$- KCNTATCAT	QRLTNFLVRS	SHNLGAALPP	TKVGSNTY-$CONH_2$
Pig	$^{+}H_3N$- KCNTATCAT	QRLTNFLVRS	SHNLGAALLP	TDVGSNTY-$CONH_2$

(C)

S20G hIAPP	$^{+}H_3N$- KCNTATCAT	QRLANFLVHS	GNNFGAILSS	TNVGSNTY-$CONH_2$
Pramlintide	$^{+}H_3N$- KCNTATCAT	QRLANFLVHS	SNNFGPILPP	TNVGSNTY-$CONH_2$
I26P hIAPP	$^{+}H_3N$- KCNTATCAT	QRLANFLVHS	SNNFGAPLSS	TNVGSNTY-$CONH_2$
3XL hIAPP	$^{+}H_3N$- KCNTATCAT	QRLANLLVHS	SNNLGAILSS	TNVGSNTL-$CONH_2$

Figure 1.10: (A) Primary sequence of IAPP from human and some mammalian species; residues that are different from human IAPP are colored red. (A) Primates and cats IAPP are amyloidogenic, (B) cows, dogs, rats, and pigs are non-amyloidogenic. (C) Some important human IAPP mutants; S20G mutant is the only known naturally found human IAPP mutant.

2. Using natural and unnatural amino acids to study the role of serine 20 in amyloid formation by islet amyloid polypeptide

2.1 Introduction

Islet amyloid polypeptide (IAPP) is one of the most amyloidogenic proteins known, but there are mutations, which accelerate IAPP amyloid formation. The serine 20 to glycine mutant is the only known naturally occurring mutation found in mature human IAPP. *In vitro* studies showed the evidence that S20G IAPP is more amyloidogenic than wild type IAPP (66,69, 70). The S20G mutant may be weakly correlated with early onset diabetes in Asian populations (60-63). *In vitro* studies showed that S20G IAPP is similarly toxic to cultured cell as wild type IAPP. The sequence of IAPP is well conserved and mostly the variations within positions 18-29 in IAPP led to variation in amyloid formation (94,95). A recently proposed IAPP amyloid model and 2DIR studies showed that Ser20, which belongs to the conservative region, is not in the distinct well-ordered β-sheet region of the amyloid fibrils (90,92,112). Our previous studies showed that mutation with a bulky charged residue lysine at position 20 of IAPP slowed the rate of amyloid formation (69). Recent *in silico* studies suggested that membrane bound condition S20G IAPP exhibits an L-shaped helical motif. *In silico* studies suggested that the G20 mutation facilitated long range contacts and conformational preorganization of the fibril like structure and this reduces the entropy cost for fibril assembly which may be a reason for rapid amyloid formation by the S20G IAPP mutant (113). However, the reason for rapid amyloid formation by S20G mutant is not clear. Because of the lack of a β-carbon side chain, glycine has more conformational flexibility in its backbone more than do residues with sidechains. There is high frequency of glycine with positive dihedral ϕ angle (Ramachandran plot, Figure 2.1) (114). We

tested that the accelerated amyloid formation by the S20G mutant may be result of the requirement for a positive dihedral ϕ angle geometry at residue 20 in its backbone that may be increased the stability of the amyloid fibril. Therefore, we rationally designed hIAPP mutant peptide to test this hypothesis. We used D-amino acids that are energetically favorable with a positive ϕ angle. It is known that replacement of glycine with a D-amino acid mutant stabilizes the turn in a β-hairpin if the additional methyl group does not cause any steric clash (115). Other possible reasons for fast amyloid formation by the S20G mutant may be; glycine reduces steric clash due to the Ser sidechain, or eliminates unfavorable hydrogen bonds that are not compatible with amyloid formation, or glycine facilitate helix-helix interaction as *in vitro* studies shows that helical intermediate formation may be on the pathway of amyloid formation(76,77). To check those possibilities we chose another two single point IAPP mutants; serine 20 to alanine (S20A IAPP) and serine 20 to 2-aminobutanoic (S20Abu IAPP). Alanine is the closest in size and in hydrophobicity to a glycine residue and 2-amino butanoic acid (2-Abu) is an unnatural amino acid that is isosteric amino acid of serine; however, it is a non-polar amino acid. Alanine and 2-aminobutanoic acid are highly helical propensity residues. Solid phase peptide synthesis makes it easy to incorporate non-coded amino acids.

2.2 Materials & Methods

2.2.1 Peptide Synthesis

Human IAPP, S20d-S IAPP, S20d-A IAPP, S20A IAPP and S20Abu were synthesized by using standard Fmoc (9-fluorenylmethoxycarbonyl) solid phase methods on a 0.1 mmol scale using a CEM Liberty 12-Channel Automated microwave peptide synthesizer. Pure S20G peptides were obtained from the former lab member Dr. Ping Cao. PAL-PEG-PS resin was used to obtain the amidated C-terminus and HBTU was used as coupling agent. Fmoc protected pseudoproline dipeptide derivatives were used at the position 9 - 10 and 27 - 28 to facilitate the synthesis (117, 118). The first residue attached to the resin, pseudoproline dipeptide derivatives, and all β-branched residues were double coupled (119). Peptides were synthesized using standard Fmoc reaction cycles (120, 121). The peptides were cleaved and deprotected from the resin by treatment with standard trifluoroacetic acid (TFA) with 3% (v/v) anisole, 3% (v/v) thioanisole, and 3% (v/v) 1,2-ethanedithiol at room temperature for 3 hours. The resin was filtered, rinsed with TFA and the filtrate was concentrated under a stream of nitrogen. The crude peptide was precipitated using cold diethyl ether, filtered with fine fritted funnel, rinsed with cold diethyl ether. Scavengers were removed under the vacuum and the crude peptide was lyophilized. Solvents used were ACS grade. Fmoc-protected pseudoproline (oxazolidine) dipeptide derivatives were purchased from Novabiochem. All other reagents were purchased from Advanced Chemtech, PE Biosystems, Sigma, and Fisher Scientific.

2.2.2. Peptide Purification and Oxidation

Crude peptides were partially dissolved in 20% acetic acid (v/v) to increase its solubility and were freeze-dried with lyophilizer. The dry polypeptides were dissolved in 100% of DMSO and

allowed to stand at room temperature for a minimum of 24 hrs to promote the formation of the Cys-2-Cys-7 disulfide bond via oxidation by DMSO (122, 123). The peptides were purified via reversed phase HPLC using a Vydac C18 preparative column (10 mm X 250 mm). An A-B gradient system was used where buffer A was consisting of 100% H_2O and 0.045% HCl (v/v) and buffer B was consisting of 80% acetonitrile, 20% H_2O, and 0.045% (v/v) HCl . The gradient was 20-60% buffer B in 40 minutes or 20-70% buffer B in 50 minutes. The pure peptides are usually eluted around 24 to 32 minutes. There is some variation between the corresponding to a percent of buffer B of different peptide (Figure 2.2). HCl was utilized as the ion-pairing agent instead of TFA since TFA can influence the rate of aggregation. After the initial purification, the peptide was redissolved in HFIP and was subjected to a second round of HPLC purification. This procedure was necessary to remove residual scavengers. The purity of peptide was checked by HPLC using a Vydac C18 reversed-phase analytic column (4.6 mm X 250 mm). The identities of the purified peptides were confirmed by mass spectrometry using a Bruker MALDI-TOF MS (matrix assisted laser desorption ionization time of flight mass spectrometry) instrument. The expected and observed molecular masses for oxidized human IAPP, expected 3903.3, observed 3902.6; S20d-S IAPP expected 3903.3, observed 3903.8; S20d-A IAPP, expected 3887.3, observed 3886.3; S20A IAPP, expected 3887.3, observed 3885.8; S20Abu IAPP, expected 3901.3, observed 3902.8.

2.2.3 Fluorescence Assays

Sample Preparation

A 1.6 mM stock solution was prepared by dissolving dry peptide (stored at -20°C inside a desiccator) in 100% Hexafluoro-2-propanol (HFIP) and the concentration was determined by

using Beckman Coulter uv/vis spectrophotometer and measuring the absorbance at 280 nm. Aliquots were stored at 4°C. Aliquots were filtered through a 0.22 μm Millex syringe-driven filter before the solution was prepared for the experiment.

Thioflavin-T Binding Kinetic Assays

Thioflavin-T binding fluorescence experiments were used to measure the development of structurally ordered fibrils over time. Fluorescence experiments with HFIP were performed on an Applied Phototechnology fluorescence spectrophotometer using an excitation wavelength of 450 nm and an emission wavelength of 485 nm. The excitation and emission slits were set at 6 nm. A 1.0 cm cuvette was used, and each point was averaged for 1 min. A16 μM peptide solution in 2% HFIP was used to keep consistency with previously published experiment condition. Solutions were prepared via dilution of the filtered stock peptide solution into 20 mM Tris-HCl buffer (pH 7.4) and 32 μM thioflavin-T solution immediately before the measurement. The final experiment conditions were as follows: 16 μM peptide, 32 μM thioflavin-T in 2% HFIP, 25°C, and pH 7.4 with continuous stirring. Stirring is known to accelerate amyloid formation.

Fluorescence experiments without HFIP were performed on a Beckman Coulter DTX 880 Multimode Detector platereader. Thioflavin T fluorescence was measured at 430 nm excitation wavelength and 485 nm emission wavelength. Corning 96-well non-binding surface black plate with a lid was used for the assay. The experiments were done with paraffin sealed wells. Fluorescence intensity was detected from the bottom of the plate. The experiments were performed at 16 μM peptide concentration. Measured amount of filter aliquots were lyophilized to remove HFIP. Lyophilized dry peptides were dissolved in 20 mM Tris-HCL buffer (pH 7.4) containing 32μM thioflavin-T solution right before the assays. The final experiment condition

was as follows: 16 μM peptide, 32 μM thioflavin-T, no HFIP, and pH 7.4 at 25 °C without stirring.

Seeding Assays

To obtain the fibril as seed, a fibril solution was prepared from diluting 1.6 mM filter aliquot in HFIP to 16 μM peptide concentration using 20 mM Tris- HCl buffer containing 32 μM Thioflavin-T in 2% HFIP solution. Experimental conditions were as follows: 10% seed (1.6 μM in monomer units), 90% of 16 μM peptide, 32 μM Thioflavin T, 2% HFIP in 20 mM Tris buffer at pH 7.4, at 25 °C, with constant stirring.

2.2.4 Circular Dichroism (CD) Experiments

CD experiments were performed using an Applied Photophysics Chirascan circular dichroism spectrophotometer. CD spectra were recorded from the sample collected at the end of the kinetic experiments conducted with 2% HFIP and from the seeding experiments. Spectra were recorded from 190 to 260 nm at 1 nm intervals using a 0.1 cm quartz cuvette and the final spectra was the average of three times repeating result. A background spectrum was subtracted from the collected data. Data were collected at 25 °C.

2.2.5 Transmission Electron Microscopy (TEM)

TEM images were taken using an FEI EM microscope at the Life Science Microscopy Center at the Stony Brook University. TEM samples were prepared from the solutions used for the fluorescence measurements. 15 μL peptide solution was taken out at the end of the 16 μM IAPP in 2% HFIP kinetic experiments and the seeding kinetic experiments, and was blotted onto a

carbon-coated Formvar 300 mesh copper grid for 1 minute and then negatively stained with saturated uranyl acetate for 1 min. Images were taken at 80kV. Images were collected using a 68,000x magnification and 100 nm under focus.

2.3 Results & Discussion

2.3.1 Analysis of amyloid formation by D-amino acid mutants confirm the normal backbone conformation of S20G IAPP

Two single serine 20 mutant of hIAPP were synthesized using unnatural D-amino acids; D-Serine and D-Alanine (Figure 2.3). These two polypeptides are denoted as S20d-S IAPP and S20d-A IAPP. The d-A and d-S residues were well fit at position 20 in an x-ray crystalline model of IAPP fibrils (Figure 2.9). The clash score was obtained by using the Molprobity program with a distance cut off for overlap set to >0.4 Å (124). The clash score for mutant fibrils are similar as wild type fibrils.

The rates of amyloid formation by S20d-S IAPP and S20d-A IAPP were measured using Thioflavin-T binding fluorescence assays, performed in the presence of 2 % HFIP with stirring (Figure 2.3B) and in absence of HFIP (Figure 2.4) at pH 7.4. The kinetic curves show that the rate of amyloid formation by S20d-S IAPP is similar to that observed for wild type IAPP, while the rate of amyloid formation by S20d-A is much slower than wild type IAPP and both are slower than S20G (Figure 2.5). Circular dichroism (CD) scans were taken at the end of the kinetic run. CD scans confirmed that the presence of β-sheet structure in wild type IAPP fibrils and mutant fibrils (Figure 2.7). Samples for taking TEM images were collected at the end of the

kinetic run. TEM images showed all the mutants formed amyloid fibrils as wild type IAPP (Figure 2.8).

It is also notable that the shape of the kinetics curves (timescale normalized with their own t_{50} – time to rich 50% of final intensity) for the two D-amino acids mutant are different than wild type (Figure 2.6) which suggests a different amyloid formation mechanism adopted by these two peptide. Comparing S20G IAPP and S20d-S IAPP, S20d-A IAPP suggests that during amyloid formation, residue 20 does not adopt positive ϕ angle in its backbone.

2.3.2 Amyloid formation by wild type IAPP can be seeded by D-amino acids mutant fibrils

The potential structural similarities between wild type IAPP and mutant fibrils were studied by seeding experiments. A small amount of preformed fibril acts as a seed in amyloid formation which allows the lag phase to be by passed. Seeding specificity helps to distinguish differences between fibril structures. Both homologous and heterologous seeding efficiency were studied in the presence of 2 % HFIP with continuous stirring at pH 7.4. Since effective seeding requires similar fibril structure, seeds were most efficient in homologous seeding. WT IAPP was seeded by its own fibrils (Figure 2.10, green curve). WT IAPP was also seeded by S20d-S IAPP fibrils and S20d-A IAPP fibrils (Figure 2.10) and compared with previously published results on wild type IAPP seeded by S20G IAPP fibrils. All of the mutant fibrils can seed amyloid formation by wild type IAPP, which indicates some structural similarity between mutant fibrils. However, mutant fibrils were less effective at seeding wild type than was wild type IAPP itself. Seeding effectiveness is more qualitative than quantitative. The seed concentration was measured at monomer unit basis. Though the same concentration of fibril (monomer units) used each time, the distribution of fibrils and the distribution of fibril length in each sample is unknown and this

makes a detailed comparison difficult. CD scans were taken at the end of the seeding kinetic experiments and all of the peptide formed β-sheet structure (Figure 2.11). Samples were also collected at the end of seeding kinetic experiments for TEM and all of the peptides form amyloid fibrils (Figure 2.12).

Each d-amino mutant peptide was seeded by its own fibrils. Analysis of the homologous seeding kinetics results (timescale normalized by the peptide t_{50} value) showed that the seeding kinetics curve of S20d-S IAPP (blue) and S20d-A IAPP (orange) were different from wild type IAPP (green) (Figure 2.13). This also suggests that the amyloid formation pathway of S20d-S IAPP and S20d-A IAPP may be different from that of wild type IAPP and it also reflects the results we saw before in the figure 2.6. CD spectroscopy confirmed the presence of β-sheet in the fibrils (Figure 2.14). TEM images were taken at the end of seeding kinetics and confirmed fibril formation (Figure 2.15).

2.3.3 Analysis of hydrophobic and isosteric amino acid mutants of serine suggests that steric clashes and incorrect side chain hydrogen bonding does not cause rapid amyloid formation by S20G IAPP

Removal of steric clashes or incorrect side chain hydrogen bonding by the Ser to Gly mutant might account for the faster rate of amyloid formation. This was checked by another two point mutants, serine 20 to alanine and serine 20 to 2-amino butanoic acid. 2-aminobutonic acid (Abu) is an unnatural, non-polar amino acid that is isosteric to serine (Figure 2.16A). The trend in hydrophobicity and in Van der Waals volume is Gly<Ala<Abu (125). These two peptides were denoted as S20A IAPP and S20Abu IAPP.

The rate of amyloid formation by S20A IAPP and S20Abu IAPP were monitored by Thioflavin-T binding fluorescence assays, in the presence of 2 % HFIP with stirring (Figure 2.16B) and in the absence of HFIP (Figure 2.17) at pH 7.4. In the presence of 2% HFIP, the kinetic curve showed that the rate of amyloid formation by S20A IAPP and S20Abu was much slower than wild type IAPP (Figure 2.18A). In absence of HFIP, the rate of amyloid formation by S20Abu IAPP was similar to WT IAPP, while S20A IAPP was much slower than WT IAPP (Figure 2.18B) was. None of the mutants formed amyloid as fast as S20G IAPP. Comparing the hydrophobicity trend (Abu>Ala>Gly>Ser) to the trend in the rate of amyloid formation (Gly>Ser>Abu>Ala), suggests that hydrophobic interactions do not have any significant effect on amyloid formation at this position. It is also noticeable that the rate of amyloid formation by S20A IAPP and S20Abu IAPP (Gly>Abu>Ala) did not follow the trend in Van der Waals volume of the amino acids (Abu>Ala>Gly). Comparing amyloid formation to the Van der Waals volume of the three residues at position 20; Serine, 2-aminobutaonic acid, suggests that even though serine and 2-aminobutanoic acid are opposite in polar characteristics, the size of the serine plays an important role in fibril packing.

Comparing the shape of the kinetics (timescale normalized with own t_{50} –time to reach 50% of its final intensity) of S20A IAPP and S20Abu IAPP, it is found that the shape of the curves are similar as WT IAPP (Figure 2.19). This analysis suggests that these two mutant peptides may follow the similar amyloid formation pathway as WT IAPP. CD scans recorded at the end of the each experiment, confirmed that the presence of β-sheet structure in wild type IAPP fibrils and mutant fibrils (Figure 2.20). Samples for TEM were collected at end of the kinetic run. TEM images showed all the mutants formed amyloid fibrils similar to wild type IAPP (Figure 2.21). Both alanine and 2-amino butanoic amino acid residues were well fit at

position 20 in the Eisenberg et al. model of hIAPP fibrils. S20A IAPP and S20Abu IAPP mutant fibrils were built from Eisenberg model using the program Chimera (Figure 2.22) (126). Steric clashes were checked using Molprobity program with a distance cut off set to >0.4 Å (124). The clash score for mutant fibrils are similar as wild type fibrils.

2.3.4 S20A IAPP and S20Abu IAPP fibrils can seed wild type IAPP amyloid formation

The structural similarity between wild type IAPP and S20A IAPP and S20Abu IAPP fibrils was studied by seeding experiments. Both homologous and heterologous seeding were studied in presence of 2% HFIP with continuous stirring at pH 7.4. WT IAPP was seeded by its own fibrils (green). WT IAPP was also seeded by S20A IAPP fibrils (orange) and S20Abu IAPP fibrils (purple) and was also compared with previously published results wild type IAPP seeded by S20G IAPP fibrils (blue) (Figure 2.23). All of the mutant fibrils can seed the amyloid formation by wild type IAPP, indicating some structural similarity between mutant fibrils. However, mutant fibrils were less effective seeds than wild type IAPP itself. The seed concentration was measure as a monomer unit basis. The same concentration of fibril (monomer units) was used each time, but it is unknown if the amount of fibrils and the distribution of fibril lengths are the same in each sample, which makes it hard to quantitatively compare different studies. CD scans were taken at the end of the seeding kinetic experiments and all of peptides contain β-sheet structure of the fibrils (Figure 2.24). Samples were also collected at the end of seeding kinetic experiments for TEM and all of the peptide forms amyloid fibrils (Figure 2.25).

S20A IAPP and S20Abu IAPP are seeded by their own fibrils. Analysis of the homologous seeding kinetics results (timescale normalized with own t_{50} value) showed that seeding kinetic curve of S20A IAPP (orange) and S20Abu IAPP (purple) were similar as wild

type IAPP (green) (Figure 2.26). The analysis of seeding kinetics suggested that the amyloid formation pathway by S20A IAPP and S20Abu IAPP might be similar to wild type IAPP. This analysis also reflected the similar results that we saw before in the unseeded amyloid kinetic profile in the figure 2.19. CD scans done at the end of the kinetics confirmed the presence of β-sheet in the fibrils (Figure 2.27). TEM images taken at the end of seeding kinetics confirmed fibril formation (Figure 2.28).

2.4 Conclusion

In summary, the analysis D-amino acid mutant kinetics confirm that accelerated amyloid formation by S20G mutant is not the result of a requirement to adopt a positive dihedral ϕ angle geometry at residue 20. Amyloid kinetics of the D-amino acid mutants variant suggests that the amyloid formation mechanism by D-amino acid mutant may be different from that of wild type IAPP. These results are also supported by the homologous seeding kinetics i.e. when peptides are seeded by their own fibrils. However, analysis of seeding kinetics of wild type IAPP by D-amino acid mutants fibrils confirmed that single point mutation did not perturbed the final fibril structure hugely as each fibril acts as a good seed for amyloid formation. CD spectra confirmed the similar secondary β- sheet structure formation and TEM images confirmed the similarity in final fibril structure.

Analysis of alanine and 2-aminobutanoic acid variants kinetics confirmed that accelerated amyloid formation by the S20G mutant is not the result of the relief from unusual steric clashes. The studies also confirmed that rapid amyloid formation is not the result of removal of unfavorable hydrogen bond interactions that hindered amyloid formation. Seeding kinetics are consistent with the D-amino acid mutants i.e. a single point mutation with a hydrophobic

residues does not severely change the final fibril morphology. Both mutants fibrils can seed wild type IAPP amyloid formation which indicates the structural similarity between the fibrils. CD and TEM images indicate similar fibril conformation.

Analysis of the kinetics of serine, D-serine and 2-amino butanoic acid mutants confirmed that these peptides are more amyloidogenic compare to alanine mutant. Serine and 2-aminobutanoic acid are polar and non-polar residue, respectively, however, the rate of amyloid formation in absence of co-solvent is not significantly different. These kinetics results indicate that the structural conformation like serine residue at position 20 is important for amyloid formation. This β-carbon may destabilize the unfolded state or stabilize the folded state packing.

Alanine is a residue with helical propensity and helical intermediates formation may be on the pathway of amyloid formation. Both Ala and D-Ala mutant showed slow amyloid formation. It may be that alanine mutant stabilizes helix- helix interaction and prevents conversion from helical form to β-sheet form which slows down the amyloid formation. Alanine can stabilize folded state of helical protein more than glycine (127).

An alternative explanation for the effect of the S20G mutant is that it could lead to better packing of monomer during oligomer formation. Analysis of non-redundant pdb set, Eisenberg et al. suggests that both GXXXG motif and AXXXA motifs are found in soluble proteins in helix-helix interactions (128). They found that AXXXA motif are more available in thermophile that they suggest contributes the thermo stability in protein. They found that the GXXXG motifs in helix-helix interaction in soluble proteins are similar to these seen in glycophorin A, a transmembrane protein. Backbone to backbone atomic contacts involving C_{α}—H···O stabilize helix- helix interaction in glycophorin A (129). Glycine mutation at position 20 in hIAPP creates

a GXXXG motif. It could be possible that enhanced amyloid formation by the S20G mutant is the results of early oligomarization driven by GXXXG motif.

Acknowledgement

I thank Dr. Ping Cao and L.H. Tu for the S20G IAPP mutant peptide and experimental data.

2.5 Figures

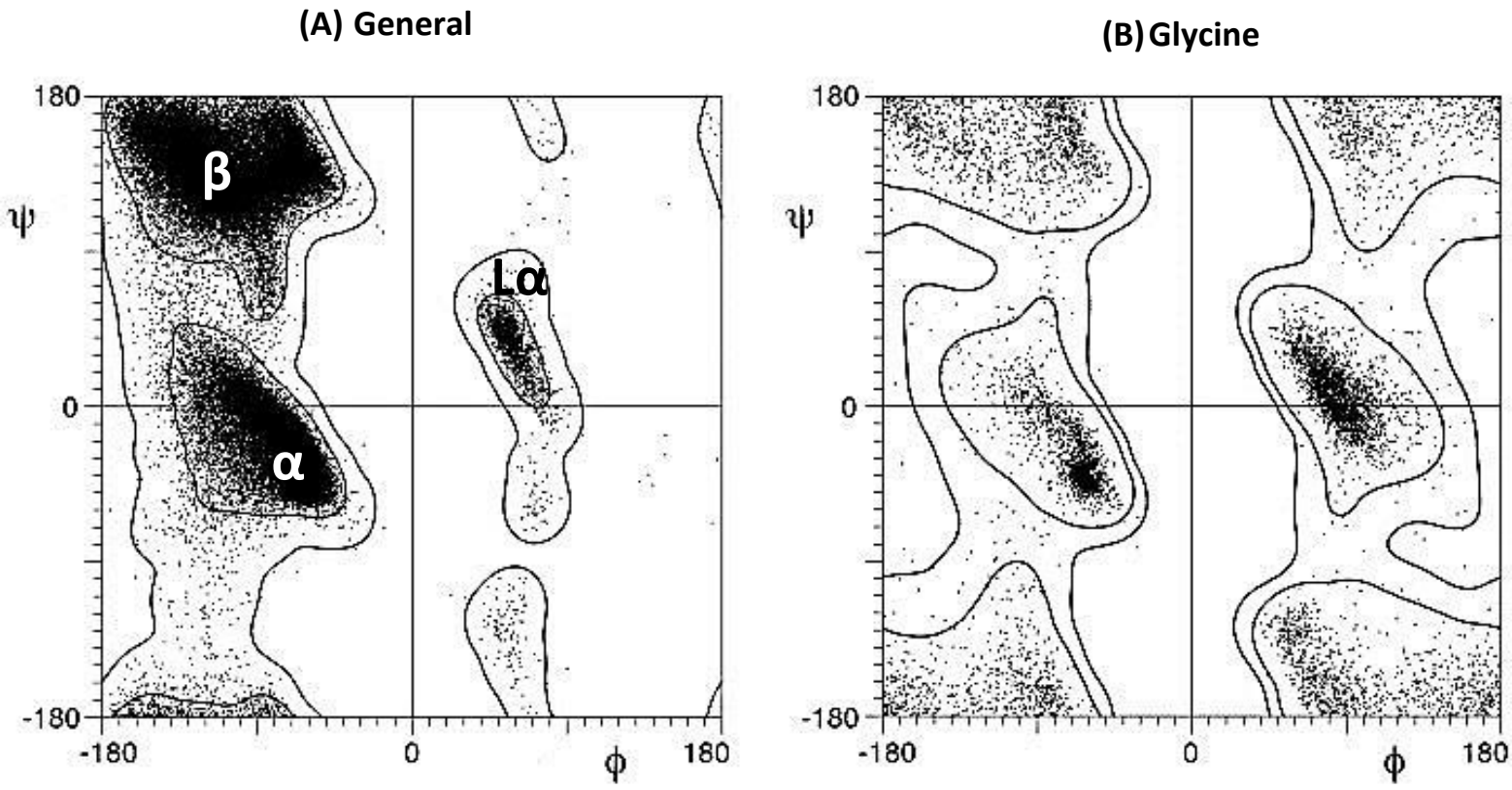

Figure 2.1: ϕ,ψ angle (Protein backbone dihedral angles) distribution of amino acids in the Ramachandran plot from 500 protein structure. (A) ϕ,ψ angle distribution for non-glycine , non-proline residues. Protein secondary structures regions are showed in the plot. (B) Backbone dihedral angle distribution for glycine residues. (Figure was taken from the Lovell et al. (2003), Proteins 50, 437-450) (111).

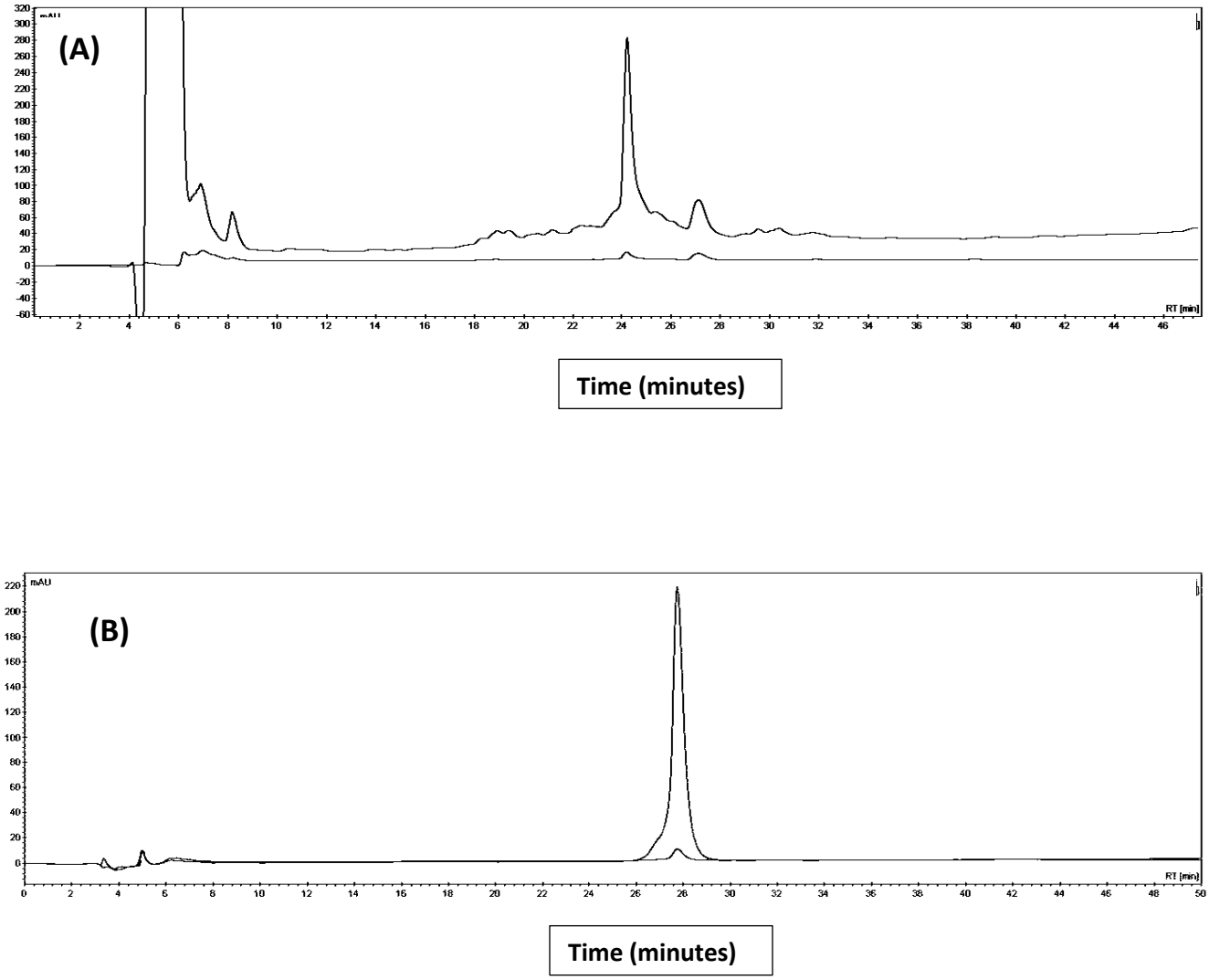

Figure 2.2.1: HPLC traces of wild type IAPP using an analytical C18 column. (A) Crude wild type (eluted at ~24 minutes), (B) Pure wild type (eluted at 28 minutes) (A-B buffer gradient system: A: 100 % DDI H_2O&0.045 % HCl, B: 80% ACN & 0.45% HCl (v/v), gradient: 20-70 % B in 50 minutes).

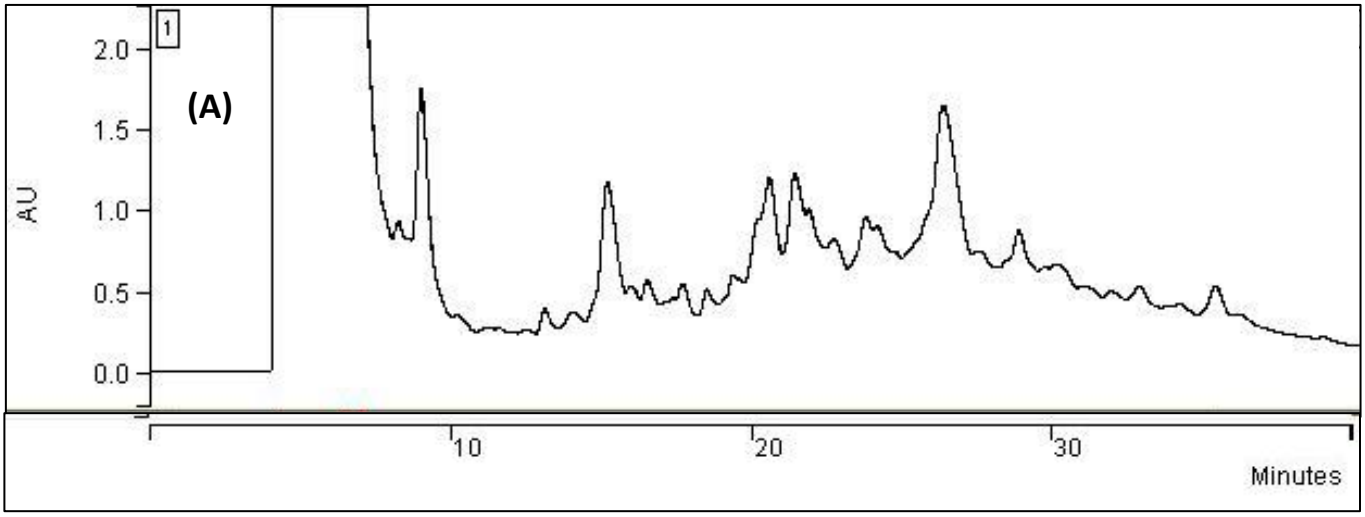

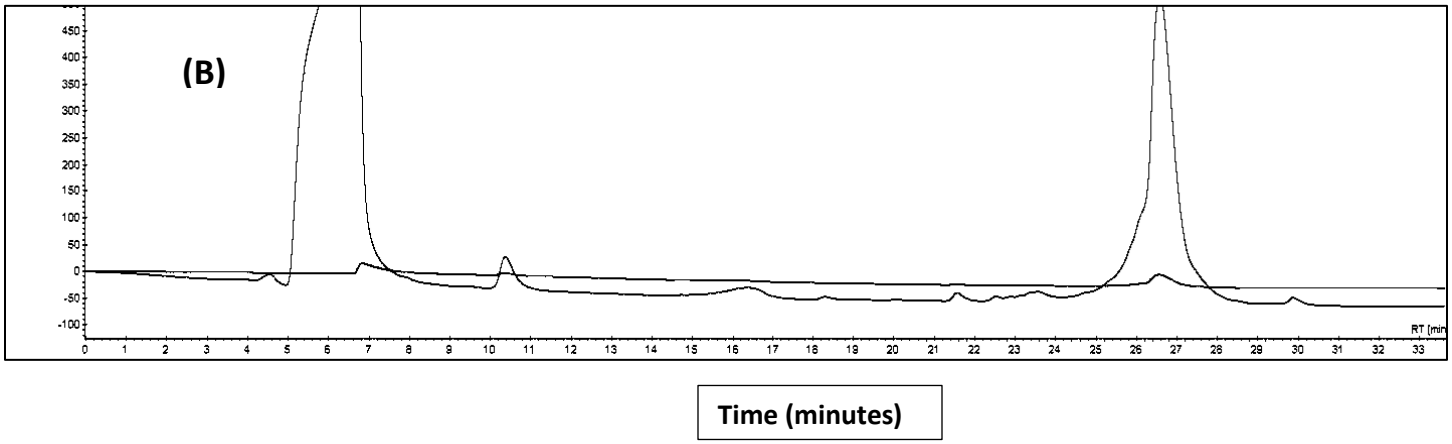

Figure 2.2.2: HPLC traces of S20d-A IAPP using an analytical C18 column. (A) Crude S20d-A IAPP (eluted at~ 24 minutes, gradient: 20-40 % B in 60 minutes), (B) Pure S20d-A IAPP(eluted at ~27 minutes, gradient : 20-50 % B in 50 minutes) (A-B buffer gradient system: A: 100 % DDI H_2O&0.045 % HCl, B: 80% ACN & 0.45% HCl (v/v)).

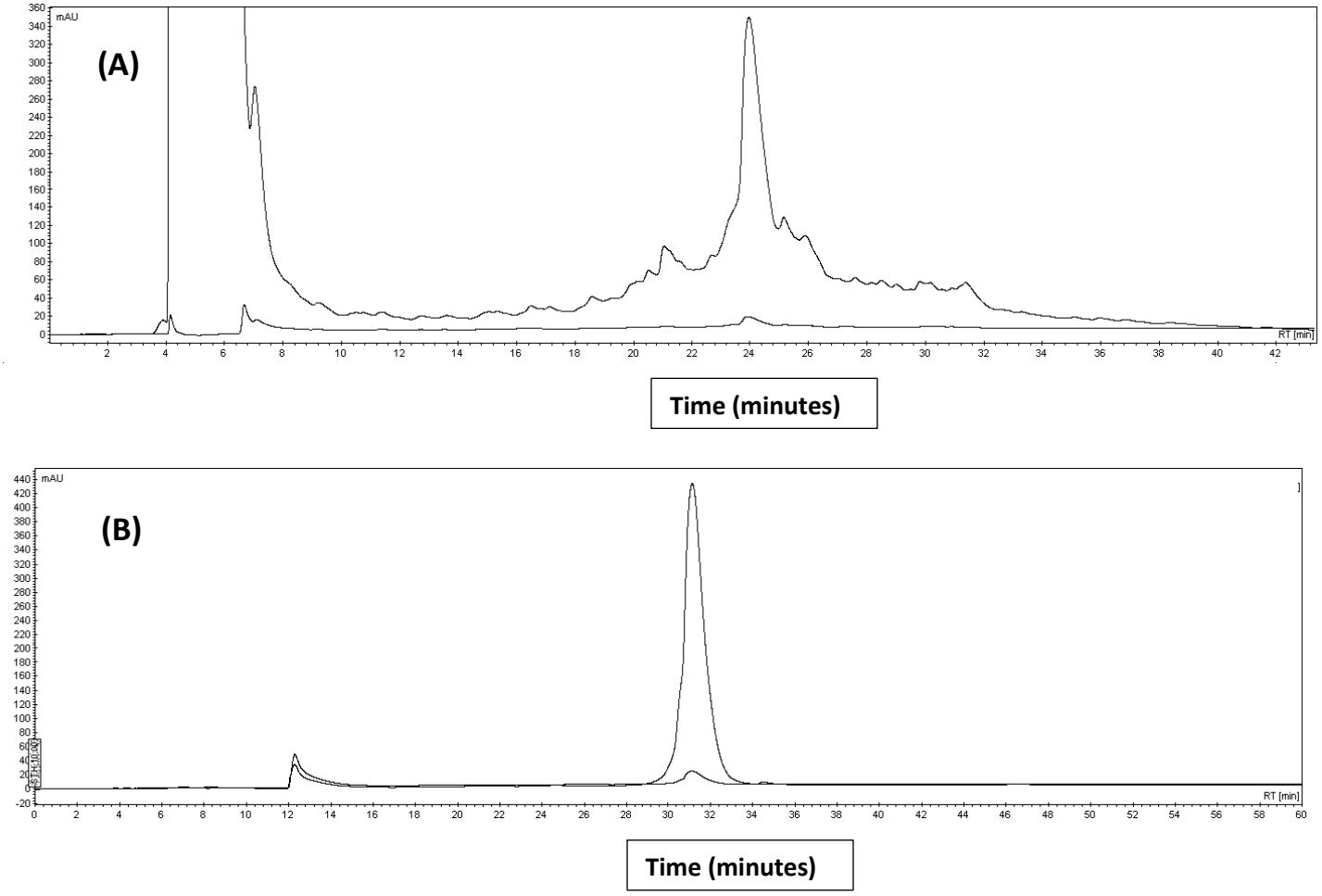

Figure 2.2.3: HPLC traces of S20d-S IAPP using an analytical C18 column. (A) Crude S20d-S IAPP (eluted at ~24 minutes, gradient: 20-70 % B in 50 minutes), (B) Pure S20d-S IAPP (eluted at 32 minutes, gradient: 20-40 % B in 20 minutes & 40-60 % in 40 minutes) (A-B buffer gradient system: A: 100 % DDI H_2O&0.045 % HCl, B: 80% ACN & 0.45% HCl (v/v)).

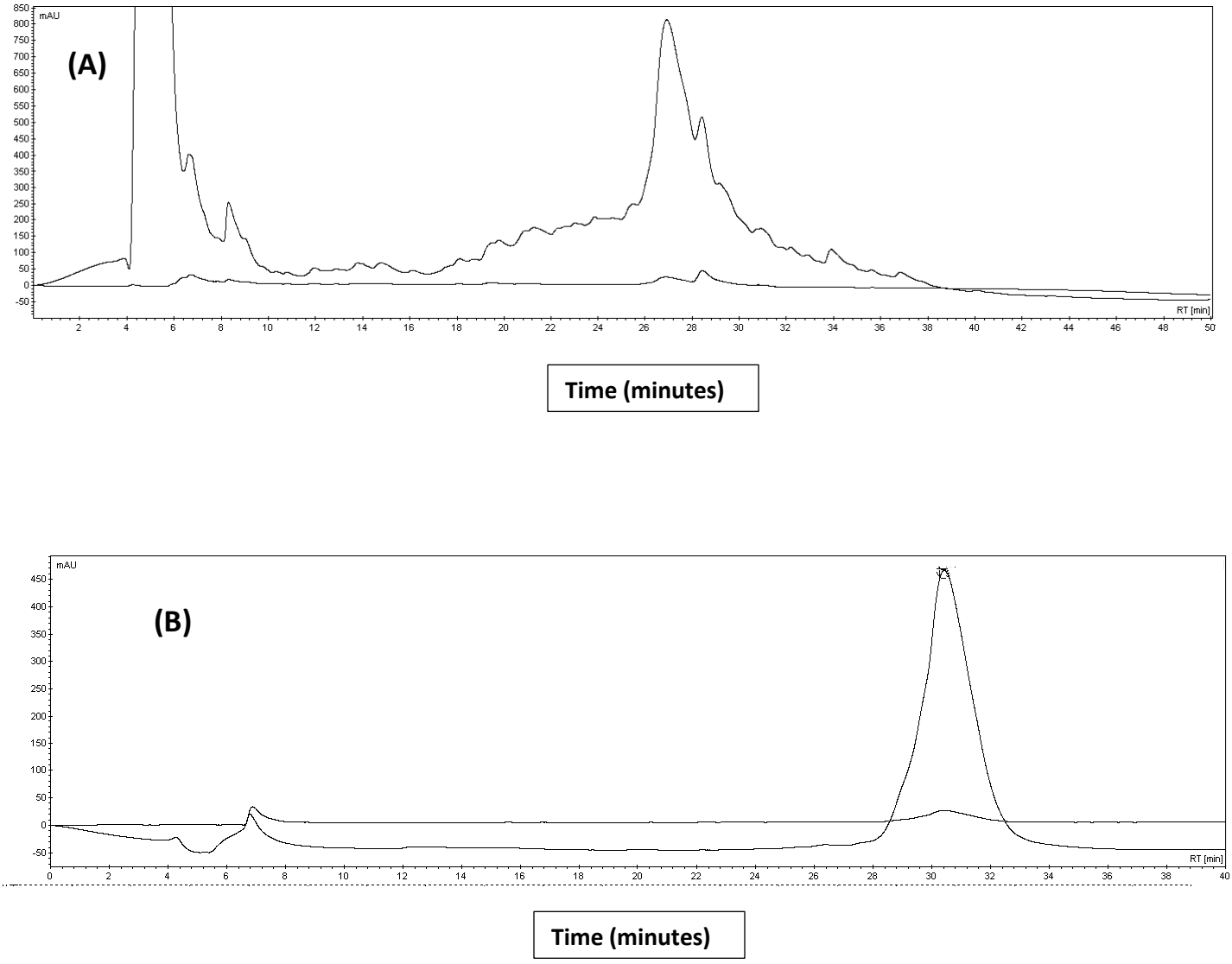

Figure 2.2.4: HPLC traces of S20A IAPP using an analytical C18 column. (A) Crude S20A IAPP (eluted at ~ 24 minutes, gradient : 20-70 % B in 50 minutes), (B) Pure S20A IAPP (eluted at ~30 minutes, gradient : 20-40 % B in 60 minutes) (A-B buffer gradient system: A: 100 % DDI H_2O&0.045 % HCl, B: 80% ACN & 0.45% HCl (v/v)).

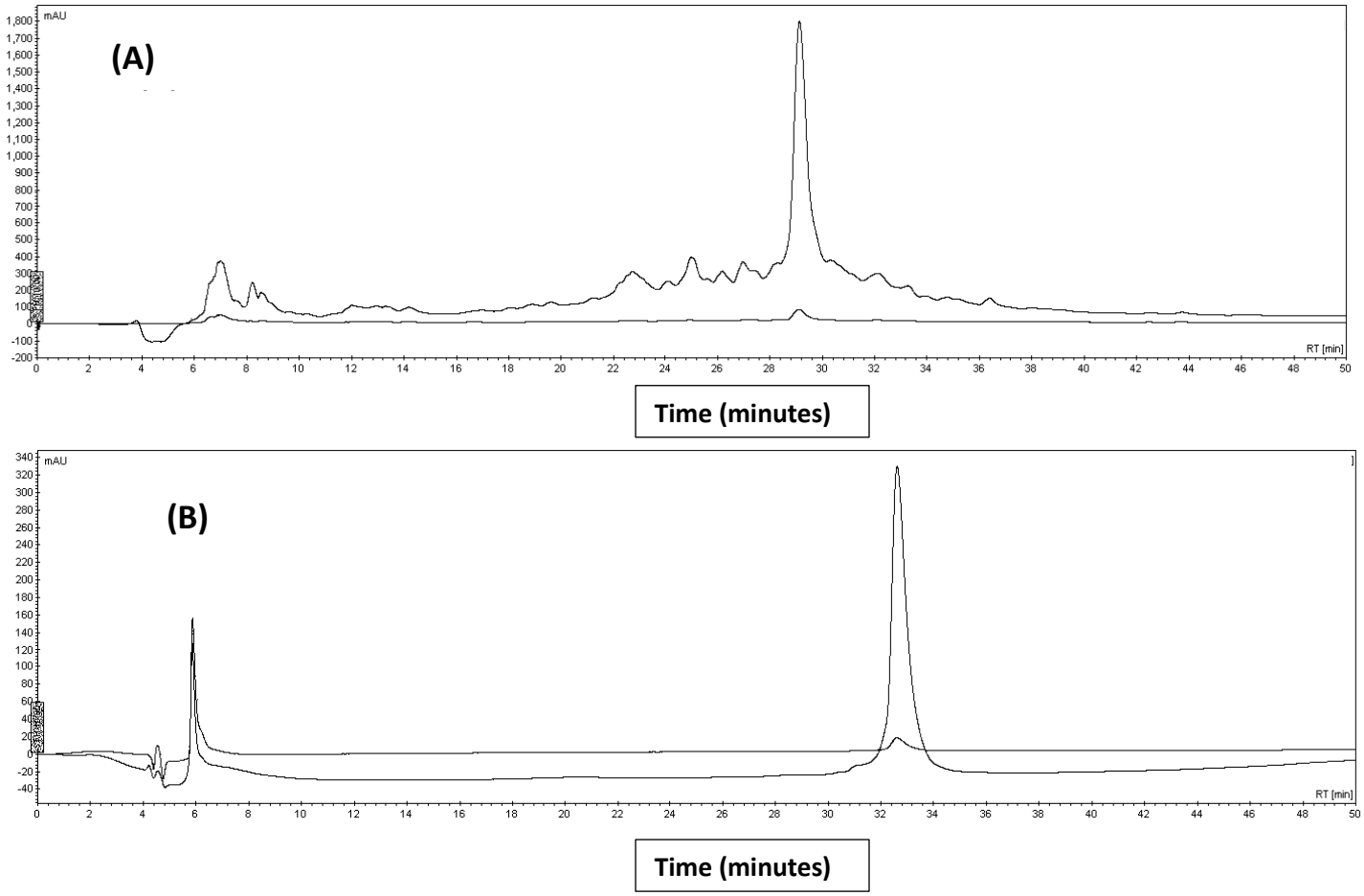

Figure 2.2.5: HPLC traces of S20Abu IAPP using an analytical C18 column. (A) Crude S20Abu IAPP (eluted at ~28 minutes), (B) Pure S20Abu IAPP (eluted at ~32 minutes) (A-B buffer gradient system: A: 100 % DDI H_2O&0.045 % HCl, B: 80% ACN & 0.45% HCl (v/v), gradient : 20-70 % B in 50 minutes).

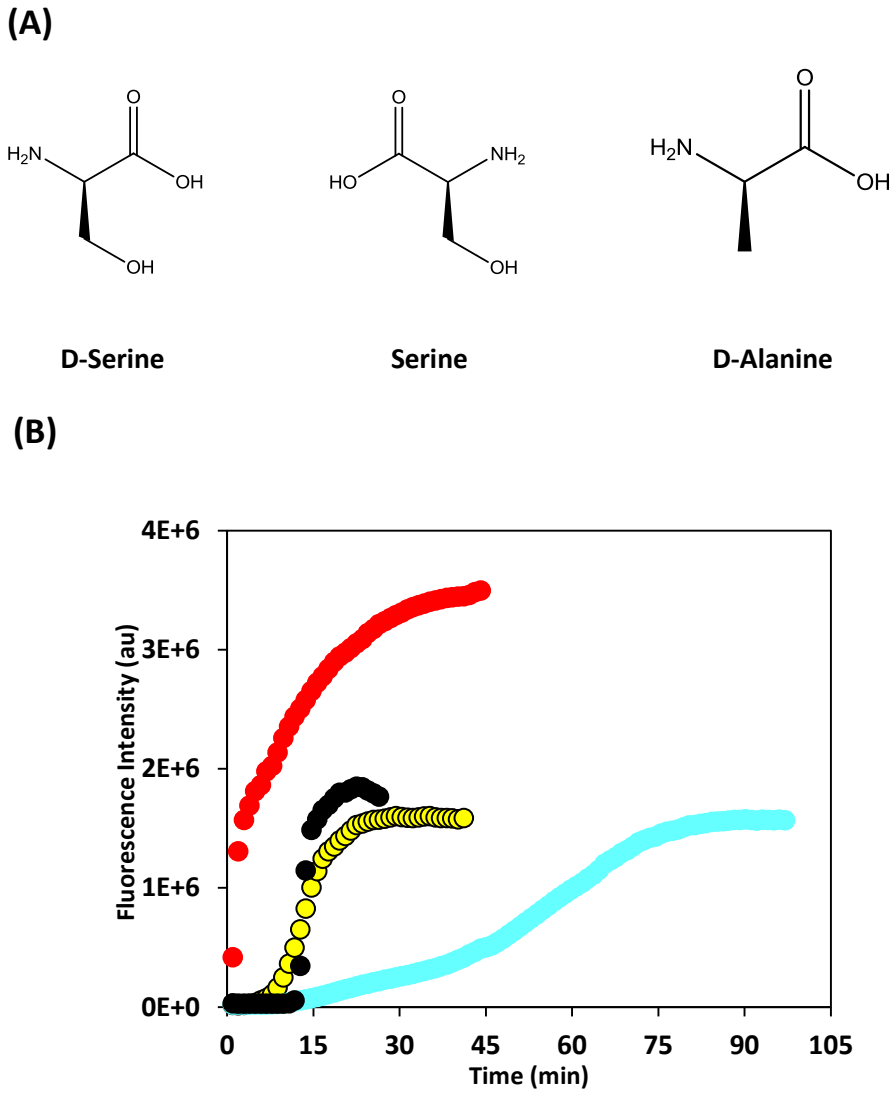

Figure 2.3: (A) Molecular structure of serine, D-serine, and D-alanine amino acid, (B) Kinetics of amyloid formation obtained from Thioflavin-T fluorescence dye binding assay in presence of 2% HFIP with constant stirring. Thioflavin-T assays were monitored in 20 mM Tris buffer (pH 7.4) at 25°C; wild type IAPP-black, S20G IAPP-red, S20d-S IAPP-yellow, and S20d-A IAPP-cyan colored.

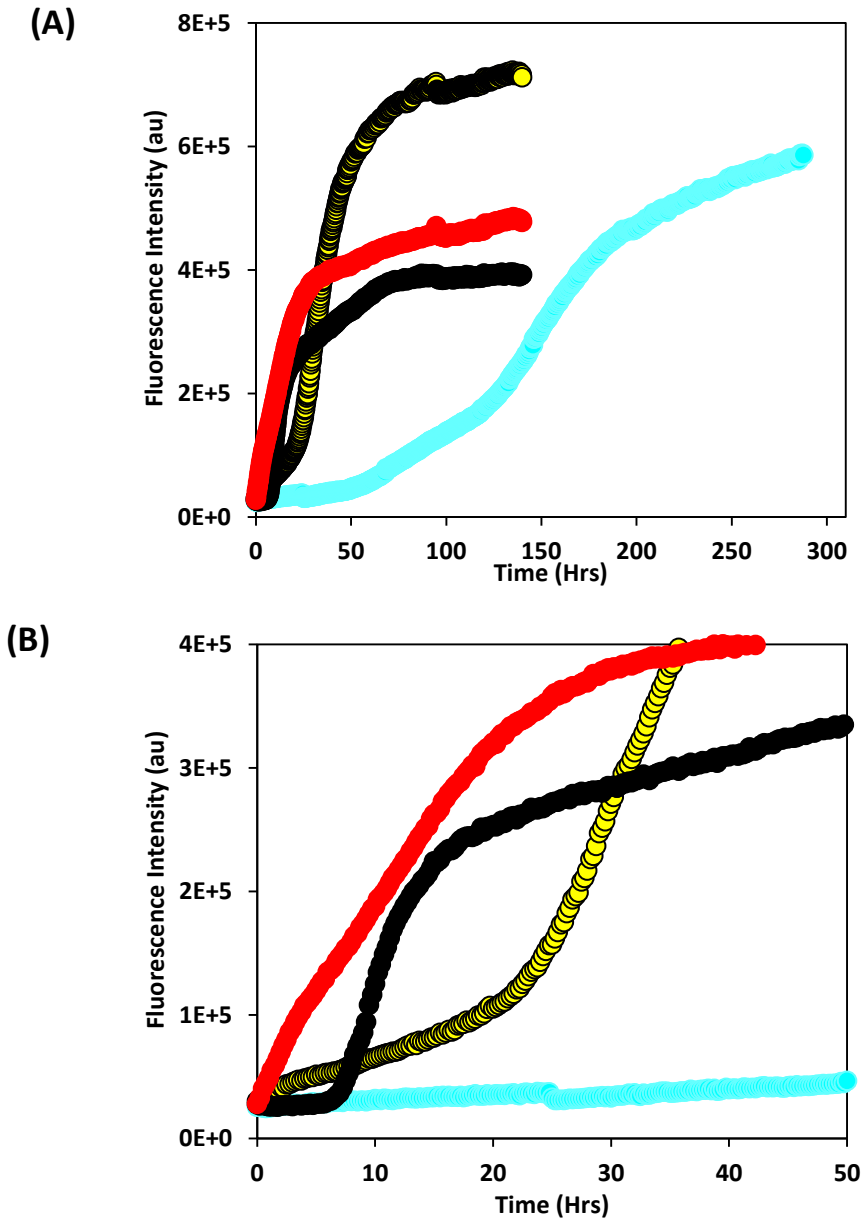

Figure 2.4: (A) Kinetics of amyloid formation obtained from Thioflavin-T fluorescence dye binding assay without HFIP and no stirring. Thioflavin-T assays were monitored in 20 mM Tris buffer (pH 7.4) at 25°C; wild type IAPP-black, S20G IAPP-red, S20d-S IAPP-yellow, and S20d-A IAPP-cyan colored. (B) Enlarged view of figure A.

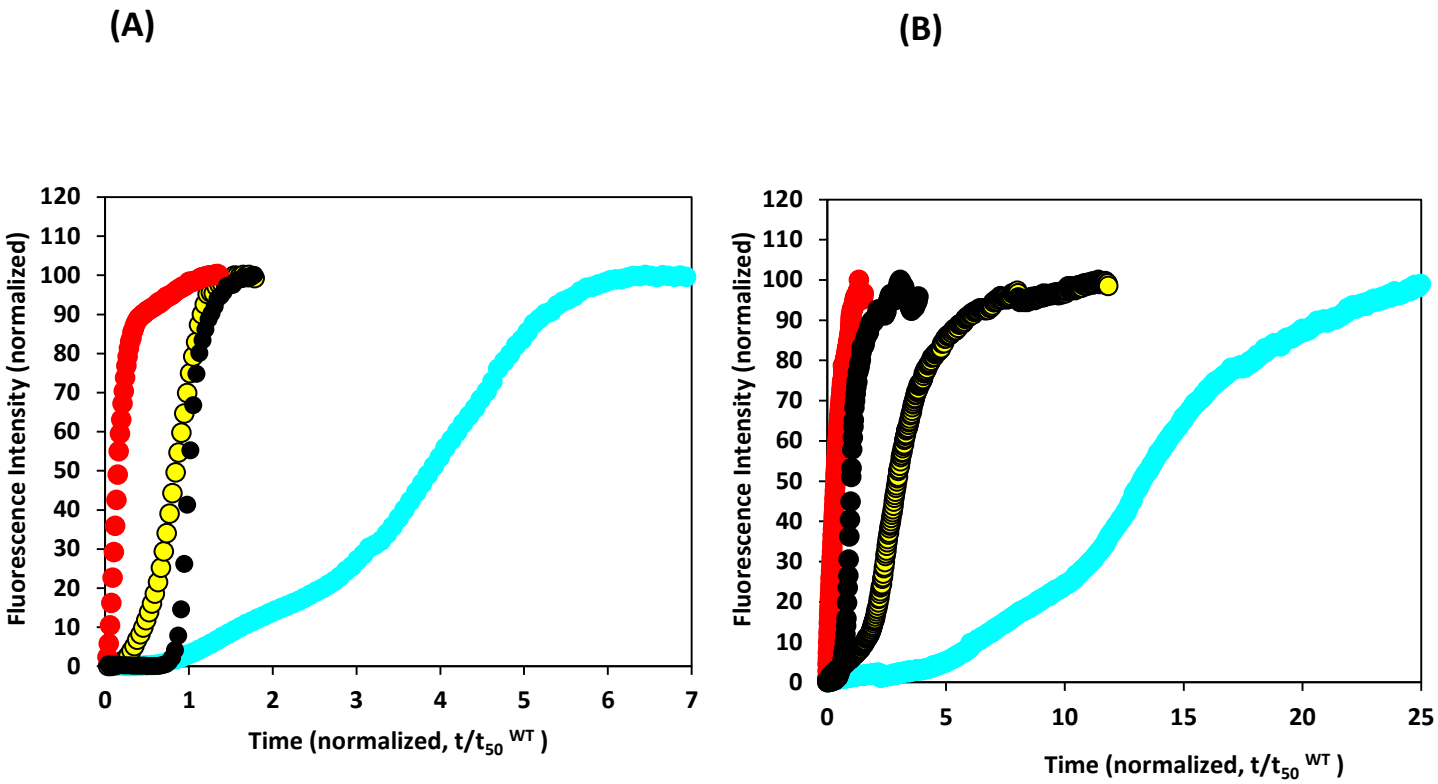

Figure 2.5: (A) The left panel shows the kinetics of amyloid formation obtained from Thioflavin-T fluorescence dye binding assay in presence of 2% HFIP with constant stirring, (B) The right panel shows the similar experiment results obtained in absence of HFIP without stirring experiment condition. The time axis is normalized to t_{50}^{wt} and fluorescence axis is normalized to final intensity of the peptide. Thioflavin-T assays were monitored in 20 mM Tris buffer (pH 7.4) at 25°C; wild type IAPP-black, S20G IAPP-red, S20d-S IAPP-yellow, and S20d-A IAPP-cyan colored.

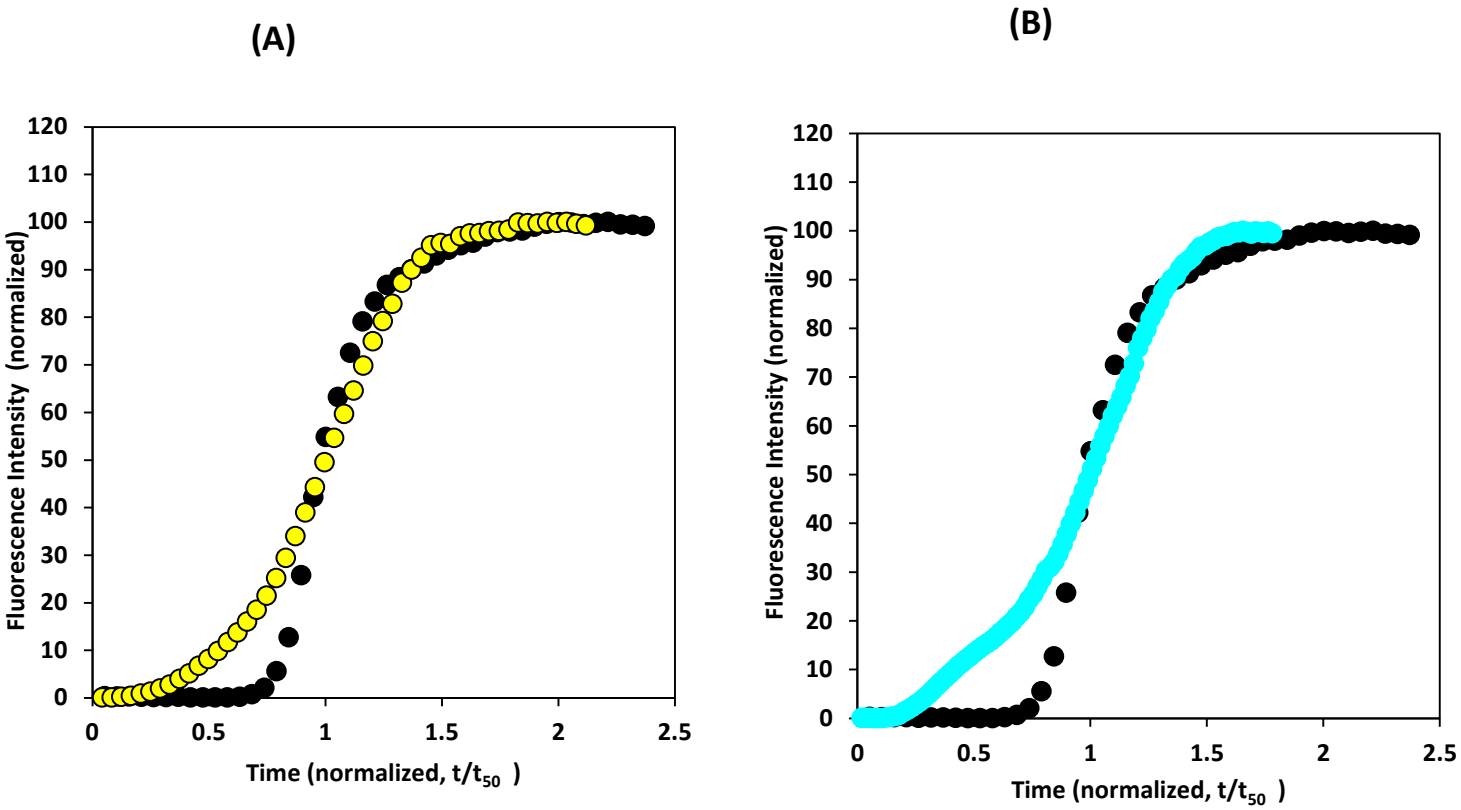

Figure 2.6: The kinetics of amyloid formation by S20d-S IAPP and S20d-A IAPP are different from WT IAPP. The time axis is normalized to t_{50} of own fibrils and fluorescence axis is normalized to final intensity of the peptide. Thioflavin-T assay were monitored in 20 mM Tris buffer (pH 7.4) at 25°C: (A) S20d-S IAPP (yellow) and WT IAPP (black), (B) S20d-A IAPP (cyan) and WT IAPP (black).

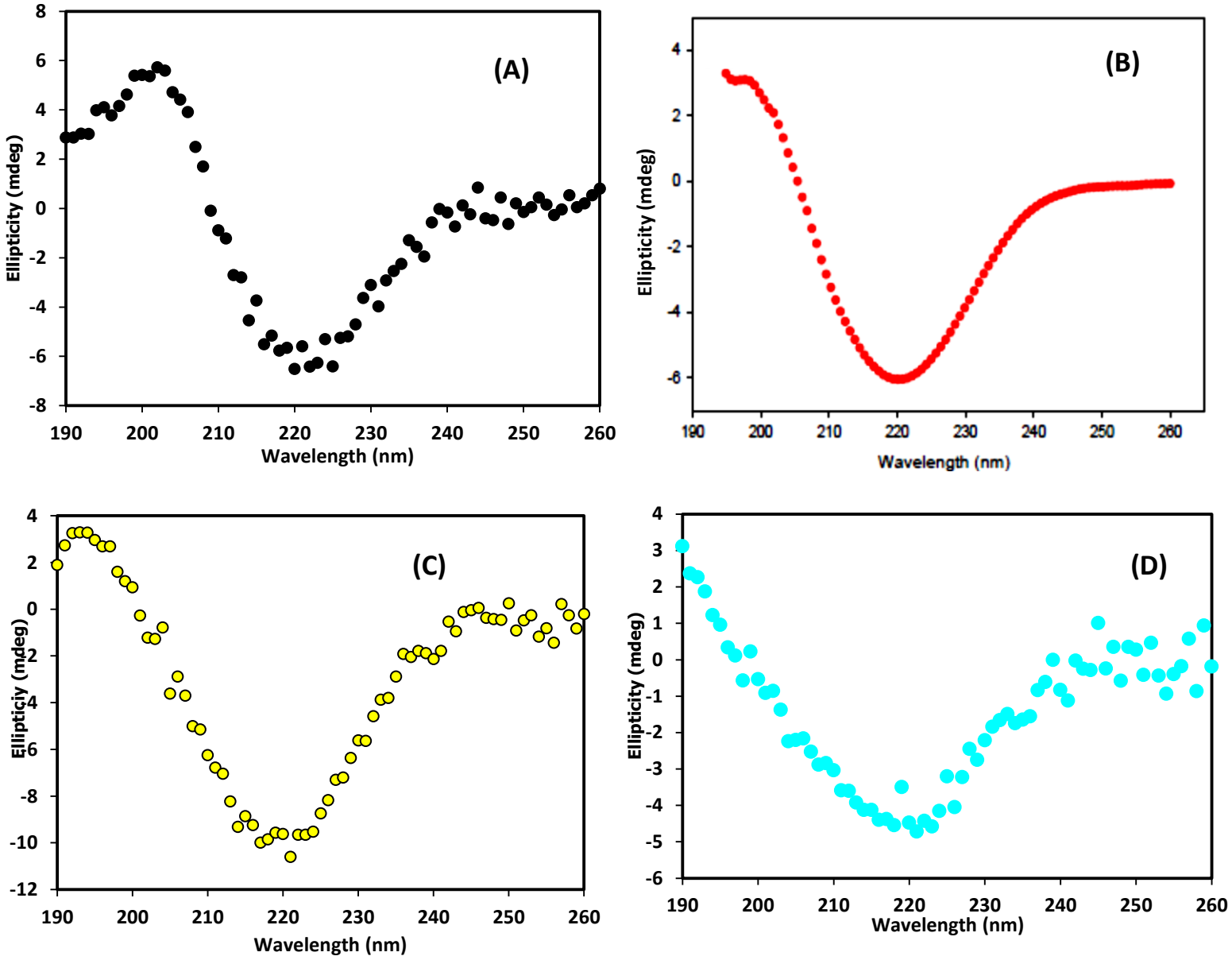

Figure 2.7: Circular dichroism (CD) spectra confirms the presence of β-sheet structure in (A) wild type IAPP fibrils (black), (B) S20G IAPP mutant fibrils (red) (S20G mutant figure is taken from Cao et al. JMB, 2012)(69), (C) S20d-S IAPP mutant fibrils (yellow), and (D) S20d-A IAPP mutant fibrils (cyan). Samples were collected at the end of each experiment conducted with 16 μM IAPP in 2% HFIP with continuous stirring in 20 mM Tris buffer, pH 7.4, at 25°C.

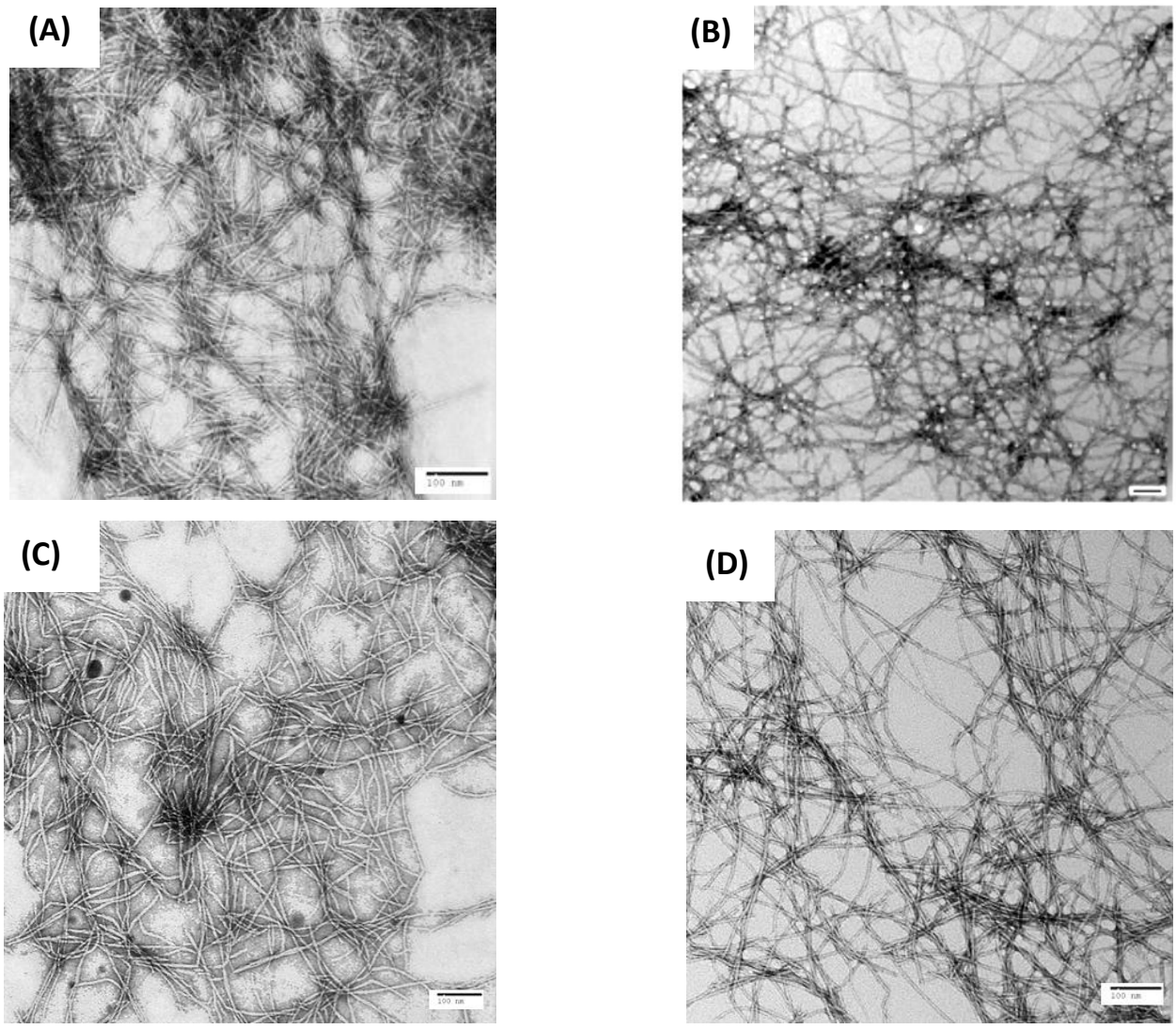

Figure 2.8: Transmission emission microscopy (TEM) images confirm amyloid fibril formation by (A) wild type IAPP, (B) S20G IAPP mutant (S20G mutant figure is taken from Cao et al. JMB, 2012) (69), (C) S20d-S IAPP mutant, and (D) S20d-A IAPP mutant. Samples were collected at the end of each experiment conducted with 16 μM IAPP in 2% HFIP with continuous stirring in 20 mM Tris buffer, pH 7.4, at 25°C. The scale bar in the images is 100 nm.

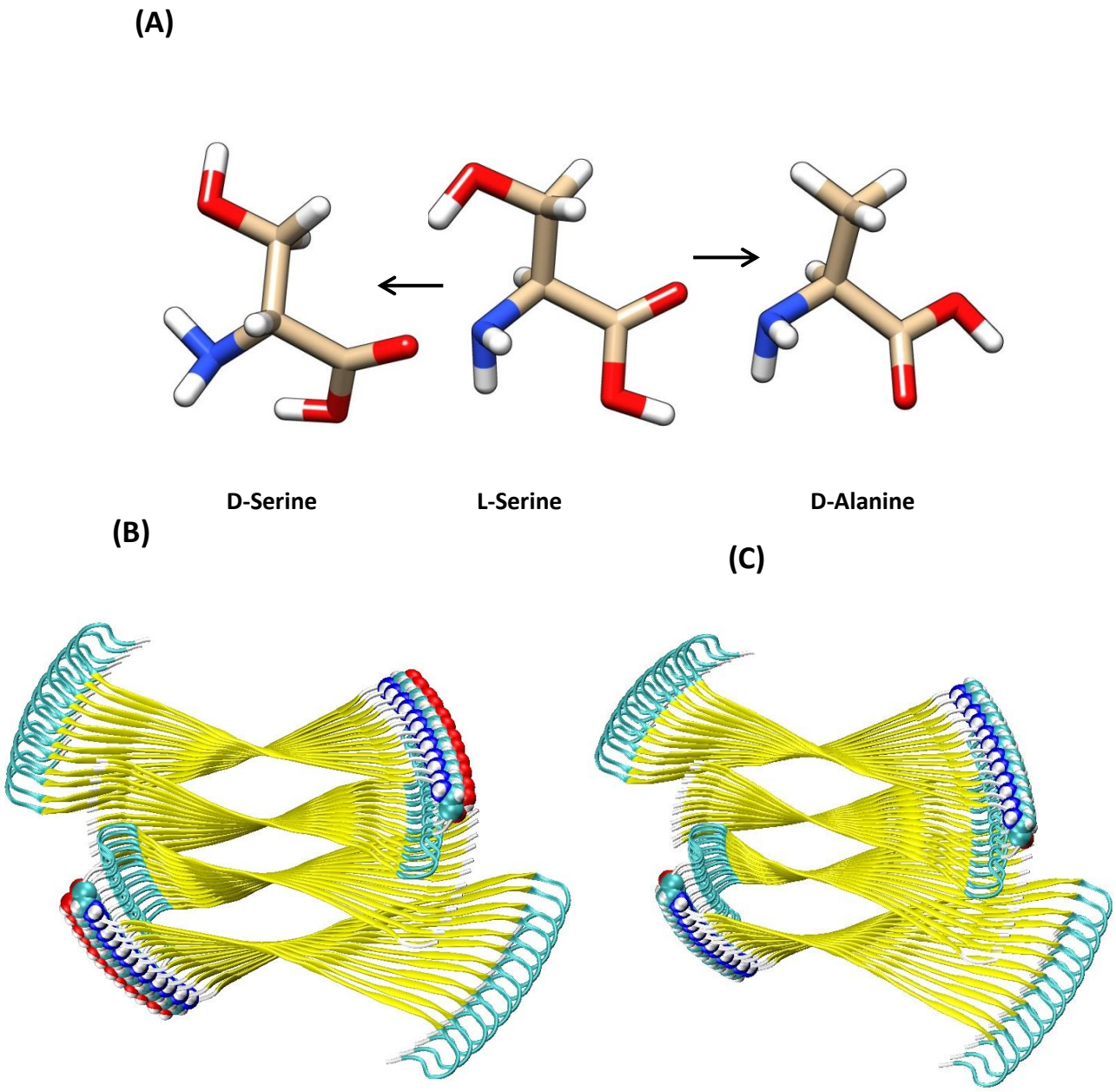

Figure 2.9: D-Serine and D-Alanine side chains make no steric clash in the amyloid fibril model of the UCLA group (10). (A) Three dimensional structure of D-Serine and D-Alanine which are used for mutation at position 20 of IAPP, (B, C) S20d-S IAPP (Figure B) and S20d-A IAPP (Figure C) mutant fibril structure built from Eisenberg et al. proposed "Steric zipper" structure model using Chimera (92, 126). Mutant residues are shown in space filling representation. D-Alanine and D-Serine are well fit in the position 20. There is no steric clash due to these residues.

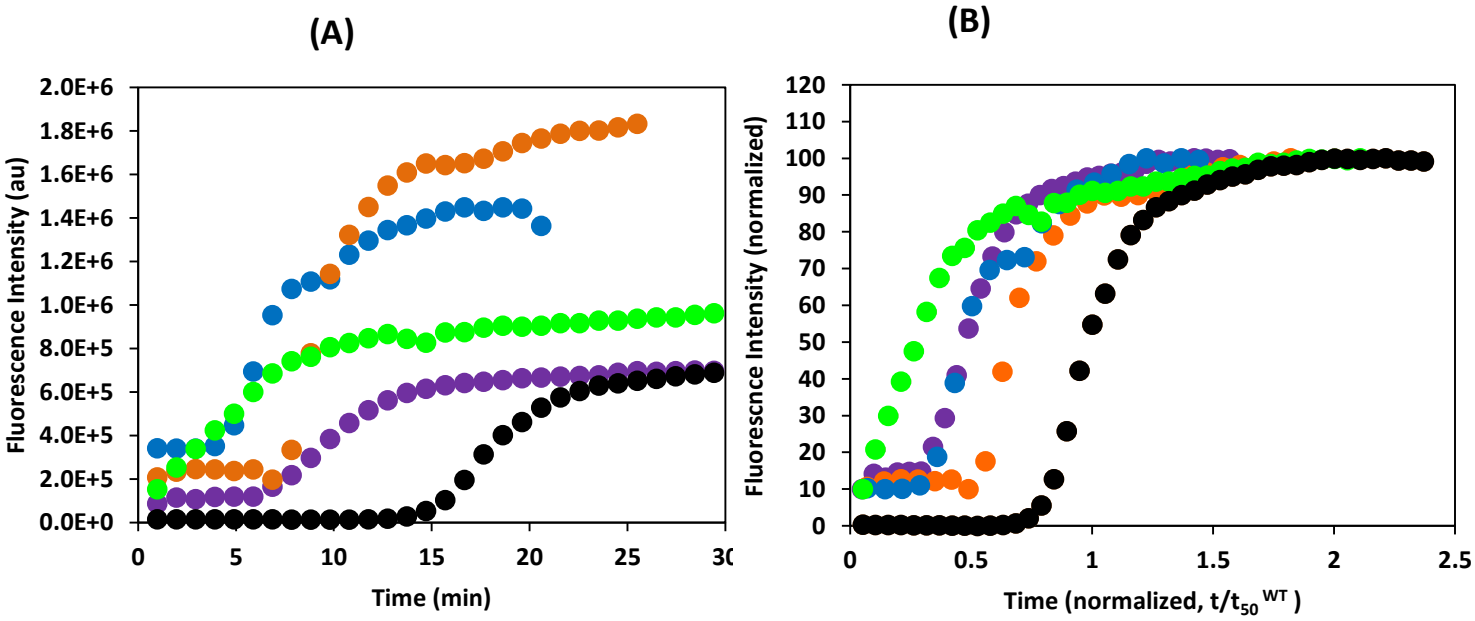

Figure 2.10: (A) Wild type IAPP can be seeded by both S20d-S IAPP fibrils and S20d-A IAPP fibrils. Thioflavin-T fluorescent assays: unseeded wild type-IAPP (black); wild type IAPP seeded by wild type IAPP fibrils (green), wild type IAPP seeded by S20G IAPP fibrils (blue), wild type IAPP seeded by S20d-S IAPP fibrils (purple), and wild type IAPP seeded by S20d-A IAPP fibrils (orange). (B) The time axis is normalized to t_{50}^{wt} (for an unseeded reaction) and fluorescence axis is normalized to final intensity of the kinetics. Thioflavin-T assay were monitored for 16 μM IAPP with 10% seed (monomer units) in 2 % HFIP in 20 mM Tris buffer (pH 7.4) with 32 μM Thioflavin T solution at 25°C with constant stirring.

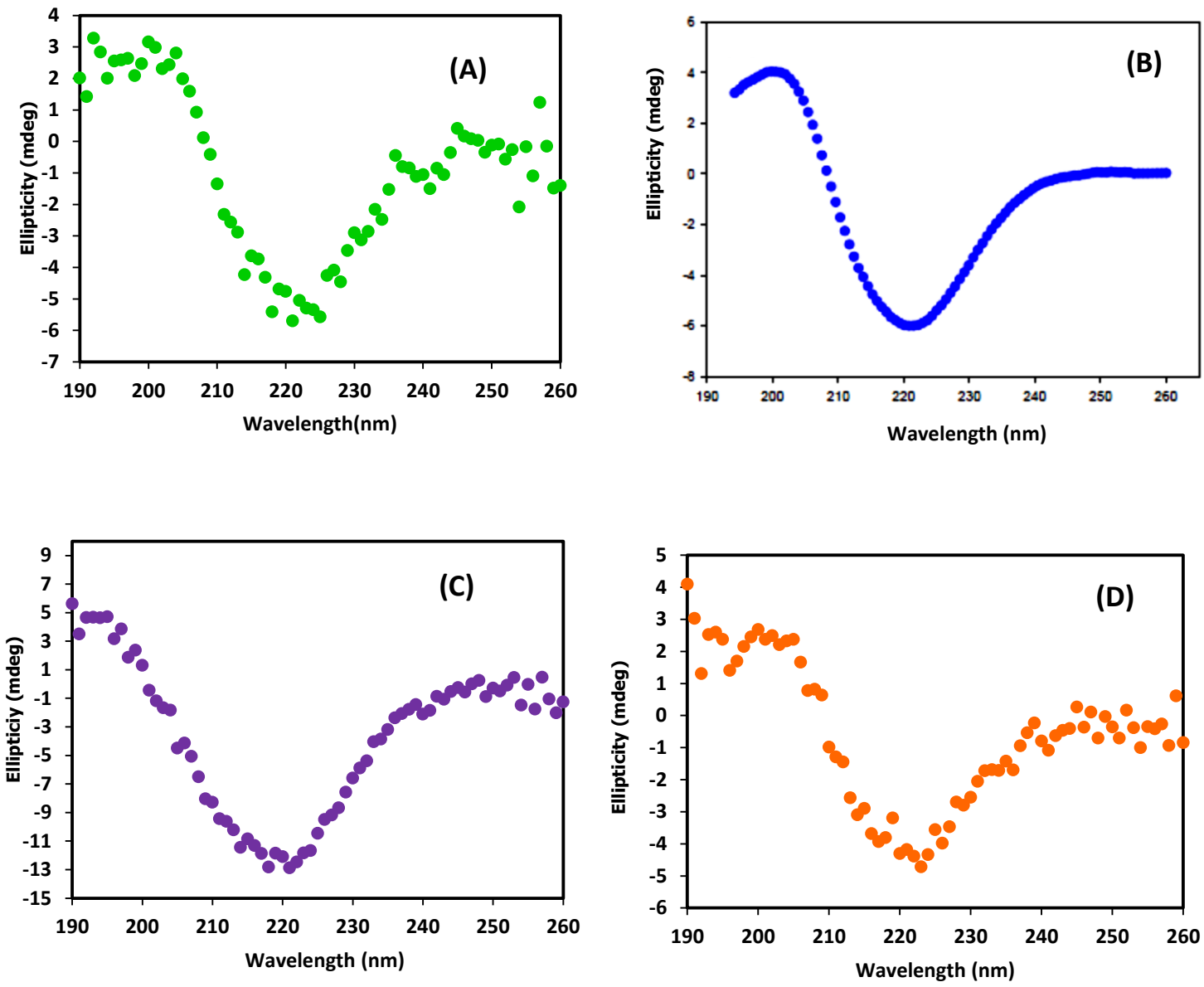

Figure 2.11: Circular dichroism (CD) spectra confirms the presence of β-sheet structure when wild type IAPP is seeded by: (A) wild type IAPP fibrils (green), (B) S20G IAPP mutant fibrils (blue) (S20G mutant figure is taken from Cao et al. JMB, 2012) (69), (C) S20d-S IAPP mutant fibrils (purple), and (D) S20d-A IAPP mutant fibrils (orange). CD scans were taken the end of seeding kinetic experiment.

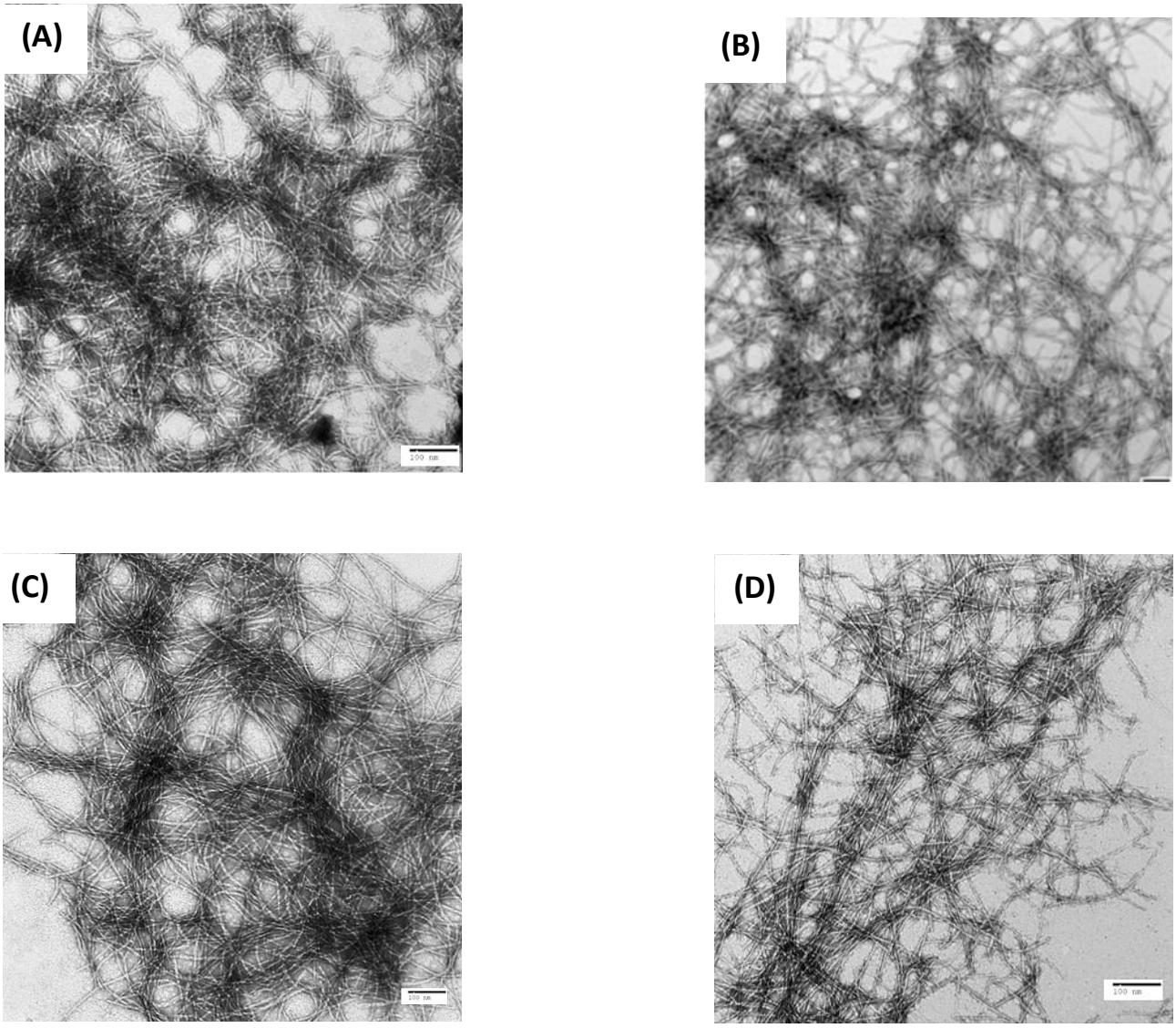

Figure 2.12: Transmission emission microscopy (TEM) images confirm amyloid fibril formation; when wild type IAPP is seeded by: (A) wild type IAPP fibrils , (B) S20G IAPP fibrils (S20G mutant figure is taken from Cao et al. JMB, 2012) (69), (C) S20d-S IAPP mutant fibrils, and (D) S20d-A IAPP mutant fibrils. Samples were collected at the end of each seeding kinetic experiment. The scale bar in the images is 100 nm.

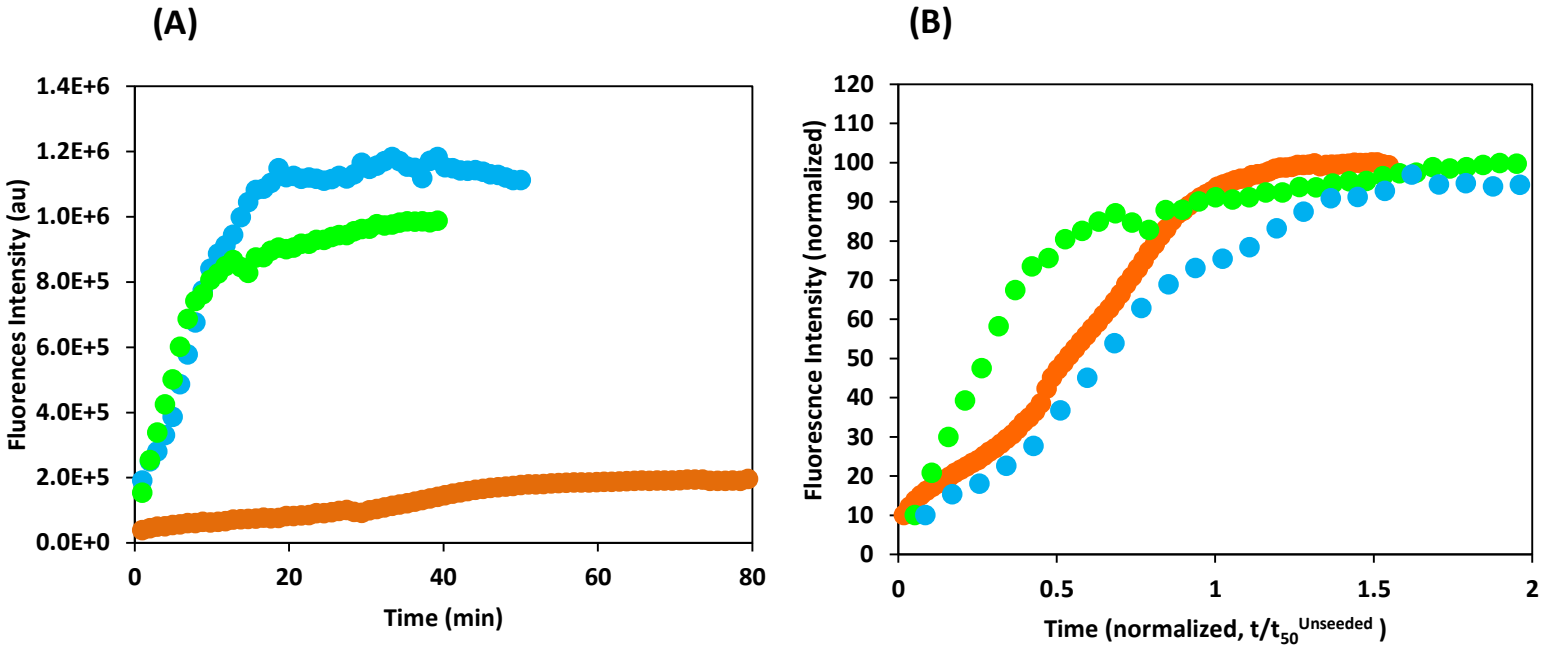

Figure 2.13: (A) Homologous seeding (each peptide is seeded by its own fibrils) kinetics of S20d-S IAPP and S20d-A IAPP are different from those of WT IAPP. Figure shows Thioflavin-T fluorescent assay results : wild type IAPP seeded by wild type IAPP fibrils (green), S20d-S IAPP was seeded by S20d-S IAPP fibrils (blue), S20d-A IAPP was seeded by S20d-A IAPP fibrils (orange). (B) The time axis is normalized to t_{50} of own kinetics and fluorescence axis is normalized to final intensity of the kinetics. Thioflavin-T assays were monitored for 16 μM IAPP with 10% seed (monomer units) in 2 % HFIP in 20 mM Tris buffer (pH 7.4) with 32 μM Thioflavin T solution at 25 °C with constant stirring.

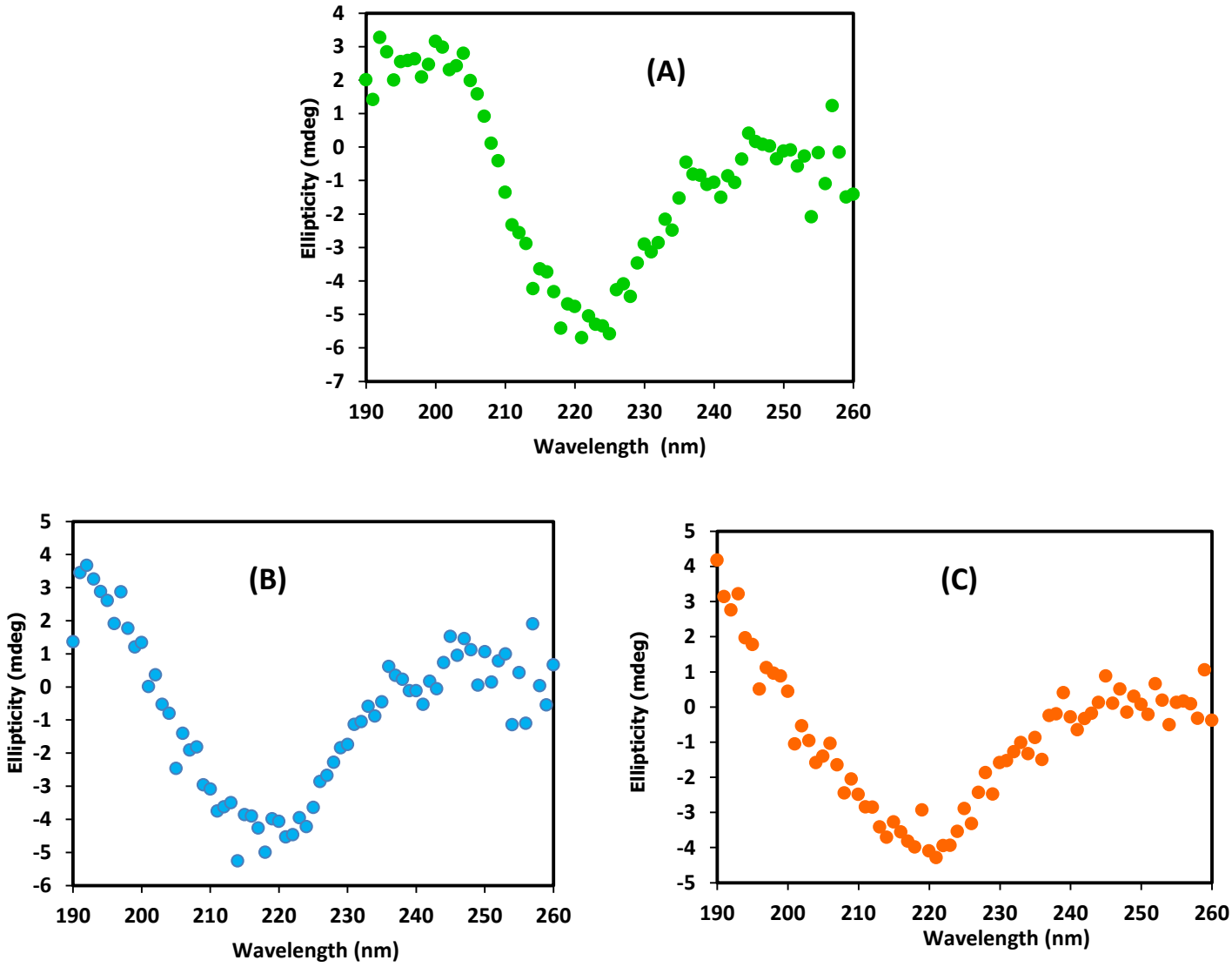

Figure 2.14: Circular dichroism (CD) spectra confirms the presence of β-sheet structure when; (A) wild type IAPP is seeded by wild type IAPP fibrils (green), (B) S20d-S IAPP mutant fibrils is seeded by S20d-S IAPP fibrils (blue), and (C) S20d-A IAPP mutant fibrils is seeded by S20d-A IAPP fibrils (orange). CD scans were taken the end of seeding kinetic experiments.

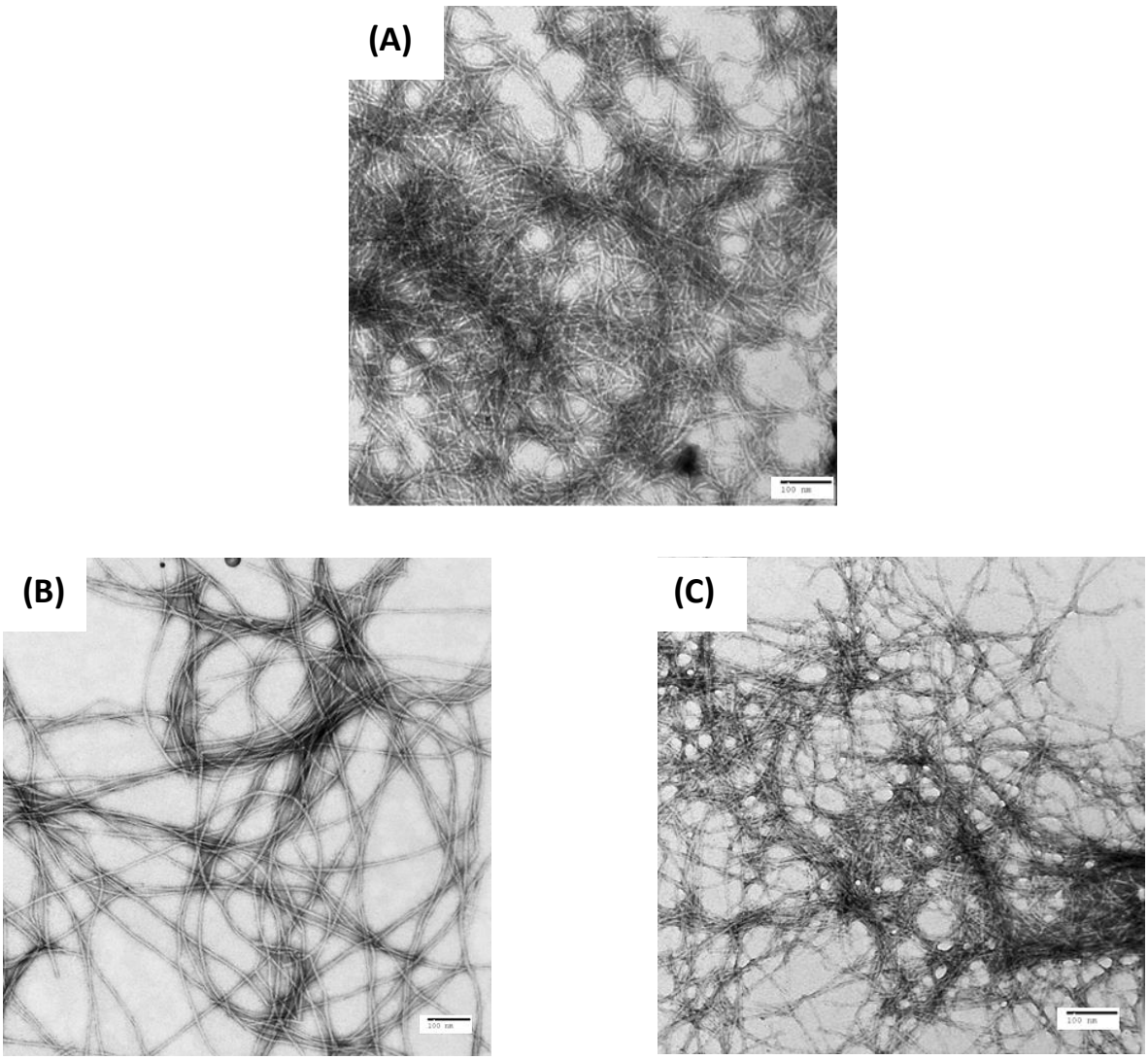

Figure 2.15: Transmission emission microscopy (TEM) images confirm amyloid fibril formation; (A) wild type IAPP is seeded by wild type IAPP fibrils , (B) S20d-S IAPP mutant fibrils is seeded by S20d-S IAPP fibrils, and (C) S20d-A IAPP mutant fibrils is seeded by S20d-A IAPP fibrils. Samples were collected at the end of each seeding kinetic experiments. The scale bar in the images is 100 nm.

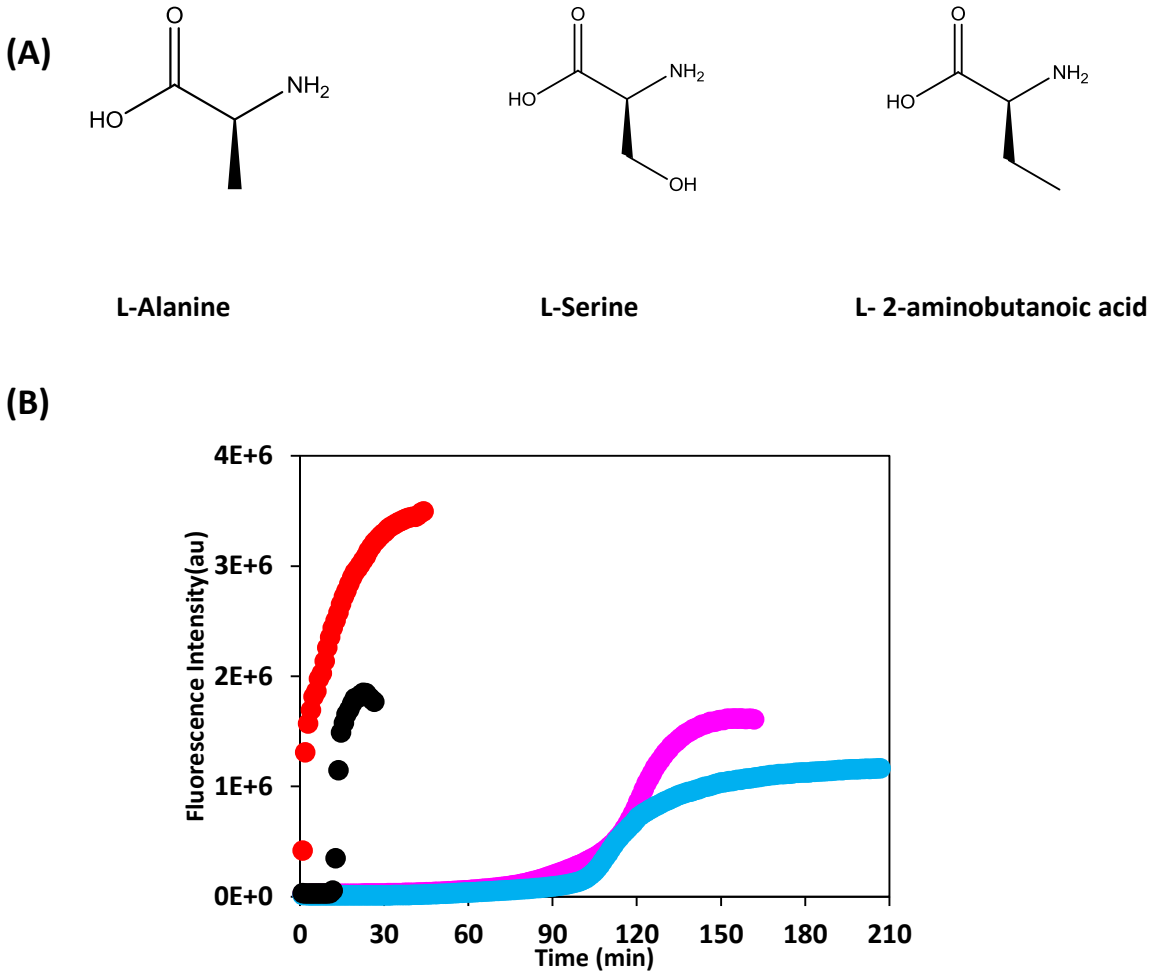

Figure 2.16: (A) Molecular structure of L-serine, L-alanine and L-2-aminobutanoic acid, (B) Kinetics of amyloid formation obtained from Thioflavin-T fluorescence dye binding assay in presence of 2% HFIP with constant stirring. Thioflavin-T assay were monitored in 20 mM Tris buffer (pH 7.4) at 25 °C; wild type IAPP-black, S20G IAPP-red, S20A IAPP-blue, and S20Abu IAPP-pink colored.

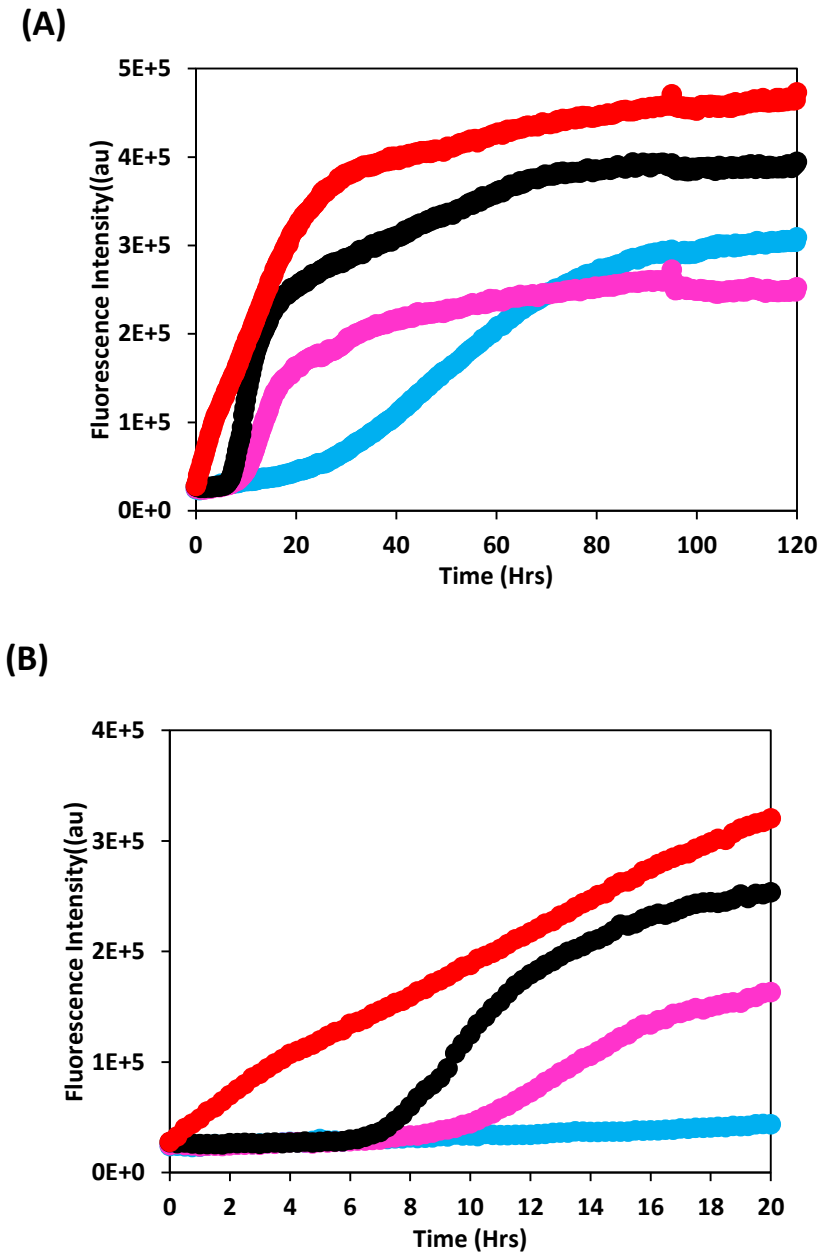

Figure 2.17: (A) Kinetics of amyloid formation obtained from Thioflavin-T fluorescence dye binding assay without HFIP and no stirring. Thioflavin-T assay were monitored in 20 mM Tris buffer (pH 7.4) at 25 °C; wild type IAPP-black, S20G IAPP-red, S20A IAPP-blue, and S20Abu IAPP-pink colored. (B) Enlarged view of figure A.

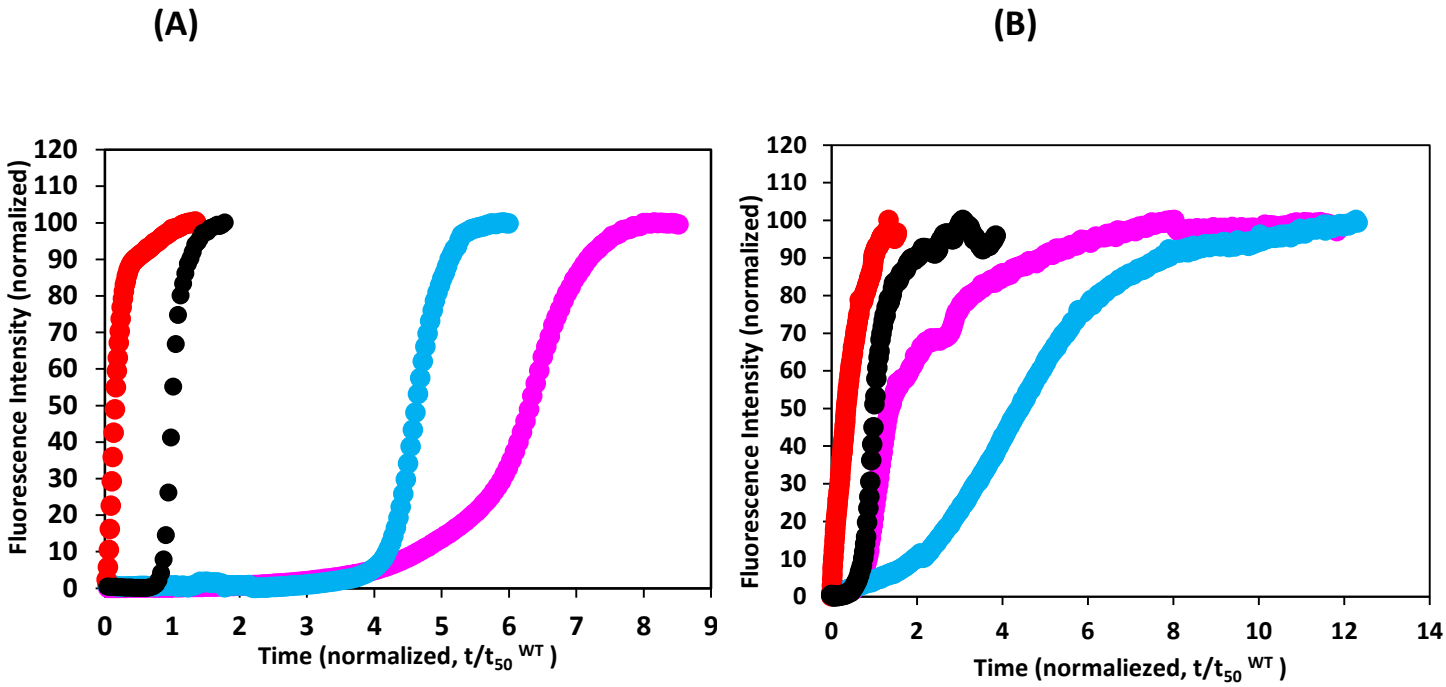

Figure 2.18: Relief of steric clashes or unfavorable hydrogen bond interactions are not the reason for rapid amyloid formation by S20G IAPP. (A) The left panel shows the kinetics of amyloid formation obtained from Thioflavin-T fluorescence dye binding assay in presence of 2% HFIP with constant stirring, (B) The right panel shows the similar experiment results obtained in absence of HFIP without stirring experiment condition. The time axis is normalized to t_{50}^{wt} and fluorescence axis is normalized to final intensity of the peptide. Thioflavin-T assay were monitored in 20 mM Tris buffer (pH 7.4) at 25 °C; wild type IAPP-black, S20G IAPP-red, S20A IAPP-blue, and S20Abu IAPP-pink colored.

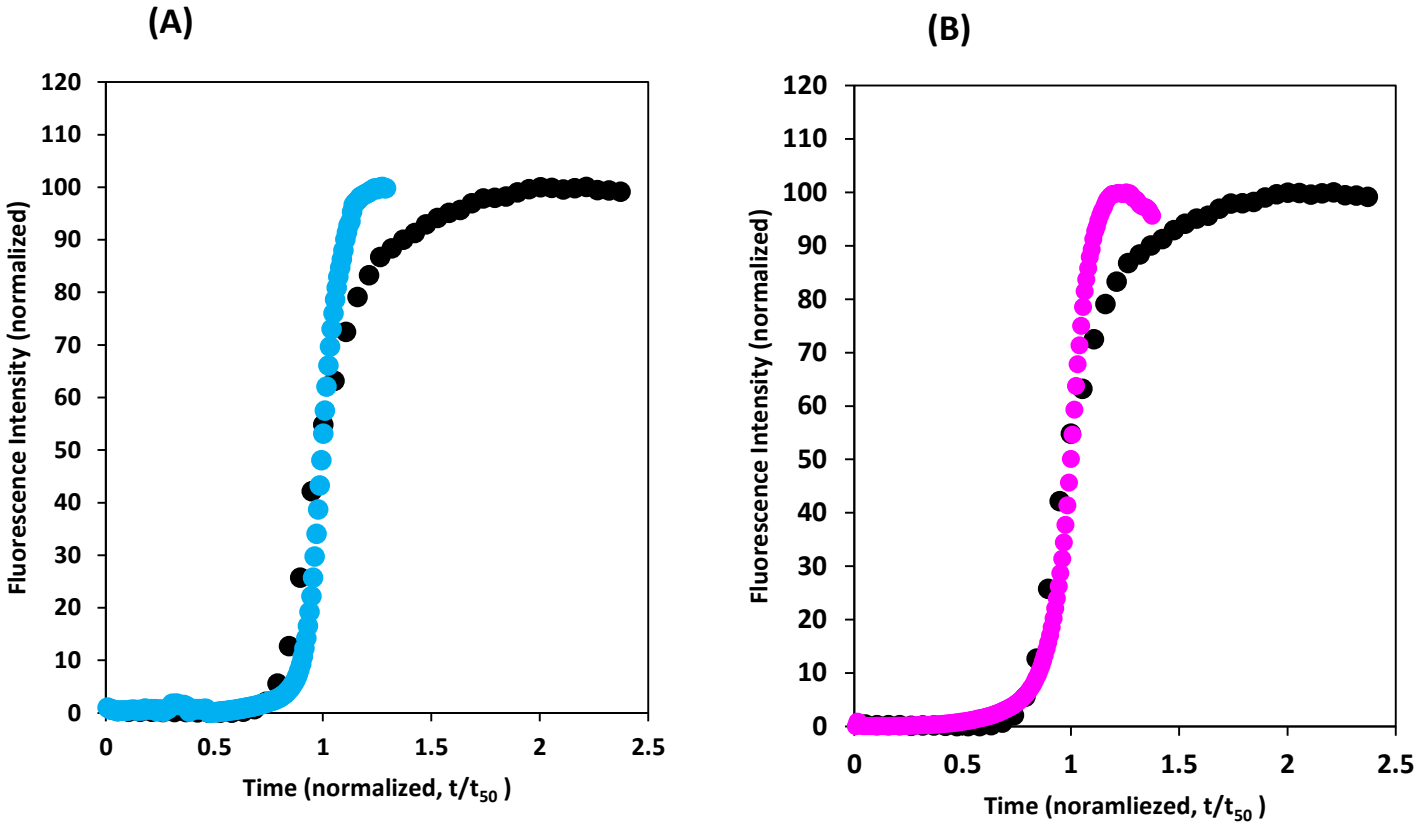

Figure 2.19: S20AbuIAPP and S20A IAPP show similar kinetic profile as WT IAPP. The time axis is normalized to t_{50} of each peptide and the fluorescence axis is normalized to final intensity of the peptide. Thioflavin-T assay were monitored in 20 mM Tris buffer (pH 7.4) at 25 °C: (A) S20A IAPP (blue) and WT IAPP (black)), (B) S20AbuIAPP (pink) and WT IAPP (black).

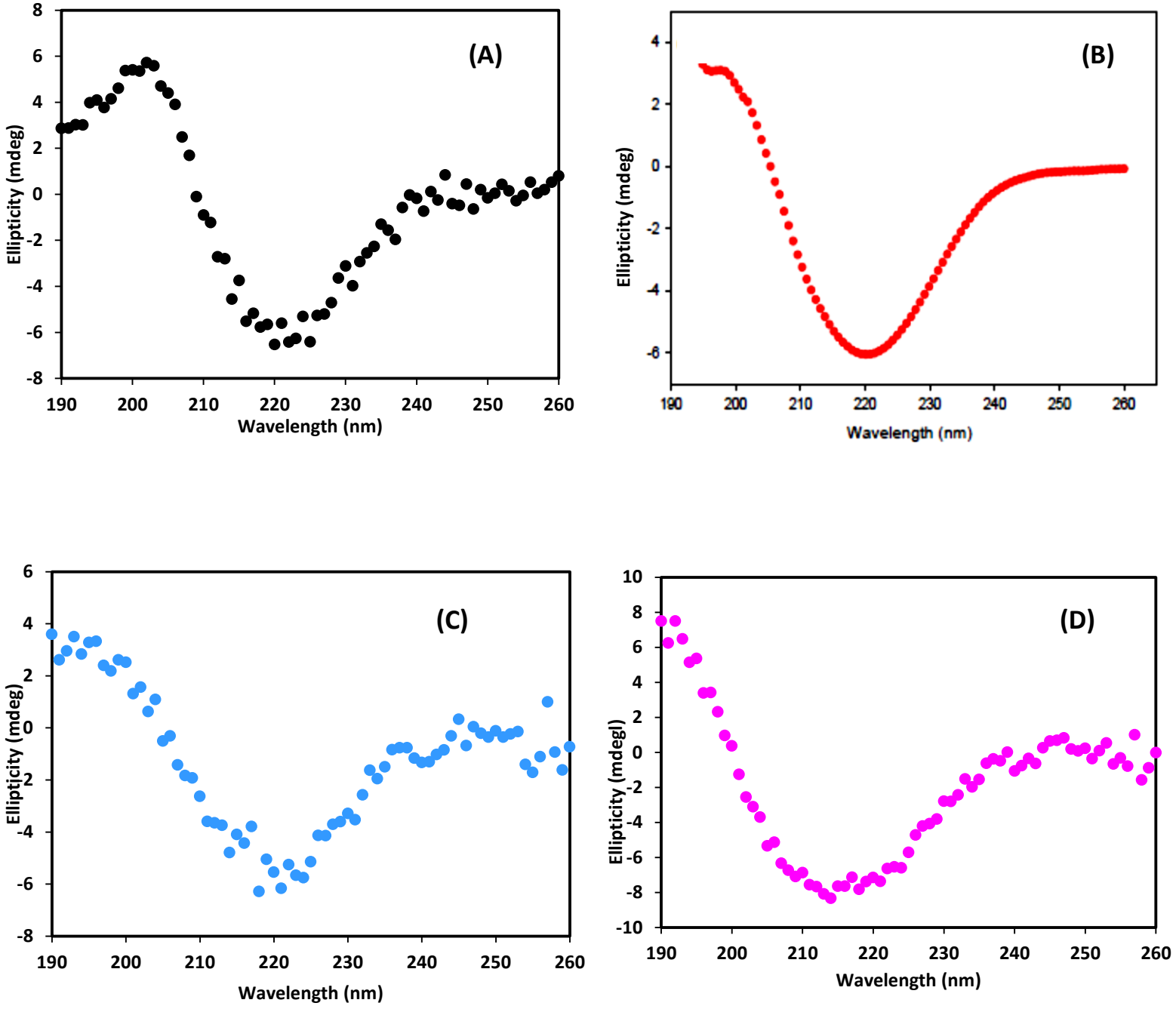

Figure 2.20: Circular dichroism (CD) spectra confirms the presence of β-sheet structure in (A) wild type IAPP fibrils (black), (B) S20G IAPP mutant fibrils (red) (S20G mutant figure is taken from Cao et al. JMB, 2012) (69),, (C) S20A IAPP mutant fibrils (blue), and (D) S20Abu IAPP mutant fibrils (pink). Samples were collected at the end of each experiment conducted with 16 μM IAPP in 2% HFIP with continuous stirring in 20 mM Tris buffer, pH 7.4, at 25°C.

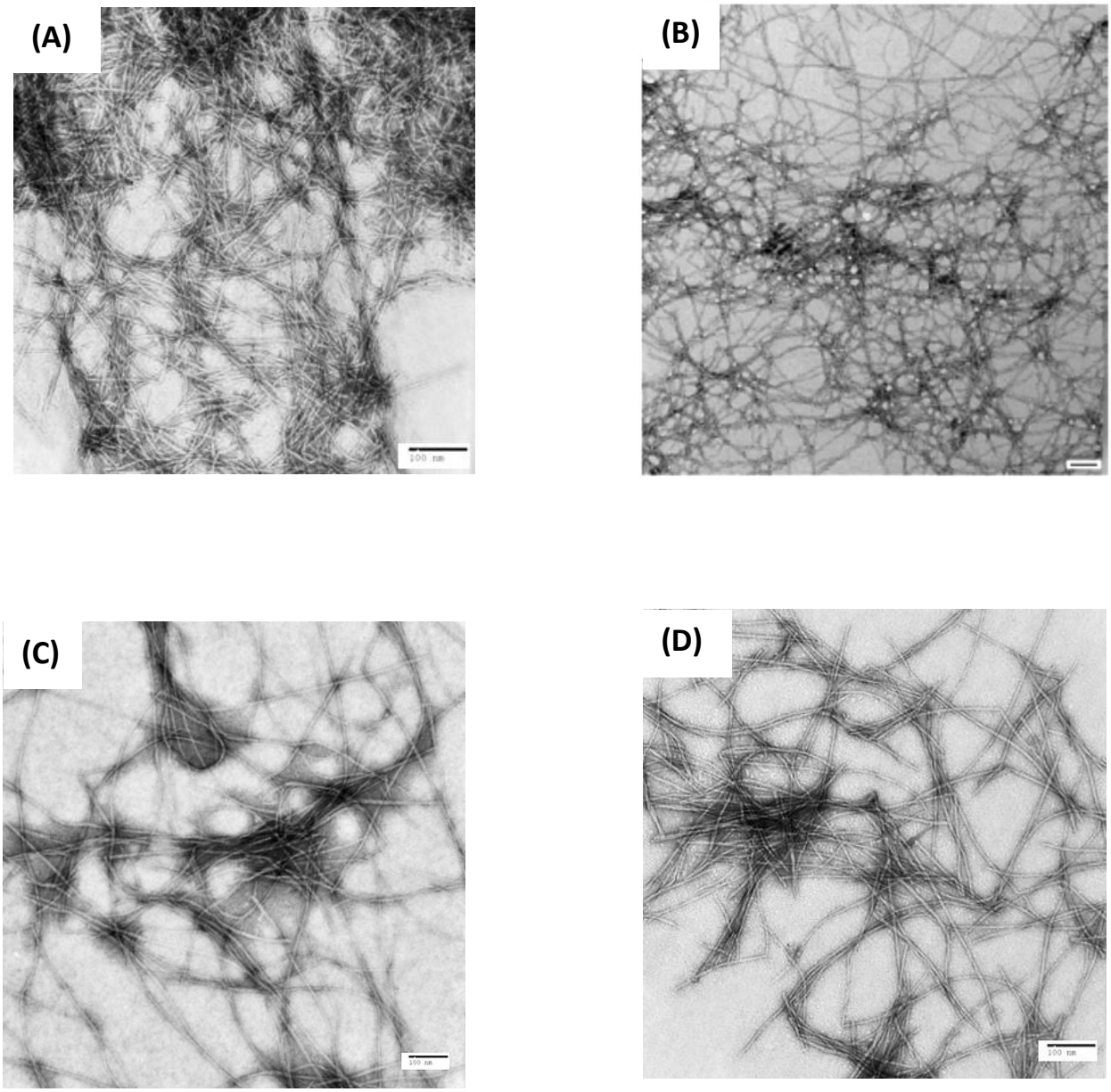

Figure 2.21: Transmission emission microscopy (TEM) images confirm amyloid fibril formation by (A) wild type IAPP, (B) S20G IAPP mutant (S20G mutant figure is taken from Cao et al. JMB, 2012) (69), (C) S20A IAPP mutant, and (D) S20Abu IAPP mutant. Samples were collected at the end of each experiment conducted with 16 μM IAPP in 2% HFIP with continuous stirring in 20 mM Tris buffer, pH 7.4, at 25°C. The scale bar in the images is 100 nm.

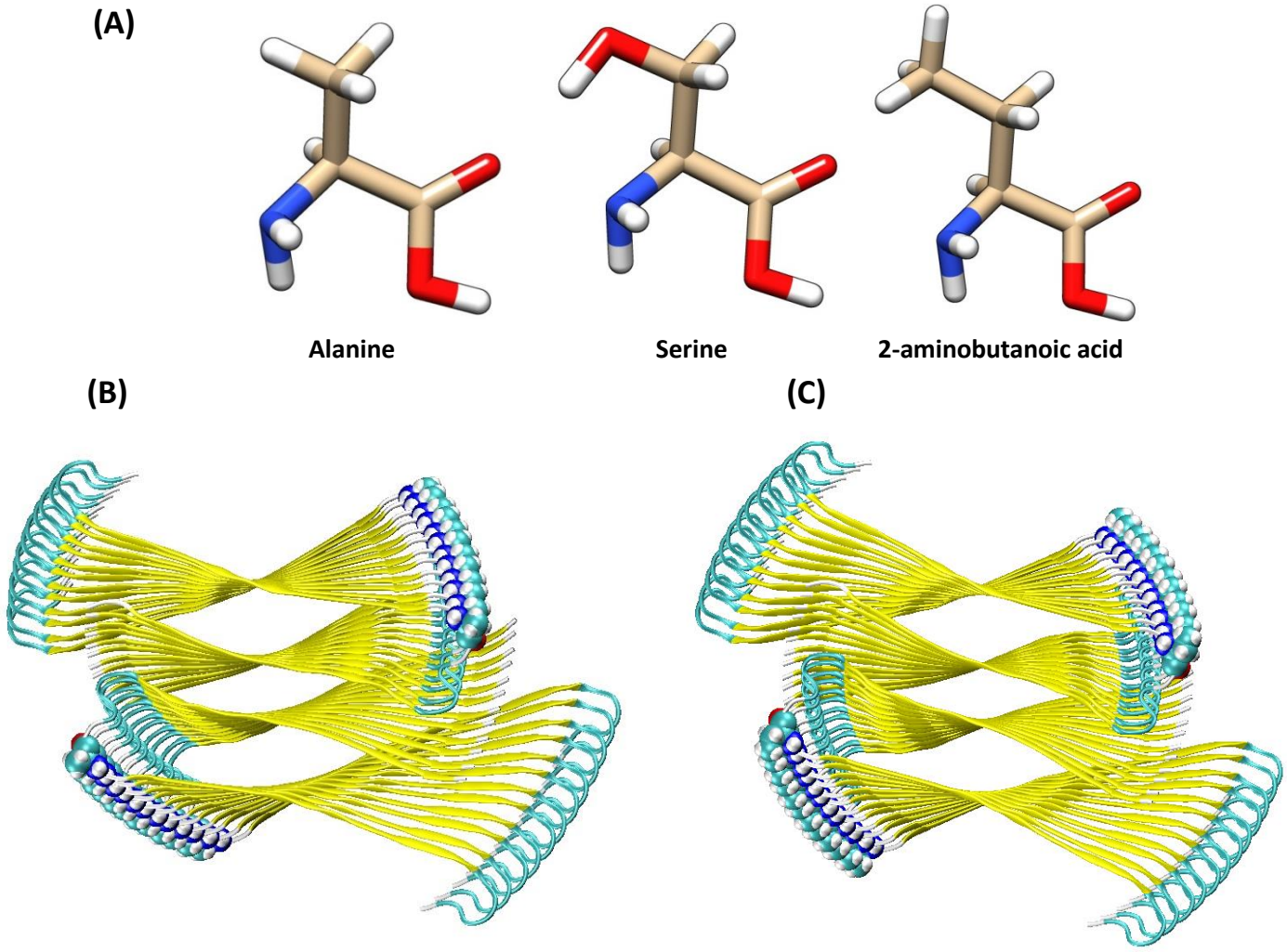

Figure 2.22: The alanine and 2-aminobutanoic acid side chains make no steric clashes in the IAPP amyloid fibril model. (A) Three dimensional structure of alanine and 2-aminobutanoic acid (B, C) S20A IAPP (Figure B) and S20Abu IAPP (Figure C) mutant fibril structure built from Eisenberg et al. proposed "Steric zipper" structure model using Chimera (92,126). Mutant residues are shown in space filling representation. D-Alanine and D-Serine are well fit in the position 20. There is no steric clash in the residues.

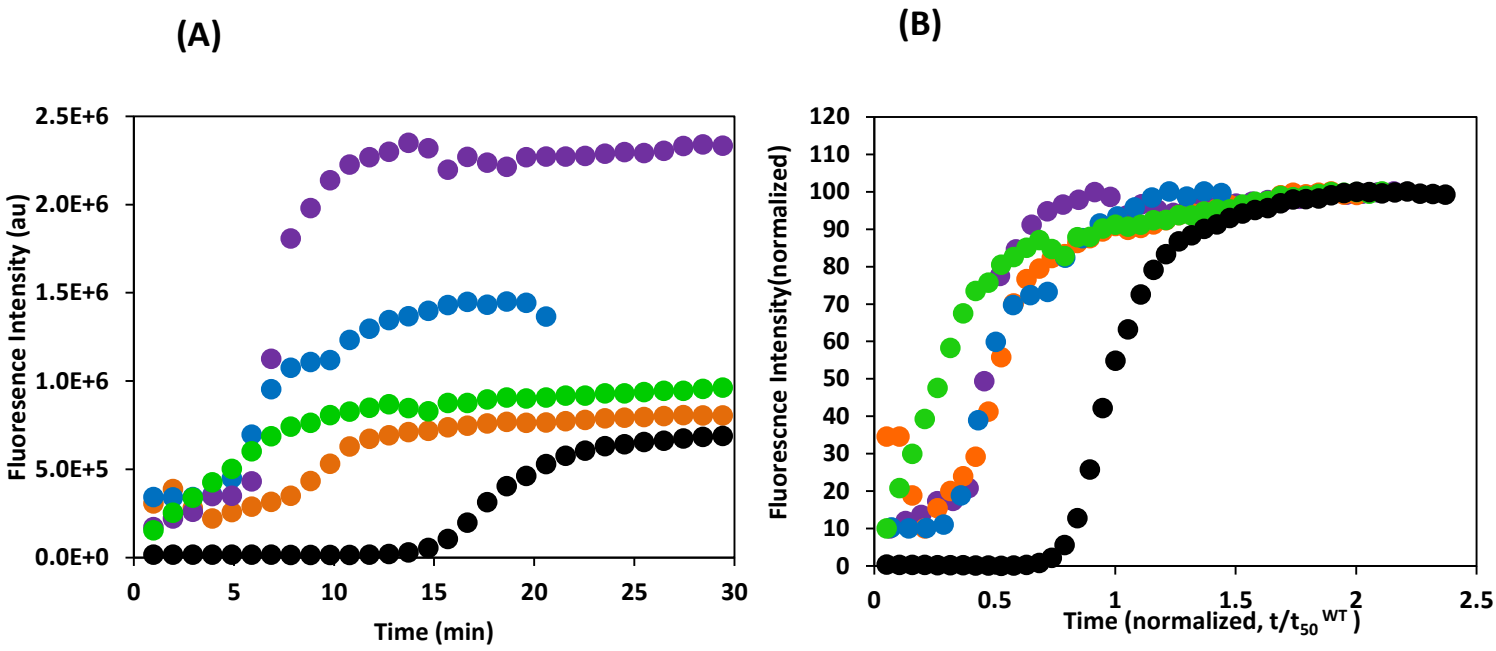

Figure 2.23: (A) Wild Type IAPP can be seeded by both S20A IAPP fibrils and S20Abu IAPP fibrils. Figure shows Thioflavin-T fluorescent assay results : unseeded wild type-IAPP (black); wild type IAPP was seeded by wild type IAPP fibrils (green), wild type IAPP was seeded by S20G IAPP fibrils (blue), wild type IAPP was seeded by S20A IAPP fibrils (orange), and wild type IAPP was seeded by S20Abu IAPP fibrils (purple). (B) The time axis is normalized to t_{50}^{wt} and fluorescence axis is normalized to the final fluorescent intensity. Experiments were conducted with 16 μM IAPP with 10% seed (monomer units) in 2% HFIP in 20 mM Tris buffer (pH 7.4) with 32 μM Thioflavin T solution at 25°C with constant stirring.

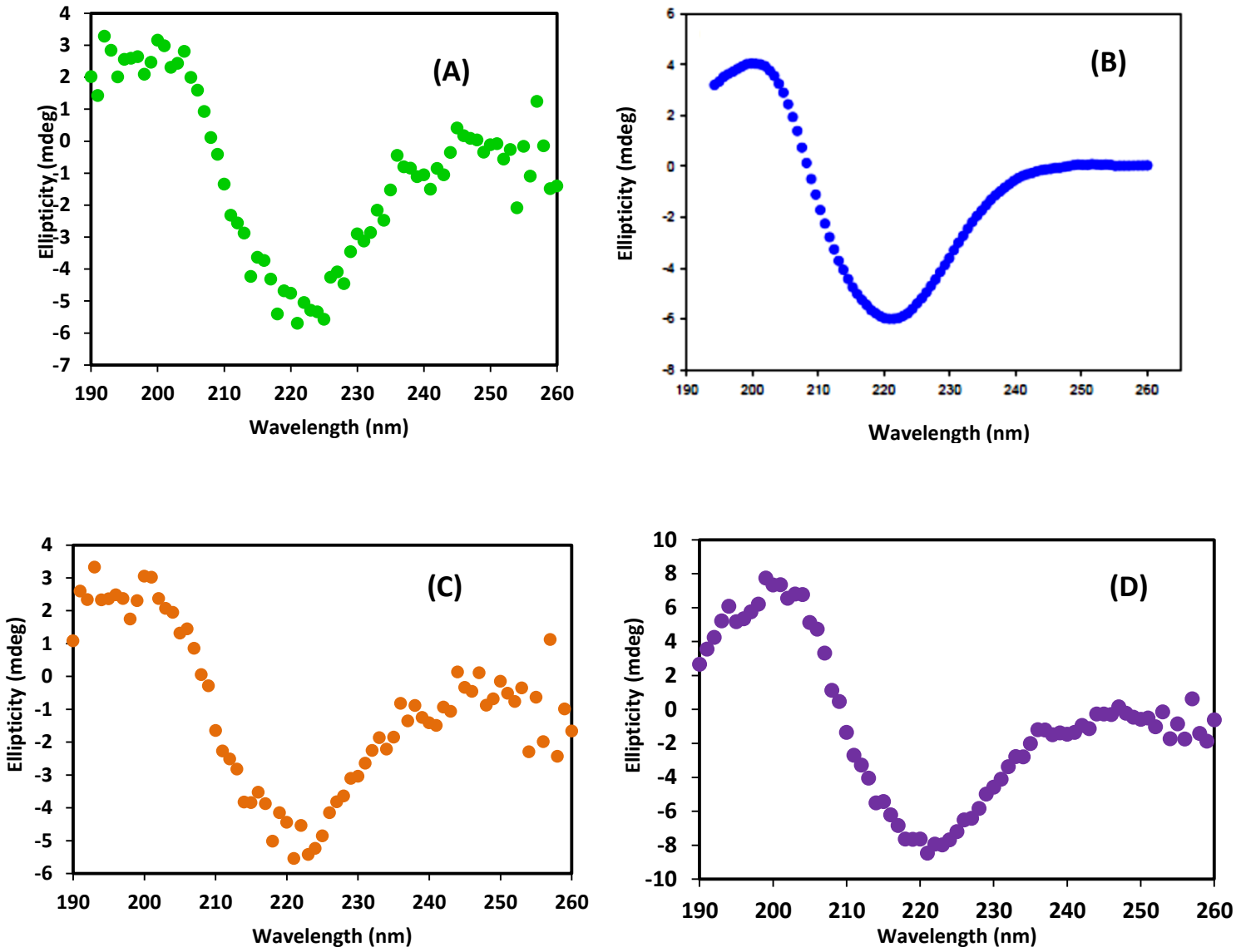

Figure 2.24: Circular dichroism (CD) spectra confirm the presence of β-sheet structure when wild type IAPP is seeded by: (A) wild type IAPP fibrils (green), (B) S20G IAPP mutant fibrils (blue) (S20G mutant figure is taken from Cao et al. JMB, 2012) (69), (C) S20A IAPP fibrils(purple) and (C) S20Abu IAPP mutant fibrils (orange). CD scans were taken at the end of seeding kinetic experiments.

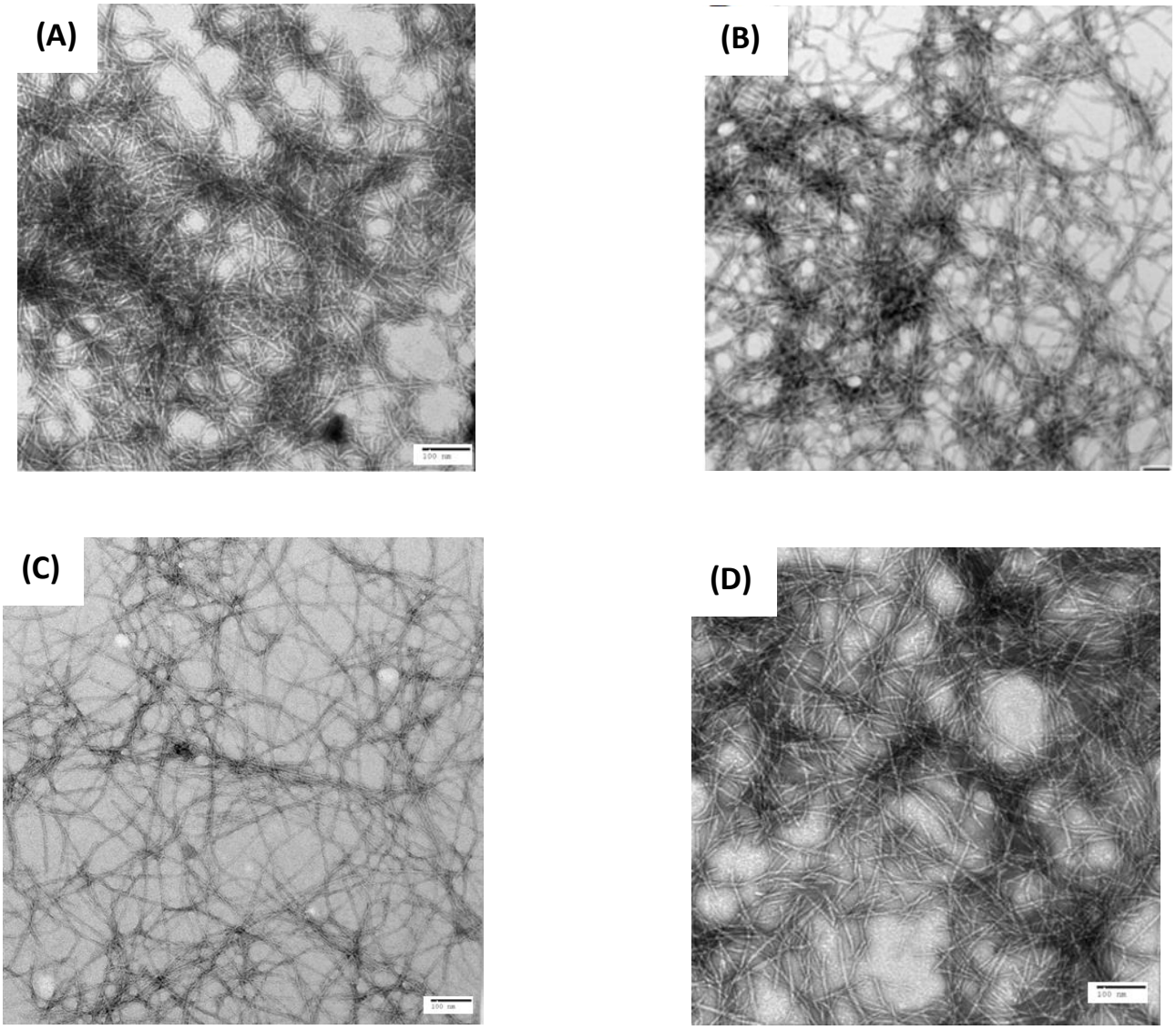

Figure 2.25: Transmission emission microscopy (TEM) images confirm amyloid fibril formation and when wild type IAPP is seeded by: (A) wild type IAPP fibrils, (B) S20G IAPP fibrils, (S20G mutant figure is taken from Cao et al. JMB, 2012) (69), (C) S20A IAPP fibrils, and (D) S20Abu IAPP fibrils. Samples were collected at the end of each seeding kinetic experiments. The scale bar in the images is 100 nm.

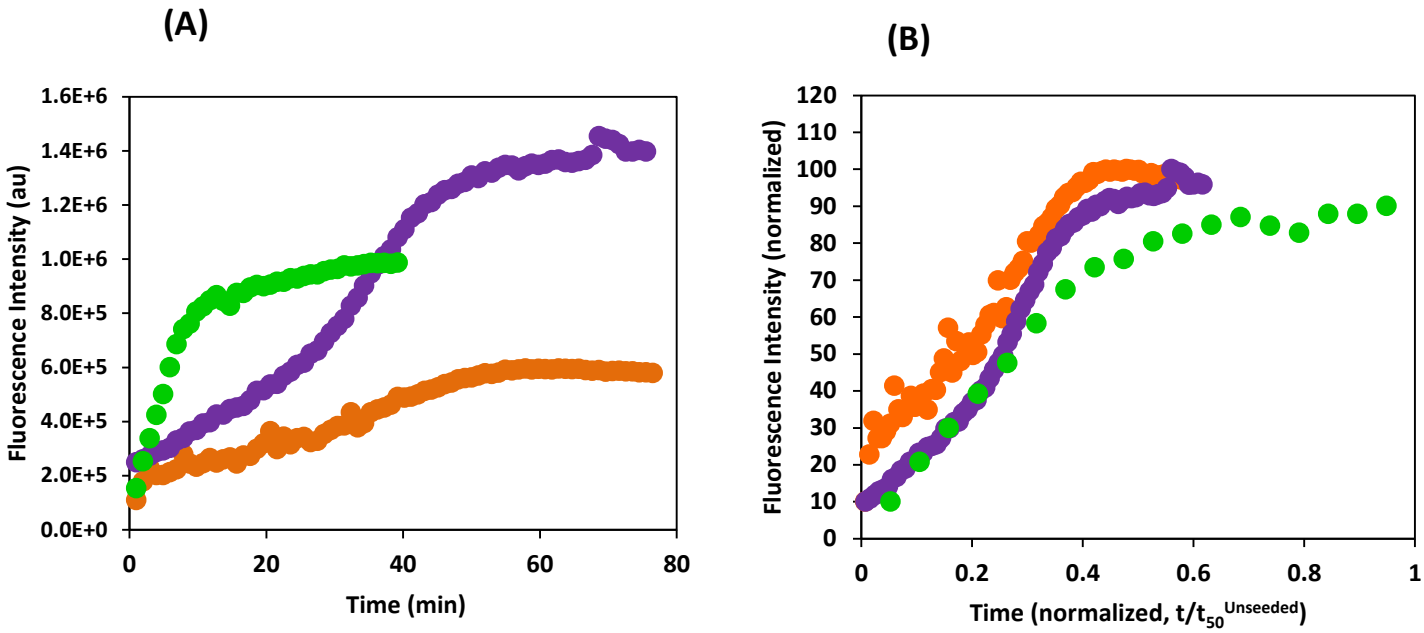

Figure 2.26: (A) Homologous seeding (each peptide is seeded by its own fibrils) kinetics of S20A IAPP and S20Abu IAPP were similar to those WT IAPP. Figure shows Thioflavin-T fluorescent assay results: wild type IAPP was seeded by wild type IAPP fibrils (green), S20A IAPP was seeded by S20AIAPP fibrils (orange), and S20Abu IAPP was seeded by S20Abu IAPP fibrils (purple). (B)The time axis is normalized to t_{50} of own kinetic and fluorescence axis is normalized to final intensity of the kinetics. Thioflavin-T assay were monitored for 16 μM IAPP with 10% seed (monomer units) in 2% HFIP in 20 mM Tris buffer (pH 7.4) with 32 μM Thioflavin T solution at 25°C with constant stirring.

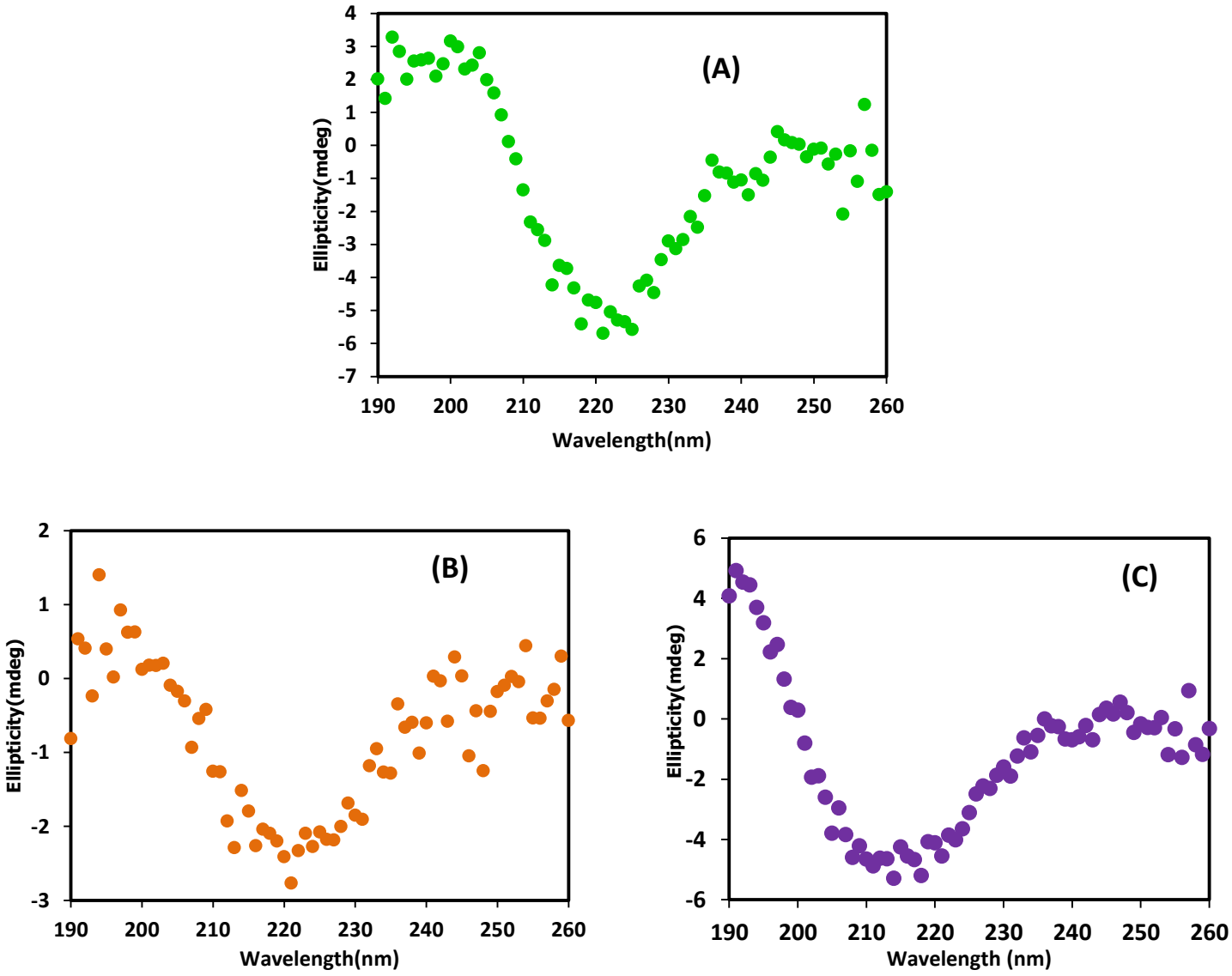

Figure 2.27: Circular dichroism (CD) spectra confirms the presence of β-sheet structure when; (A) wild type IAPP is seeded by wild type IAPP fibrils (green), (B) S20A IAPP mutant fibrils is seeded by S20A IAPP fibrils (orange), and (C) S20Abu IAPP mutant fibrils is seeded by S20Abu IAPP fibrils (purple). CD scans were taken at the end of seeding kinetic experiments.

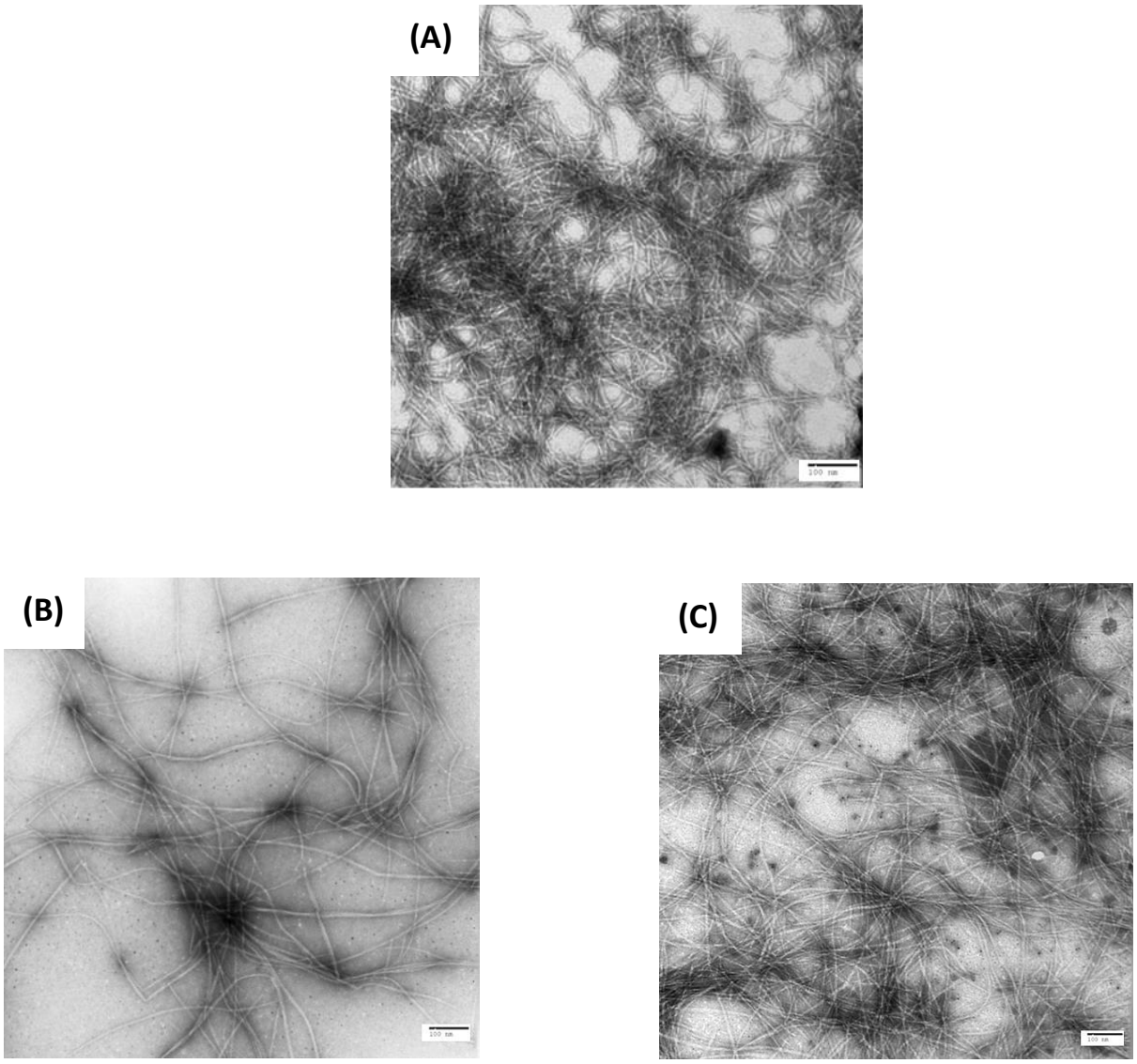

Figure 2.28: Transmission emission microscopy (TEM) images confirm amyloid fibril formation by (A) wild type IAPP seeded by wild type IAPP fibrils, (B) S20A IAPP mutant fibrils seeded by S20A IAPP fibrils, and (C) S20Abu IAPP mutant fibrils seeded by S20Abu IAPP fibrils. Samples were collected at the end of each seeding kinetic experiments. The scale bar in the images is 100 nm.

3. Analysis of a serine 19 to glycine mutation on IAPP amyloid formation

3.1 Introduction

In addition to the pathological importance, the S20G IAPP mutation is very important in considering the primary sequence of IAPP. IAPP amyloid formation is related to the primary sequence of the protein. Recently published all of the IAPP proposed models showed that serine 20 is not in the distinct β-sheet region of amyloid fibrils. Serine 20 is in the turn region between two β-strands of amyloid fibrils (90, 92). Two-dimensional infrared (2D IR) studies with $^{13}C^{18}O$ isotope labeled side chain also showed the evidence that S20 is not in β sheet structure of amyloid fibrils (112). In membrane mimic conditions, NMR studies, and *in silico* studies showed evidence that the serine 20 is in the turn region between two helices of the IAPP monomer (41, 113). There is another serine residue in a similar region of hIAPP at position19 (Figure 3.1). As S20G forms amyloid faster than wild type IAPP, we are interested to see if S19G mutation does this. To check the sensitivity of serine 20 to glycine mutation in amyloid formation at that region, I have studied the serine 19 to glycine mutant (S19G IAPP). Here, I have tested the kinetics of amyloid formation of the S19G mutant in the presence and the absence of co-solvent at physiological pH. I have also compared the structural similarity of the S19G mutant with wild type IAPP by cross-seeding experiments. Comparing S19G mutant results with previously published S20G mutant results (69), confirms the distinct amyloidgenic profile of S20G IAPP.

3.2 Materials & methods

3.2.1 Peptide Synthesis

S19G IAPP was synthesized using the same protocol described in chapter 2.

3.2.2. Peptide Purification and Oxidation

Peptides were purified and were oxidized using the same protocol described in chapter 2. The pure peptides were eluted from reverse phase HPLC column around ~24 min (Figure 3.2). The expected and observed molecular masses for oxidized S19G IAPP are 3873.3 and 3873.4 respectively.

3.2.3 Fluorescence Assays

Sample Preparation

Samples were prepared using the same protocol described in chapter 2.

Thioflavin-T Binding Kinetic Assays

Thioflavin-T binding fluorescence assays were done using the same protocol as described in chapter 2.

Seeding Assays

Seeding assays were performed using the same method as described in chapter 2.

3.2.4 Circular Dichroism (CD) Experiment

CD spectrum were collected using the same conditions as described in chapter 2.

3.2.5 Transmission Electron Microscopy (TEM)

TEM images were collected as described in chapter 2.

3.3 Results & Discussion

3.3.1 Analysis of amyloid formation by serine to glycine mutants in the turn region

The primary sequences of human IAPP is shown in figure 3.1. Human IAPP has serine residues in its sequence at positions19 and 20 (red colored in figure 3. 1A). Figure 3.1B shows the human IAPP fibril model proposed by Eisenberg et al. built from an x-ray crystallography structure of small segment of IAPP. The IAPP fibril model showed that serine residue 19 and 20 are in the turn region of IAPP. Single mutant structure of serine 19 and serine 20 to glycine were built from the Eisenberg proposed model using Chimera (2.1C, D) (126). The hIAPP and its mutant structures showed no side chain hydrogen bond interactions at residue 19 and 20 with >4Å and 30° cut off, which was checked using VMD (111). S19G IAPP and S20G IAPP were synthesized to compare the sensitivity of serine to glycine mutation in loop region.

Amyloid formation by S19G IAPP and S20G IAPP was examined using Thioflavin-T binding fluorescence assays. Thioflavin-T shows very low fluorescent intensity in solution but its quantum yields significantly increases when it binds to the amyloid fibrils. Thioflavin-T assay were conducted in the presence of 2% hexafluoroisopropyl alcohol (HFIP) (with stirring) and in absence of HFIP (non- stirring) at pH 7.4. The kinetics curves obtained from Thioflavin-T assays

for wild type hIAPP and S20G IAPP are consisted with previously reported results using similar biophysical conditions (Figure 3.3). Wild type has a distinct lag phase, followed by a growth phase and a steady state plateau phase while the kinetics curve of S20G IAPP showed that it has no lag phase and rapid growth phase. On the other hand, the kinetics of S19G IAPP showed that the rate of amyloid formation was slower than WT IAPP (Figure 3.3.1). Amyloid formation was monitored in the presence and the absence of the co-solvent HFIP at pH 7.4 to facilitate comparison to earlier studies. Amyloid formation was rapid in the presence of HFIP with stirring. However, both experiments showed that amyloid formation by S20G IAPP was faster and amyloid formation by S19G IAPP was slower than that of WT IAPP (Figure 3.3.2). The bar graph shows the comparison of the results of the lag time and the t_{50} values for all three peptide with t_{50} value of WT IAPP (t_{50}^{wt}) time scale (Figure 3.3.2). t_{50} is the time need to reach half of the final intensity in Thioflavin T assay. Circular dichroism (CD) absorption scans were taken for all three peptide when kinetic curves reached its plateau phase. CD spectroscopy confirms that all three peptide fibrils have secondary β-sheet structure in their conformation (Figure 3.4). Transmission electron microscopy (TEM) images were collected from all three peptide at the end of the experiments. All the peptide showed significant amount amyloid fibrils formation in TEM image (Figure 3.5).

3.3.2 S20G IAPP and S19G IAPP fibrils can seed the amyloid formation by WT IAPP

Structural similarities between wild type IAPP and S20G IAPP, S19G IAPP mutant fibrils were studied by seeding experiments. If two different peptide fibrils tips are similar, the monomer of the one peptide can dock on to the another peptide fibrils. Seeding specificity distinguishes the difference between the fibril structures. Seeds are more efficient when peptides are seeded by

their own fibrils. WT IAPP was seeded WT IAPP fibrils (green) and WT IAPP was seeded by S19G IAPP fibrils (orange) and S20G fibrils (blue) in presence of 2% HFIP with continuous stirring at pH7.4 (Figure 3.6). The seeding ability of the mutant fibrils indicated the structural similarity between the WT IAPP fibrils and mutant fibrils. Mutant fibrils were less effective seeds for WT IAPP than wild type IAPP fibrils (Figure 3.6). These results may suggest that the point mutation at position 19 and position 20 did not significantly change final fibril structure or the fibrils surface. Seeding effectiveness is more qualitative than quantitative. CD scans were taken at the end of the seeding kinetic experiments and all of the peptides confirmed the β-sheet structure of the fibrils (Figure 3.7). Samples were also collected at the end of seeding kinetic experiments and all of the peptide forms amyloid fibrils (Figure 3.8).

3.4 Conclusion

Kinetics curve of S19G IAPP shows that S19G mutation slows down amyloid formation. CD spectra confirm β-sheet secondary structure and TEM images confirm the fibril structure. This study confirm us the specific amyloidogenic profile of S20G mutant. Seeding kinetics of wild type IAPP by S20G and S19G mutant fibrils showed, both of them can seed amyloid formation. These seeding kinetics suggests the similarity in final fibril structure. CD spectra confirmed β-sheet structure and TEM images showed similar fibril morphology.

The kinetics data suggest that serine 19 causes favorable interaction in amyloid formation and mutation of Ser19 with glycine disrupts the favorable interaction. On the other hand, wild type IAPP is one of the most amyloidogenic proteins and S20G mutation makes it more amyloidogenic. Analysis of serine mutation with glycine at position 19 and 20 suggests that serine 19 and serine 20 has different contribution in IAPP amyloid formation.

3.5 Figures

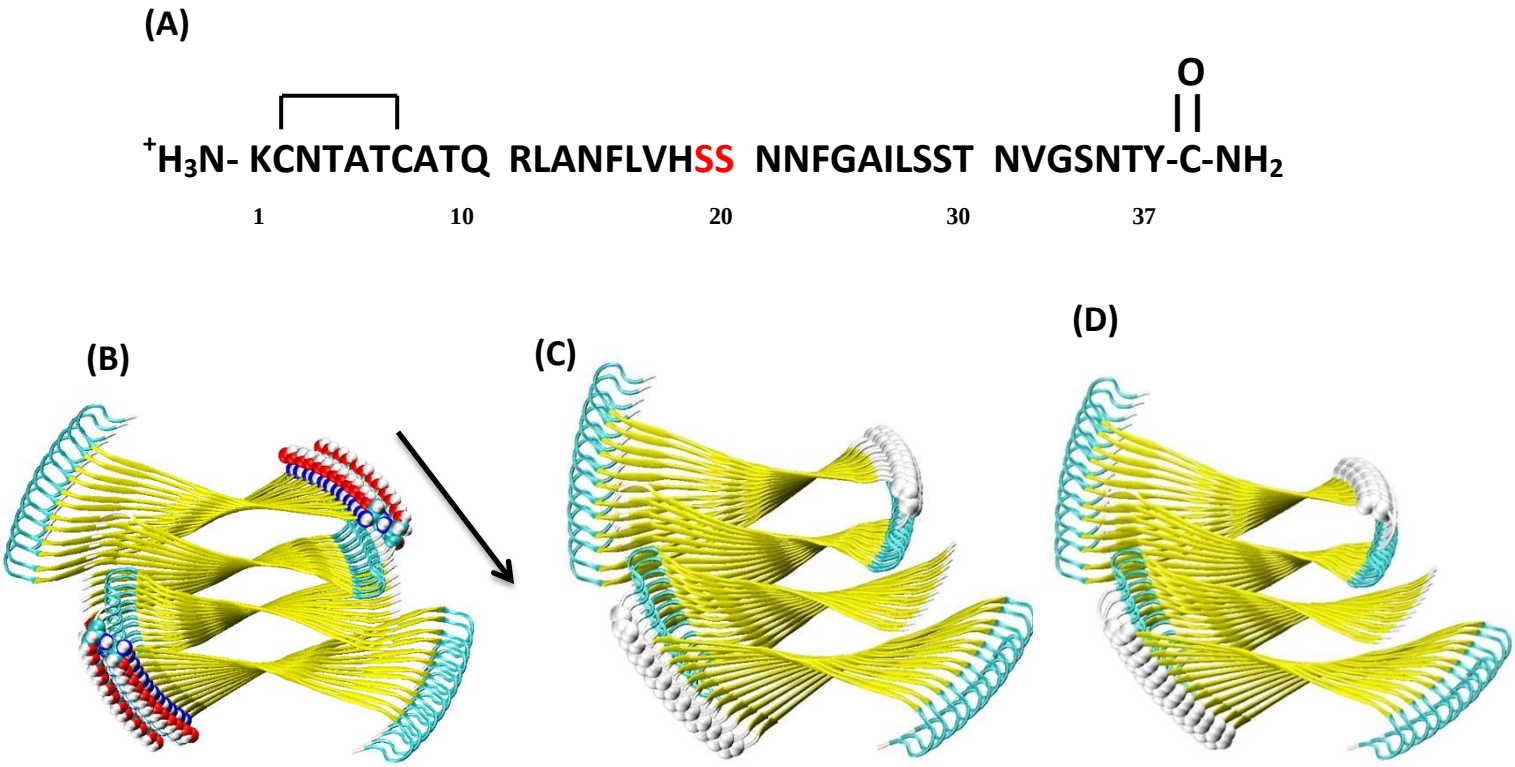

Figure 3.1: (A) Primary sequence of human IAPP (two serine residues at position 19 and 20 red colored), (B) Human IAPP fibril model, Eisenberg et al. proposed "Steric zipper" structure model, built from two small segment x-ray crystalline structures; segment of residues 21-27(NNFGAIL) and residues 28-33(SSTNVG) of hIAPP (88). Ser19 and Ser20 are shown in space filling representation. Figure shows that both of these residues are in turn region of IAPP fibrils. Fibril axis is along the black arrow. β-sheets are yellow colored in the figure. (C,D) S20G IAPP (Figure C) and S19G IAPP (Figure D) mutant fibril structure built from the above described model using Chimera (126). Figures were prepared using VMD(111).

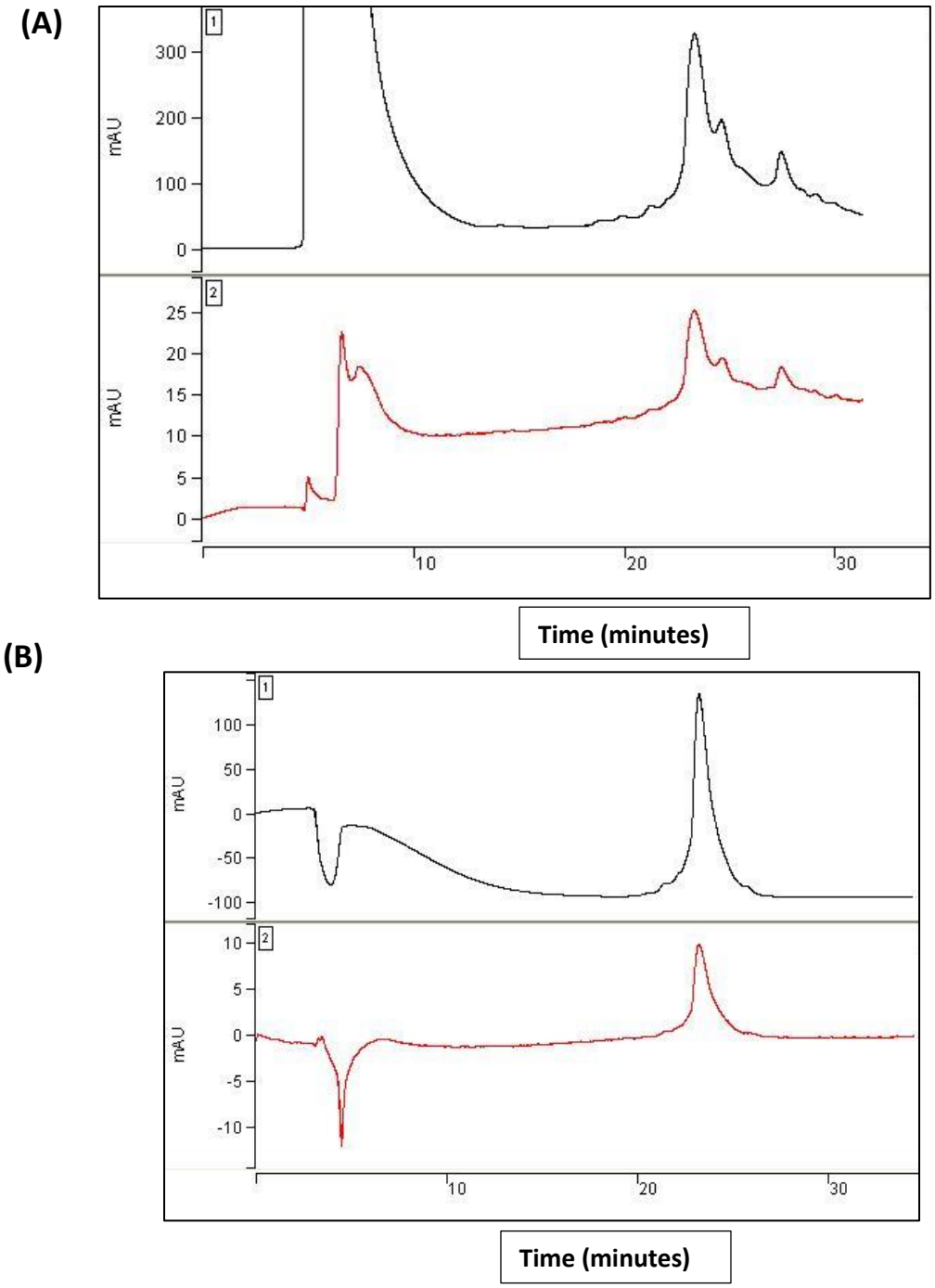

Figure 3.2: HPLC traces of S19G IAPP using an analytical C18 column. (A) Crude S19G IAPP (eluted at ~24 minutes), (B) Pure S19G IAPP (eluted at~24 minutes) (A-B buffer gradient system: A: 100 % DDI H_2O&0.045 % HCl, B: 80% ACN & 0.45% HCl (v/v), gradient: 20-60 % B in 60 minutes).

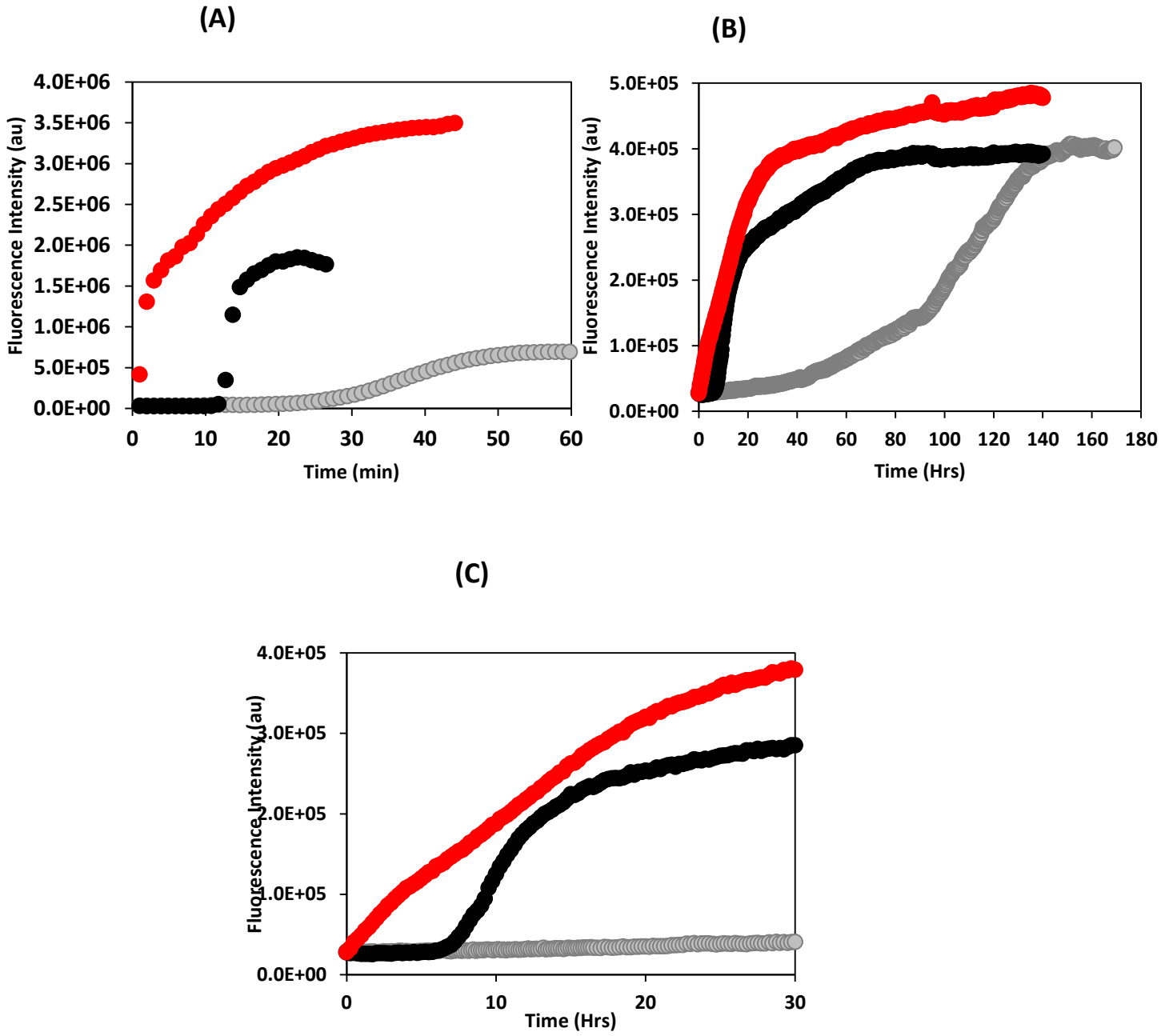

Figure 3.3.1: S19G IAPP mutant shows slow amyloid formation compared to wild type IAPP and S20G IAPP mutant. (A) The top left panel shows the kinetics of amyloid formation obtained from Thioflavin-T fluorescence dye binding assays in the presence of 2% HFIP with constant stirring, (B) The top right panel shows the similar experiment results obtained in absence of HFIP without stirring. (C) Enlarged view of figure B. Thioflavin-T assay were monitored in 20 mM Tris buffer (pH 7.4) at 25°C ; wild type IAPP-black, S20G IAPP-red and S19G IAPP-gray.

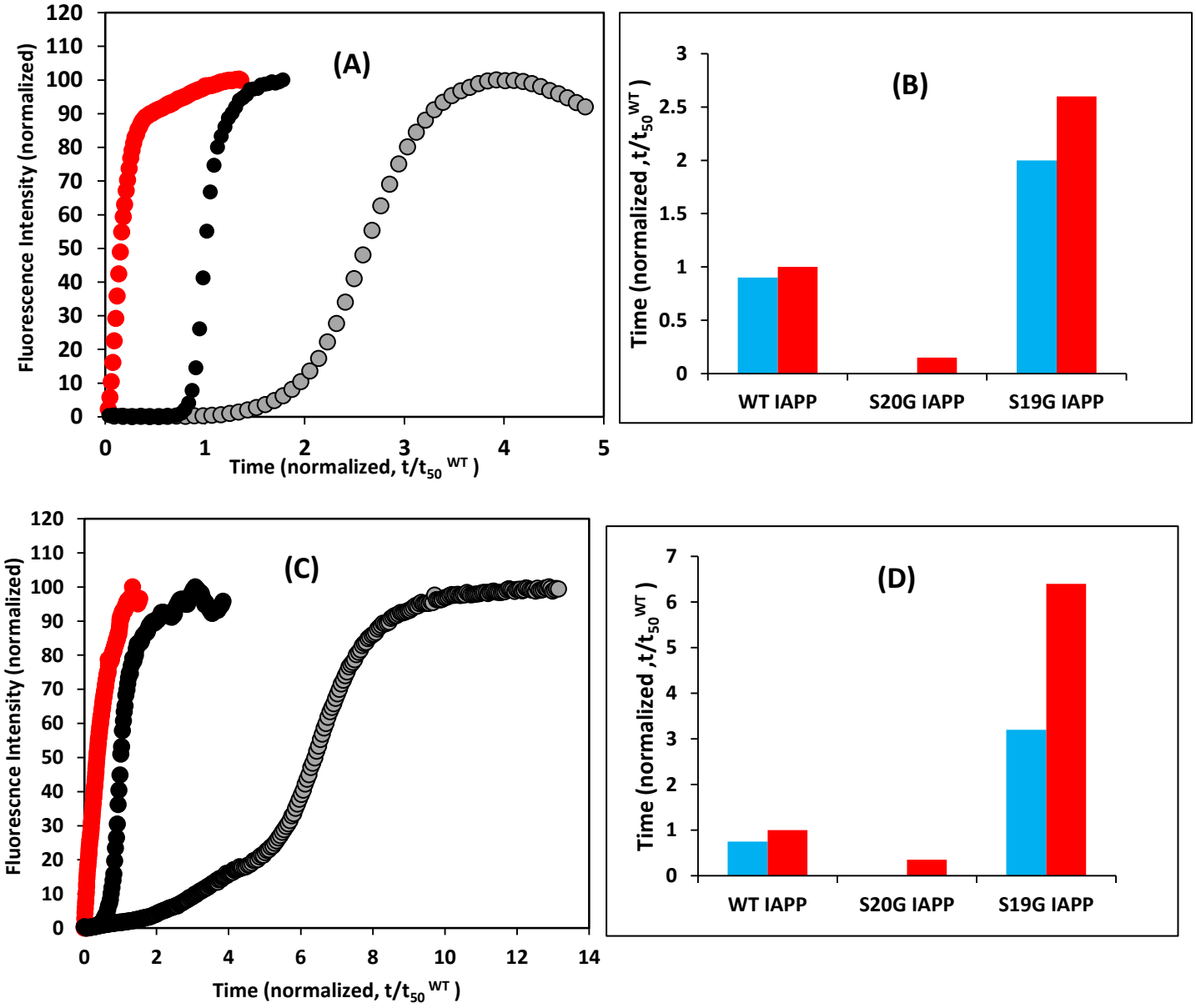

Figure 3.3.2: S19G IAPP mutant shows slow amyloid formation compared to wild type IAPP and S20G IAPP mutant. (A) The top left panel shows the kinetics of amyloid formation obtained from Thioflavin-T fluorescence dye binding assays in the presence of 2% HFIP with constant stirring, (B) The bottom left panel shows the similar experiment results obtained in absence of HFIP without stirring. The time axis is normalized to t_{50}^{wt} and the fluorescence axis is normalized to final intensity of the peptide. (C, D) The right panel bar graphs show the lag time and t_{50} comparison results obtained from kinetics results at the left panel. Thioflavin-T assay were monitored in 20 mM Tris buffer (pH 7.4) at 25°C ; wild type IAPP-black, S20G IAPP-red and S19G IAPP-gray; normalize lag time-blue bar, T_{50}-red bar.

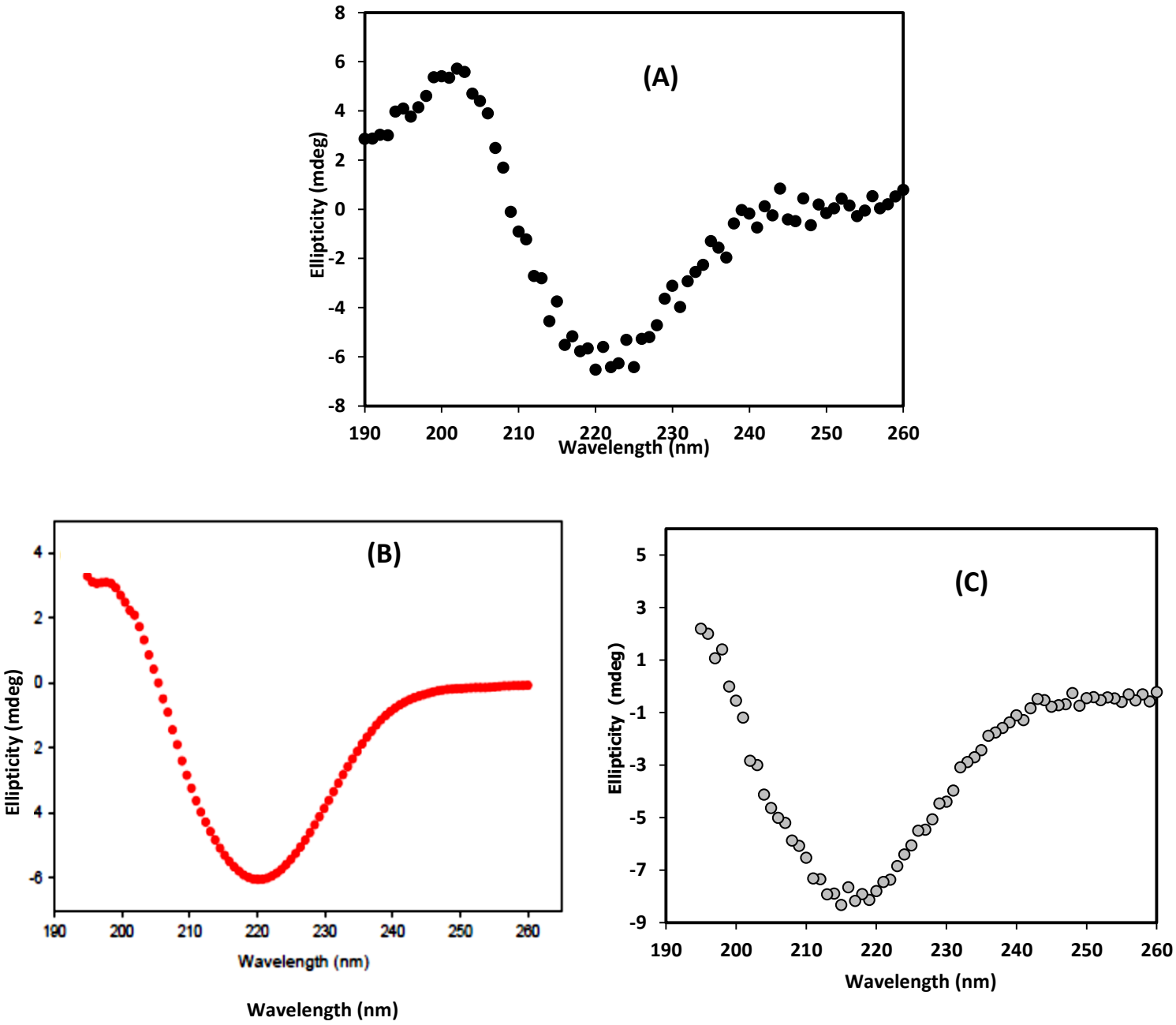

Figure 3.4: Circular dichroism (CD) spectra confirms the presence of β-sheet structure in (A) wild type IAPP fibrils (black), (B) S20G IAPP mutant fibrils (red) (S20G mutant figure is taken from Cao et al. JMB, 2012) (69), and (C) S19G IAPP mutant fibrils (gray). Samples were collected at the end of each experiment conducted with 16 μM IAPP in 2% HFIP with continuous stirring in 20 mM Tris buffer, pH 7.4, at 25°C.

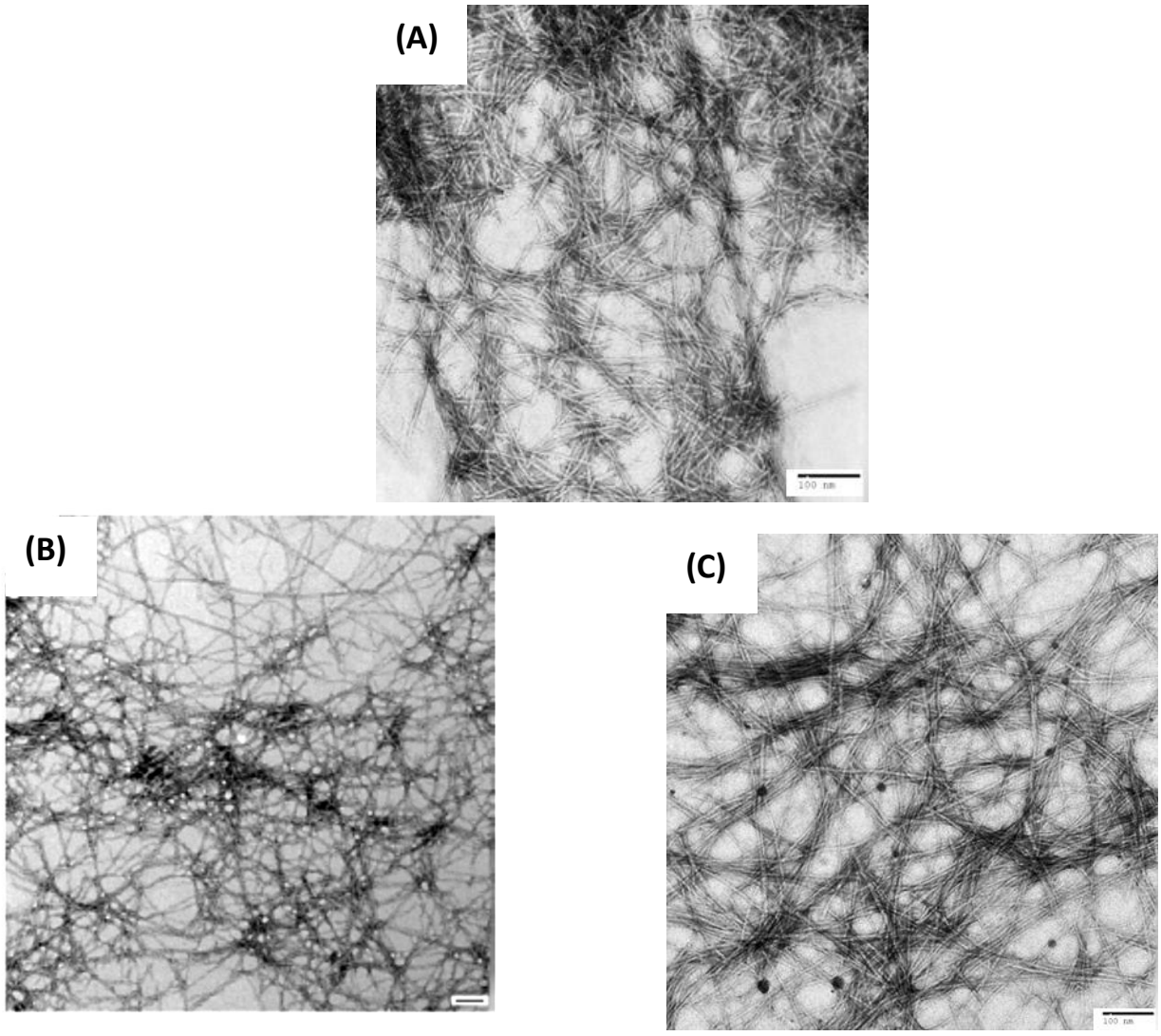

Figure 3.5: Transmission emission microscopy (TEM) images confirm amyloid fibril formation by (A) wild type IAPP, (B) S20G IAPP mutant (S20G mutant figure is taken from Cao et al. JMB, 2012) (69), and (C) S19G IAPP mutant. Samples were collected at the end of each experiment conducted with 16 μM IAPP in 2% HFIP with continuous stirring in 20 mM Tris buffer, pH 7.4, at 25°C. The scale bar in images is 100 nm.

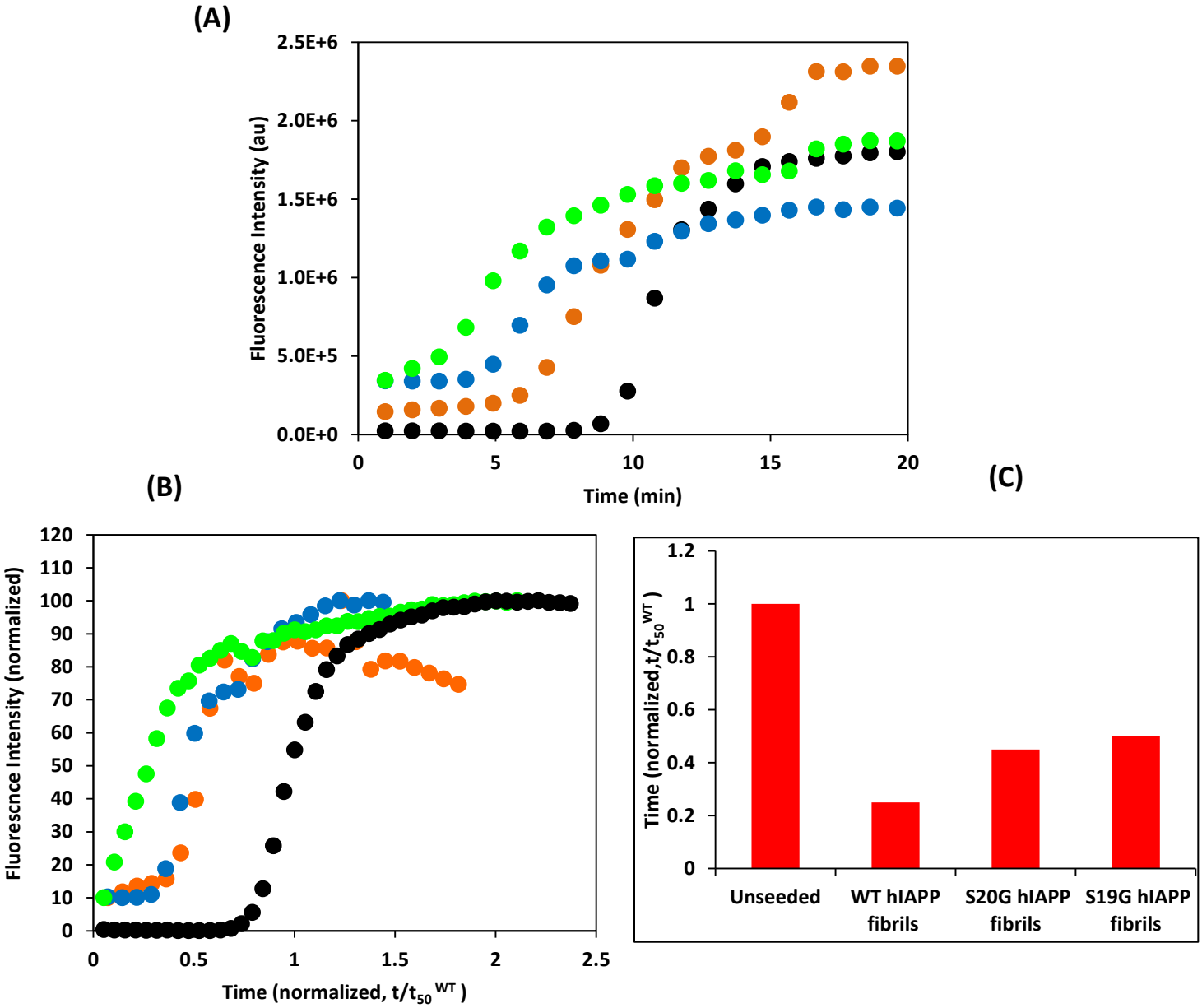

Figure 3.6: Wild Type IAPP can be seeded by both S20G IAPP fibrils and S19G IAPP fibrils. (A) The top panel shows the Thioflavin-T fluorescent assay results. Unseeded wild type-IAPP (black); wild type IAPP seeded by wild type IAPP fibrils (green), wild type IAPP seeded by S20G IAPP fibrils (blue), wild type IAPP seeded by S19G IAPP fibrils (orange). (B) The left panel shows same kinetics in figure A; here, time axis is normalized to t_{50}^{wt} and fluorescence axis is normalized to final intensity of the peptide, (C)The right panel shows the T_{50} comparison results at normalized time scale t/t_{50}^{wt} obtained from the seeding kinetics results at the left panel. Thioflavin-T assay were monitored for 16 μM IAPP with 10% seed (monomer unit) in 2 % HFIP in 20mM Tris buffer (pH 7.4) with 32 μM Thioflavin T solution at 25°C with constant stirring.

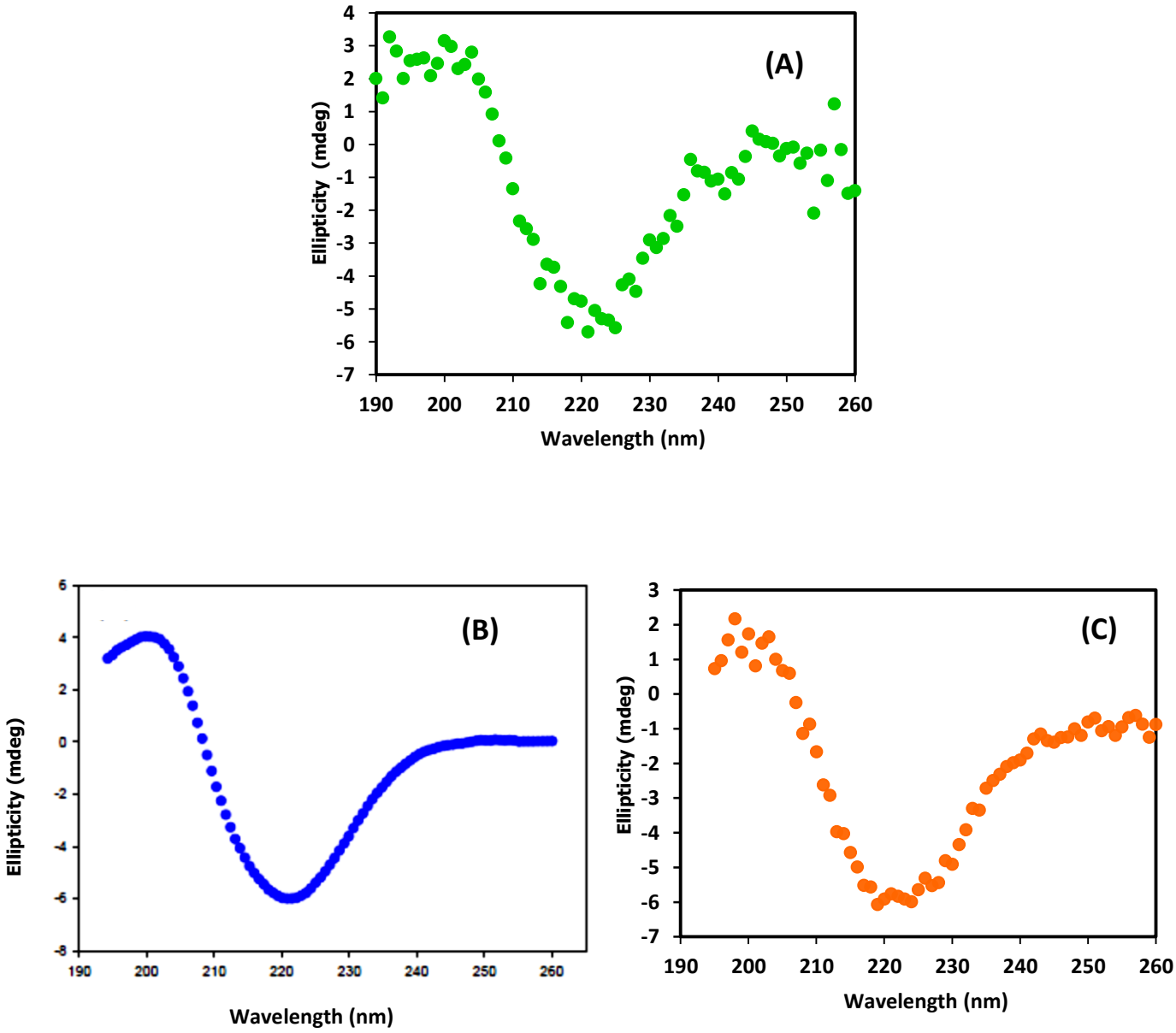

Figure 3.7: Circular dichroism (CD) spectra confirms the presence of β-sheet structure when wild type IAPP is seeded by: (A) wild type IAPP fibrils (green), (B) S20G IAPP mutant fibrils (blue), (S20G mutant figure is taken from Cao et al. JMB, 2012)(69), and (C) S19G IAPP mutant fibrils (orange). CD scans were taken the end of seeding kinetic experiments.

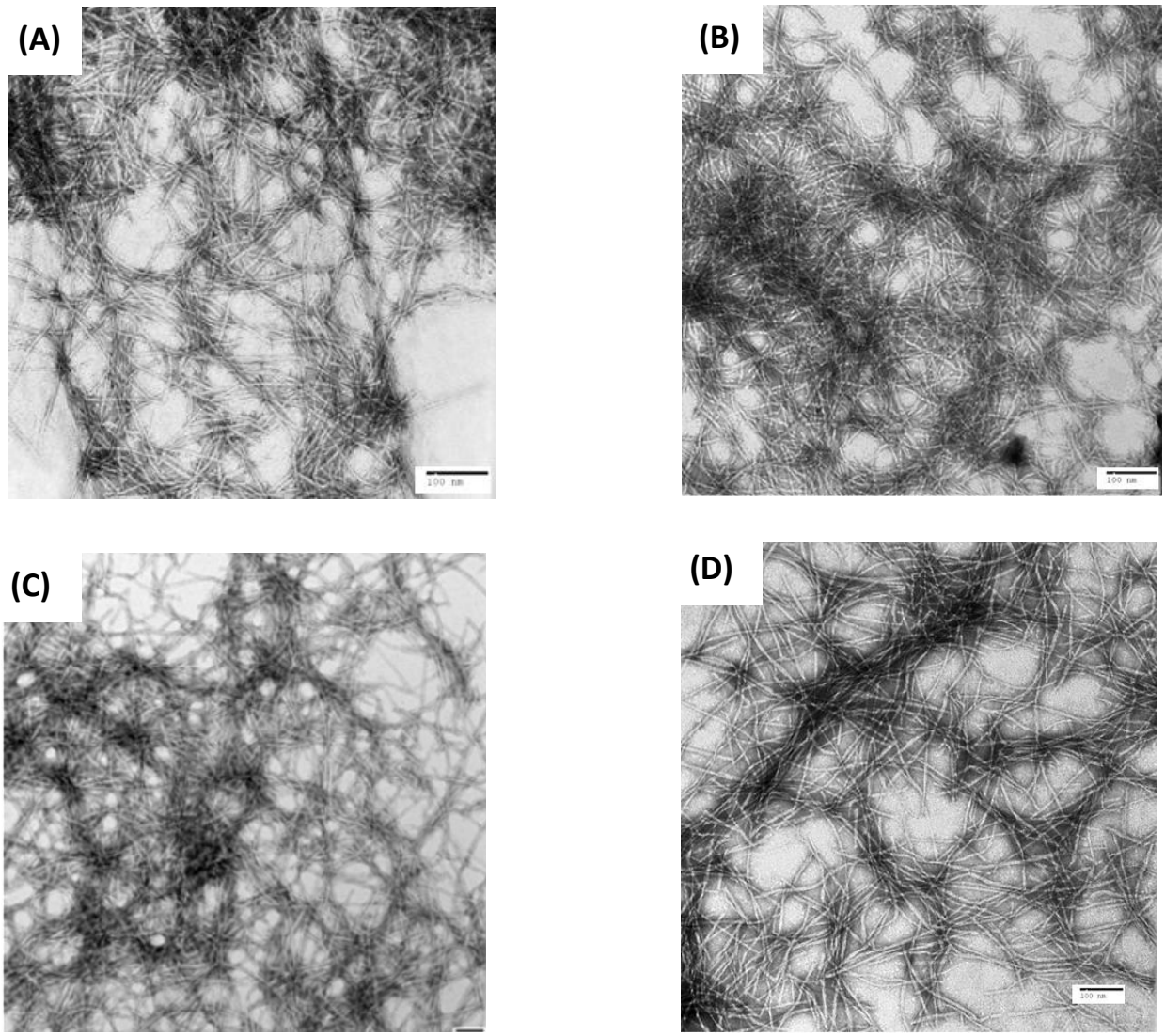

Figure 3.8: Transmission emission microscopy (TEM) images confirm amyloid fibril formation by (A) wild type IAPP and wild type IAPP : (B) seeded by wild type IAPP fibrils , (C) seeded by S20G IAPP mutant fibrils(S20G mutant figure is taken from Cao et al. JMB, 2012) (69), and (D) seeded by S19G IAPP mutant fibrils. Samples were collected at the end of each seeding kinetic experiment. The scale bar in the images is 100 nm.

4. References:

1. Rochet, J. C., and Lansbury, P. T., Jr. (2000) Amyloid fibrillogenesis: themes and variations, *Curr. Opin. Struct. Biol. 10*, 60-68.
2. Glenner, G. G., Eanes, E. D., Bladen, H. A., Linke, R. P., and Termine, J. D. (1974) Beta-pleated sheet fibrils. A comparison of native amyloid with synthetic protein fibrils, *J. Histochem. Cytochem. 22*, 1141-1158.
3. Westermark, P. (2005) Aspects on human amyloid forms and their fibril polypeptides, *FEBS J. 272*, 5942-5949.
4. Chiti, F., and Dobson, C. M. (2006) Protein misfolding, functional amyloid, and human disease, *Annu. Rev. Biochem. 75*, 333-366.
5. Selkoe, D. J. (2004) Cell biology of protein misfolding: the examples of Alzheimer's and Parkinson's diseases, *Nat. Cell. Biol. 6*, 1054-1061.
6. Sipe, J. D. (1994) Amyloidosis, *Crit. Rev. Clin. Lab. Sci. 31*, 325-354.
7. Pepys, M. B. (2006) Amyloidosis, *Annu. Rev.Med. 57*, 223-241.
8. Johansson, J., Nerelius, C., Willander, H., and Presto, J. (2010) Conformational preferences of non-polar amino acid residues: an additional factor in amyloid formation, *Biochem. Biophys. Res. Commun. 402*, 515-518.
9. Tycko, R. (2006) Molecular structure of amyloid fibrils: insights from solid-state NMR, *Q. Rev. Biophys. 39*, 1-55.
10. Makin, O. S., and Serpell, L. C. (2005) Structures for amyloid fibrils, *FEBS J. 272*, 5950-5961.
11. Sunde, M., Serpell, L. C., Bartlam, M., Fraser, P. E., Pepys, M. B., and Blake, C. C. (1997) Common core structure of amyloid fibrils by synchrotron X-ray diffraction, *J. Mol. Biol. 273*, 729-739.
12. Johnston, N. (2005) Gamma-secretase makes a splash, *Scientist 19*, 24-25.
13. Xue, W. F., Homans, S. W., and Radford, S. E. (2008) Systematic analysis of nucleation-dependent polymerization reveals new insights into the mechanism of amyloid self-assembly, *Proc. Natl. Acad. Sci. U. S. A. 105*, 8926-8931.
14. O'Nuallain, B., Williams, A. D., Westermark, P., and Wetzel, R. (2004) Seeding specificity in amyloid growth induced by heterologous fibrils, *J. Biol. Chem. 279*, 17490-17499.
15. Soto, C., Saborio, G. P., and Anderes, L. (2002) Cyclic amplification of protein misfolding: application to prion-related disorders and beyond, *Trends Neurosci. 25*, 390-394.
16. Levine, H. (1995) Thioflavine-T interaction with amyloid β-sheet structures, *Amyloid 2*, 1-6.
17. Puchtler, H., Sweat, F., and Levine, M. (1962) On binding of congo red by amyloid, *J. Histochem. Cytochem. 10*, 355-&.
18. Khurana, R., Coleman, C., Ionescu-Zanetti, C., Carter, S. A., Krishna, V., Grover, R. K., Roy, R., and Singh, S. (2005) Mechanism of thioflavin T binding to amyloid fibrils, *J. Struct. Biol. 151*, 229-238.
19. Stsiapura, V. I., Maskevich, A. A., Kuzmitsky, V. A., Uversky, V. N., Kuznetsova, I. M., and Turoverov, K. K. (2008) Thioflavin T as a molecular rotor: fluorescent properties of thioflavin T in solvents with different viscosity, *J. Phys. Chem. B 112*, 15893-15902.

20. Krebs, M. R., Bromley, E. H., and Donald, A. M. (2005) The binding of thioflavin-T to amyloid fibrils: localisation and implications, *J. Struct. Biol. 149*, 30-37.
21. Jackson, K., Barisone, G. A., Diaz, E., Jin, L. W., Decarli, C., and Despa, F. (2013) Amylin deposition in the brain: A second amyloid in Alzheimer disease?, *Annals of neurology*.
22. Gong, W., Liu, Z. H., Zeng, C. H., Peng, A., Chen, H. P., Zhou, H., and Li, L. S. (2007) Amylin deposition in the kidney of patients with diabetic nephropathy, *Kidney international 72*, 213-218.
23. Mukherjee, S., and Dey, S. G. (2013) Heme bound amylin: spectroscopic characterization, reactivity, and relevance to type 2 diabetes, *Inorg Chem 52*, 5226-5235.
24. Janson, J., Laedtke, T., Parisi, J. E., O'Brien, P., Petersen, R. C., and Butler, P. C. (2004) Increased risk of type 2 diabetes in Alzheimer disease, *Diabetes 53*, 474-481.
25. Kahn, S. E. (2003) The relative contributions of insulin resistance and β-cell dysfunction to the pathophysiology of type 2 diabetes, *Diabetologia 46*, 3-19.
26. Hoppener, J. W., and Lips, C. J. (2006) Role of islet amyloid in type 2 diabetes mellitus, *Int. J. Biochem. Cell Biol. 38*, 726-736.
27. Potter, K. J., Abedini, A., Marek, P., Klimek, A. M., Butterworth, S., Driscoll, M., Baker, R., Nilsson, M. R., Warnock, G. L., Oberholzer, J., Bertera, S., Trucco, M., Korbutt, G. S., Fraser, P. E., Raleigh, D. P., and Verchere, C. B. (2010) Islet amyloid deposition limits the viability of human islet grafts but not porcine islet grafts, *Proc. Natl. Acad. Sci. U. S. A. 107*, 4305-4310.
28. Westermark, P., Wernstedt, C., Wilander, E., Hayden, D. W., O'Brien, T. D., and Johnson, K. H. (1987) Amyloid fibrils in human insulinoma and islets of Langerhans of the diabetic cat are derived from a neuropeptide-like protein also present in normal islet cells, *Proc. Natl. Acad. Sci. U. S. A. 84*, 3881-3885.
29. Cooper, G. J., Willis, A. C., Clark, A., Turner, R. C., Sim, R. B., and Reid, K. B. (1987) Purification and characterization of a peptide from amyloid-rich pancreases of type 2 diabetic patients, *Proc. Natl. Acad. Sci. U. S. A. 84*, 8628-8632.
30. Westermark, P., Andersson, A., and Westermark, G. T. (2011) Islet amyloid polypeptide, islet amyloid, and diabetes mellitus, *Physio;. Rev. 91*, 795-826.
31. Lukinius, A., Wilander, E., Westermark, G. T., Engstrom, U., and Westermark, P. (1989) Co-localization of islet amyloid polypeptide and insulin in the β cell secretory granules of the human pancreatic islets, *Diabetologia 32*, 240-244.
32. Kahn, S. E., D'Alessio, D. A., Schwartz, M. W., Fujimoto, W. Y., Ensinck, J. W., Taborsky, G. J., Jr., and Porte, D., Jr. (1990) Evidence of cosecretion of islet amyloid polypeptide and insulin by beta-cells, *Diabetes 39*, 634-638.
33. Gedulin, B. R., Jodka, C. M., Herrmann, K., and Young, A. A. (2006) Role of endogenous amylin in glucagon secretion and gastric emptying in rats demonstrated with the selective antagonist, AC187, *Reg. Pepts. 137*, 121-127.
34. Castillo, M. J., Scheen, A. J., and Lefebvre, P. J. (1995) Amylin/islet amyloid polypeptide: biochemistry, physiology, patho-physiology, *Diabete Metab. 21*, 3-25.
35. Young, A. (2005) Inhibition of gastric emptying, *Adv. Pharmacol. 52*, 99-121.
36. Christopoulos, G., Paxinos, G., Huang, X. F., Beaumont, K., Toga, A. W., and Sexton, P. M. (1995) Comparative distribution of receptors for amylin and the related peptides calcitonin gene related peptide and calcitonin in rat and monkey brain, *Can. J. Physiol. Pharmacol. 73*, 1037-1041.

37. Gebre-Medhin, S., Mulder, H., Zhang, Y. Z., Sundler, F., and Betsholtz, C. (1998) Reduced nociceptive behavior in islet amyloid polypeptide (amylin) knockout mice, *Mol. Brain Res. 63*, 180-183.
38. Naot, D., and Cornish, J. (2008) The role of peptides and receptors of the calcitonin family in the regulation of bone metabolism, *Bone 43*, 813-818.
39. Williamson, J. A., and Miranker, A. D. (2007) Direct detection of transient alpha-helical states in islet amyloid polypeptide, *Protein Sci. 16*, 110-117.
40. Cort, J. R., Liu, Z., Lee, G. M., Huggins, K. N., Janes, S., Prickett, K., and Andersen, N. H. (2009) Solution state structures of human pancreatic amylin and pramlintide, *Protein Eng. Des. Sel. 22*, 497-513.
41. Abedini, A., and Raleigh, D. P. (2009) A role for helical intermediates in amyloid formation by natively unfolded polypeptides?, *Physical Biol.6*.
42. Nanga, R. P. R., Brender, J. R., Vivekanandan, S., and Ramamoorthy, A. (2011) Structure and membrane orientation of IAPP in its natively amidated form at physiological pH in a membrane environment, *Biochim. Biophys. Acta. 1808*, 2337-2342.
43. Patil, S. M., Xu, S. H., Sheftic, S. R., and Alexandrescu, A. T. (2009) Dynamic alpha-helix structure of micelle-bound human amylin, *J. Biol. Chem. 284*, 11982-11991.
44. Wimalawansa, S. J. (1997) Amylin, calcitonin gene-related peptide, calcitonin, and adrenomedullin: a peptide superfamily, *Crit. Rev. Neurobiol. 11*, 167-239.
45. Sanke, T., Bell, G. I., Sample, C., Rubenstein, A. H., and Steiner, D. F. (1988) An islet amyloid peptide is derived from an 89-amino acid precursor by proteolytic processing, *J. Biol. Chem. 263*, 17243-17246.
46. Westermark, P., Li, Z. C., Westermark, G. T., Leckstrom, A., and Steiner, D. F. (1996) Effects of beta cell granule components on human islet amyloid polypeptide fibril formation, *FEBS Lett. 379*, 203-206.
47. Hutton, J. C. (1989) The insulin secretory granule, *Diabetologia 32*, 271-281.
48. Kahn, S. E., Fujimoto, W. Y., D'Alessio, D. A., Ensinck, J. W., and Porte, D., Jr. (1991) Glucose stimulates and potentiates islet amyloid polypeptide secretion by the β-cell, *Horm. Metab. Res. 23*, 577-580.
49. Toshimori, H., Narita, R., Nakazato, M., Asai, J., Mitsukawa, T., Kangawa, K., Matsuo, H., and Matsukura, S. (1990) Islet amyloid polypeptide (IAPP) in the gastrointestinal tract and pancreas of man and rat, *Cell Tissue Res. 262*, 401-406.
50. Fan, L., Westermark, G., Chan, S. J., and Steiner, D. F. (1994) Altered gene structure and tissue expression of islet amyloid polypeptide in the chicken, *Mol. Endocrinol 8*, 713-721.
51. http://www.who.int/mediacentre/factsheets/fs312/en/.
52. Definition, diagnosis and classification of diabetes mellitus and its complications. Part 1: Diagnosis and classification of diabetes mellitus. Geneva, World Health Organization, 1999 (WHO/NCD/NCS/99.2).
53. Westermark, P., Johnson, K. H., O'Brien, T. D., and Betsholtz, C. (1992) Islet amyloid polypeptide--a novel controversy in diabetes research, *Diabetologia 35*, 297-303.
54. Janson, J., Soeller, W. C., Roche, P. C., Nelson, R. T., Torchia, A. J., Kreutter, D. K., and Butler, P. C. (1996) Spontaneous diabetes mellitus in transgenic mice expressing human islet amyloid polypeptide, *Proc. Natl. Acad. Sci. U. S. A. 93*, 7283-7288.
55. Clark, A., Wells, C. A., Buley, I. D., Cruickshank, J. K., Vanhegan, R. I., Matthews, D. R., Cooper, G. J., Holman, R. R., and Turner, R. C. (1988) Islet amyloid, increased α-

cells, reduced β-cells and exocrine fibrosis: quantitative changes in the pancreas in type 2 diabetes, *Diabetes Res. 9*, 151-159.
56. Hull, R. L., Westermark, G. T., Westermark, P., and Kahn, S. E. (2004) Islet amyloid: a critical entity in the pathogenesis of type 2 diabetes, *J. Clin. Endocrinol Metab. 89*, 3629-3643.
57. Westermark, G., Westermark, P., Eizirik, D. L., Hellerstrom, C., Fox, N., Steiner, D. F., and Andersson, A. (1999) Differences in amyloid deposition in islets of transgenic mice expressing human islet amyloid polypeptide versus human islets implanted into nude mice, *Metabolism 48*, 448-454.
58. Udayasankar, J., Kodama, K., Hull, R. L., Zraika, S., Aston-Mourney, K., Subramanian, S. L., Tong, J., Faulenbach, M. V., Vidal, J., and Kahn, S. E. (2009) Amyloid formation results in recurrence of hyperglycaemia following transplantation of human IAPP transgenic mouse islets, *Diabetologia 52*, 145-153.
59. Potter, K. J., Abedini, A., Marek, P., Klimek, A. M., Butterworth, S., Driscoll, M., Baker, R., Nilsson, M. R., Warnock, G. L., Oberholzer, J., Bertera, S., Trucco, M., Korbutt, G. S., Fraser, P. E., Raleigh, D. P., and Verchere, C. B. (2010) Islet amyloid deposition limits the viability of human islet grafts but not porcine islet grafts, *Proc. Natl. Acad. Sci. U. S. A. 107*, 4305-4310.
60. Sakagashira, S., Sanke, T., Hanabusa, T., Shimomura, H., Ohagi, S., Kumagaye, K. Y., Nakajima, K., and Nanjo, K. (1996) Missense mutation of amylin gene (S20G) in Japanese NIDDM patients, *Diabetes 45*, 1279-1281.
61. Seino, S. (2001) S20G mutation of the amylin gene is associated with Type II diabetes in Japanese. Study group of comprehensive analysis of genetic gactors in diabetes mellitus, *Diabetologia 44*, 906-909.
62. Lee, S. C., Hashim, Y., Li, J. K., Ko, G. T., Critchley, J. A., Cockram, C. S., and Chan, J. C. (2001) The islet amyloid polypeptide (amylin) gene S20G mutation in Chinese subjects: evidence for associations with type 2 diabetes and cholesterol levels, *Clin. Endocrinol. 54*, 541-546.
63. Cho, Y. M., Kim, M., Park, K. S., Kim, S. Y., and Lee, H. K. (2003) S20G mutation of the amylin gene is associated with a lower body mass index in Korean type 2 diabetic patients, *Diabetes Res. Clin. Pr. 60*, 125-129.
64. Chuang, L. M., Lee, K. C., Huang, C. N., Wu, H. P., Tai, T. Y., and Lin, B. J. (1998) Role of S20G mutation of amylin gene in insulin secretion, insulin sensitivity, and type II diabetes mellitus in Taiwanese patients, *Diabetologia 41*, 1250-1251.
65. Morita, S., Sakagashira, S., Ueyama, M., Shimajiri, Y., Furuta, M., and Sanke, T. (2011) Progressive deterioration of insulin secretion in Japanese type 2 diabetic patients in comparison with those who carry the S20G mutation of the islet amyloid polypeptide gene: A long-term follow-up study, *J. Diabetes Investig. 2*, 287-292.
66. Ma, Z., Westermark, G. T., Sakagashira, S., Sanke, T., Gustavsson, A., Sakamoto, H., Engstrom, U., Nanjo, K., and Westermark, P. (2001) Enhanced in vitro production of amyloid-like fibrils from mutant (S20G) islet amyloid polypeptide, *Amyloid 8*, 242-249.
67. Yamada, K., Yuan, X., Ishiyama, S., and Nonaka, K. (1998) Glucose tolerance in Japanese subjects with S20G mutation of the amylin gene, *Diabetologia 41*, 125.
68. Hayakawa, T., Nagai, Y., Ando, H., Yamashita, H., Takamura, T., Abe, T., Nomura, G., and Kobayashi, K. (2000) S20G mutation of the amylin gene in Japanese patients with type 2 diabetes, *Diabetes Res. Clin. Pr. 49*, 195-197.

69. Cao, P., Tu, L. H., Abedini, A., Levsh, O., Akter, R., Patsalo, V., Schmidt, A. M., and Raleigh, D. P. (2012) Sensitivity of amyloid formation by human islet amyloid polypeptide to mutations at residue 20, *J. Mol. Biol. 421*, 282-295.
70. Sakagashira, S., Hiddinga, H. J., Tateishi, K., Sanke, T., Hanabusa, T., Nanjo, K., and Eberhardt, N. L. (2000) S20G mutant amylin exhibits increased in vitro amyloidogenicity and increased intracellular cytotoxicity compared to wild-type amylin, *Am. J. Pathol. 157*, 2101-2109.
71. Aston-Mourney, K., Hull, R. L., Zraika, S., Udayasankar, J., Subramanian, S. L., and Kahn, S. E. (2011) Exendin-4 increases islet amyloid deposition but offsets the resultant beta cell toxicity in human islet amyloid polypeptide transgenic mouse islets, *Diabetologia 54*, 1756-1765.
72. Westermark, P. (1973) Fine structure of islets of Langerhans in insular amyloidosis, *Virchows Arch. A. 359*, 1-18.
73. O'Brien, T. D., Butler, A. E., Roche, P. C., Johnson, K. H., and Butler, P. C. (1994) Islet amyloid polypeptide in human insulinomas. Evidence for intracellular amyloidogenesis, *Diabetes 43*, 329-336.
74. Cao, P., Marek, P., Noor, H., Patsalo, V., Tu, L. H., Wang, H., Abedini, A., and Raleigh, D. P. (2013) Islet amyloid: from fundamental biophysics to mechanisms of cytotoxicity, *FEBS Lett. 587*, 1106-1118.
75. Abedini, A., and Raleigh, D. P. (2005) The role of His-18 in amyloid formation by human islet amyloid polypeptide, *Biochemistry 44*, 16284-16291.
76. Williamson, J. A., and Miranker, A. D. (2007) Direct detection of transient alpha-helical states in islet amyloid polypeptide, *Protein Sci 16*, 110-117.
77. Williamson, J. A., Loria, J. P., and Miranker, A. D. (2009) Helix stabilization precedes aqueous and bilayer-catalyzed fiber formation in islet amyloid polypeptide, *J. Mol. Biol. 393*, 383-396.
78. Wiltzius, J. J., Sievers, S. A., Sawaya, M. R., and Eisenberg, D. (2009) Atomic structures of IAPP (amylin) fusions suggest a mechanism for fibrillation and the role of insulin in the process, *Protein Sci. 18*, 1521-1530.
79. Paulsson, J. F., Andersson, A., Westermark, P., and Westermark, G. T. (2006) Intracellular amyloid-like deposits contain unprocessed pro-islet amyloid polypeptide (proIAPP) in beta cells of transgenic mice overexpressing the gene for human IAPP and transplanted human islets, *Diabetologia 49*, 1237-1246.
80. Marzban, L., Rhodes, C. J., Steiner, D. F., Haataja, L., Halban, P. A., and Verchere, C. B. (2006) Impaired NH2-terminal processing of human proislet amyloid polypeptide by the prohormone convertase PC2 leads to amyloid formation and cell death, *Diabetes 55*, 2192-2201.
81. Krampert, M., Bernhagen, J., Schmucker, J., Horn, A., Schmauder, A., Brunner, H., Voelter, W., and Kapurniotu, A. (2000) Amyloidogenicity of recombinant human pro-islet amyloid polypeptide (ProIAPP), *Chem. Biol. 7*, 855-871.
82. Meng, F., Abedini, A., Song, B., and Raleigh, D. P. (2007) Amyloid formation by pro-islet amyloid polypeptide processing intermediates: Examination of the role of protein heparan sulfate interactions and implications for islet amyloid formation in type 2 diabetes, *Biochemistry 46*, 12091-12099.

83. Park, K., and Verchere, C. B. (2001) Identification of a heparin binding domain in the N-terminal cleavage site of pro-islet amyloid polypeptide - Implications for islet amyloid formation, *J. Biol. Chem. 276*, 16611-16616.
84. Jayasinghe, S. A., and Langen, R. (2005) Lipid membranes modulate the structure of islet amyloid polypeptide, *Biochemistry 44*, 12113-12119.
85. Knight, J. D., Hebda, J. A., and Miranker, A. D. (2006) Conserved and cooperative assembly of membrane-bound alpha-helical states of islet amyloid polypeptide, *Biochemistry 45*, 9496-9508.
86. Ling, Y. L., Strasfeld, D. B., Shim, S. H., Raleigh, D. P., and Zanni, M. T. (2009) Two-dimensional infrared spectroscopy provides evidence of an intermediate in the membrane-catalyzed assembly of diabetic amyloid, *J. Phys. Chem. B 113*, 2498-2505.
87. Trikha, S., and Jeremic, A. M. (2011) Clustering and internalization of toxic amylin oligomers in pancreatic cells require plasma membrane cholesterol, *J. Biol. Chem. 286*, 36086-36097.
88. Wakabayashi, M., and Matsuzaki, K. (2009) Ganglioside-induced amyloid formation by human islet amyloid polypeptide in lipid rafts, *FEBS Lett. 583*, 2854-2858.
89. Kawahara, M., Kuroda, Y., Arispe, N., and Rojas, E. (2000) Alzheimer's beta-amyloid, human islet amylin, and prion protein fragment evoke intracellular free calcium elevations by a common mechanism in a hypothalamic GnRH neuronal cell line, *J. Biol. Chem. 275*, 14077-14083.
90. Luca, S., Yau, W. M., Leapman, R., and Tycko, R. (2007) Peptide conformation and supramolecular organization in amylin fibrils: constraints from solid-state NMR, *Biochemistry 46*, 13505-13522.
91. Petkova, A. T., Yau, W. M., and Tycko, R. (2006) Experimental constraints on quaternary structure in Alzheimer's beta-amyloid fibrils, *Biochemistry 45*, 498-512.
92. Wiltzius, J. J., Sievers, S. A., Sawaya, M. R., Cascio, D., Popov, D., Riekel, C., and Eisenberg, D. (2008) Atomic structure of the cross-beta spine of islet amyloid polypeptide (amylin), *Protein Sci. 17*, 1467-1474.
93. Bedrood, S., Li, Y. Y., Isas, J. M., Hegde, B. G., Baxa, U., Haworth, I. S., and Langen, R. (2012) Fibril structure of human islet amyloid polypeptide, *J. Biol. Chem. 287*, 5235-5241.
94. Westermark, P., Engstrom, U., Johnson, K. H., Westermark, G. T., and Betsholtz, C. (1990) Islet amyloid polypeptide: pinpointing amino acid residues linked to amyloid fibril formation, *Proc. Natl. Acad. Sci. U. S. A. 87*, 5036-5040.
95. Nishi, M., Chan, S. J., Nagamatsu, S., Bell, G. I., and Steiner, D. F. (1989) Conservation of the sequence of islet amyloid polypeptide in five mammals is consistent with its putative role as an islet hormone, *Proc. Natl. Acad. Sci. U. S. A. 86*, 5738-5742.
96. Moriarty, D. F., and Raleigh, D. P. (1999) Effects of sequential proline substitutions on amyloid formation by human amylin20-29, *Biochemistry 38*, 1811-1818.
97. Abedini, A., and Raleigh, D. P. (2006) Destabilization of human IAPP amyloid fibrils by proline mutations outside of the putative amyloidogenic domain: is there a critical amyloidogenic domain in human IAPP?, *J. Mol. Biol. 355*, 274-281.
98. Green, J., Goldsbury, C., Mini, T., Sunderji, S., Frey, P., Kistler, J., Cooper, G., and Aebi, U. (2003) Full-length rat amylin forms fibrils following substitution of single residues from human amylin, *J. Mol. Biol. 326*, 1147-1156.

99. Ratner, R. E., Dickey, R., Fineman, M., Maggs, D. G., Shen, L., Strobel, S. A., Weyer, C., and Kolterman, O. G. (2004) Amylin replacement with pramlintide as an adjunct to insulin therapy improves long-term glycaemic and weight control in Type 1 diabetes mellitus: a 1-year, randomized controlled trial, *Diabetic Med. 21*, 1204-1212.
100. Edelman, S. V., Darsow, T., and Frias, J. P. (2006) Pramlintide in the treatment of diabetes, *Int. J. Clin. Pract. 60*, 1647-1653.
101. Abedini, A., Meng, F., and Raleigh, D. P. (2007) A single-point mutation converts the highly amyloidogenic human islet amyloid polypeptide into a potent fibrillization inhibitor, *J. Am. Chem. Soc. 129*, 11300-11301.
102. Hellman, U., Wernstedt, C., Westermark, P., O'Brien, T. D., Rathbun, W. B., and Johnson, K. H. (1990) Amino acid sequence from degu islet amyloid-derived insulin shows unique sequence characteristics, *Biochem. Biophys. Res. Commun. 169*, 571-577.
103. Marek, P. J., Patsalo, V., Green, D. F., and Raleigh, D. P. (2012) Ionic strength effects on amyloid formation by amylin are a complicated interplay among Debye screening, ion selectivity, and Hofmeister effects, *Biochemistry 51*, 8478-8490.
104. Padrick, S. B., and Miranker, A. D. (2002) Islet amyloid: phase partitioning and secondary nucleation are central to the mechanism of fibrillogenesis, *Biochemistry 41*, 4694-4703.
105. Tracz, S. M., Abedini, A., Driscoll, M., and Raleigh, D. P. (2004) Role of aromatic interactions in amyloid formation by peptides derived from human amylin, *Biochemistry 43*, 15901-15908.
106. Tu, L. H., and Raleigh, D. P. (2013) Role of aromatic interactions in amyloid formation by islet amyloid polypeptide, *Biochemistry 52*, 333-342.
107. Marek, P., Abedini, A., Song, B., Kanungo, M., Johnson, M. E., Gupta, R., Zaman, W., Wong, S. S., and Raleigh, D. P. (2007) Aromatic interactions are not required for amyloid fibril formation by islet amyloid polypeptide but do influence the rate of fibril formation and fibril morphology, *Biochemistry 46*, 3255-3261.
108. Koo, B. W., Hebda, J. A., and Miranker, A. D. (2008) Amide inequivalence in the fibrillar assembly of islet amyloid polypeptide, *Protein Eng. Des. Sel. 21*, 147-154.
109. Wiltzius, J. J. W., Sievers, S. A., Sawaya, M. R., and Eisenberg, D. (2009) Atomic structures of IAPP (amylin) fusions suggest a mechanism for fibrillation and the role of insulin in the process, *Protein Sci. 18*, 1521-1530.
110. Fox, A., Snollaerts, T., Errecart Casanova, C., Calciano, A., Nogaj, L. A., and Moffet, D. A. (2010) Selection for nonamyloidogenic mutants of islet amyloid polypeptide (IAPP) identifies an extended region for amyloidogenicity, *Biochemistry 49*, 7783-7789.
111. Humphrey, W., Dalke, A., and Schulten, K. (1996) VMD: visual molecular dynamics, *J. Mol. Graphics 14*, 33-38, 27-38.
112. Wang, L., Middleton, C. T., Singh, S., Reddy, A. S., Woys, A. M., Strasfeld, D. B., Marek, P., Raleigh, D. P., de Pablo, J. J., Zanni, M. T., and Skinner, J. L. (2011) 2DIR spectroscopy of human amylin fibrils reflects stable beta-sheet structure, *J. Am. Chem.Soc. 133*, 16062-16071.
113. Duan, M., Fan, J., and Huo, S. (2012) Conformations of islet amyloid polypeptide monomers in a membrane environment: implications for fibril formation, *PloS 7*, e47150.

114. Lovell, S. C., Davis, I. W., Arendall, W. B., 3rd, de Bakker, P. I., Word, J. M., Prisant, M. G., Richardson, J. S., and Richardson, D. C. (2003) Structure validation by C alpha geometry: phi,psi and Cbeta deviation, *Proteins 50*, 437-450.
115. Anil, B., Song, B., Tang, Y., and Raleigh, D. P. (2004) Exploiting the right side of the Ramachandran plot: substitution of glycines by D-alanine can significantly increase protein stability, *J. Am. Chem. Soc . 126*, 13194-13195.
116. Abedini, A., and Raleigh, D. P. (2009) A critical assessment of the role of helical intermediates in amyloid formation by natively unfolded proteins and polypeptides, *Protein Eng. Des. Sel. 22*, 453-459.
117. Abedini, A., and Raleigh, D. P. (2005) Incorporation of pseudoproline derivatives allows the facile synthesis of human IAPP, a highly amyloidogenic and aggregation-prone polypeptide, *Org. Lett. 7*, 693-696.
118. Wohr, T., Wahl, F., Nefzi, A., Rohwedder, B., Sato, T., Sun, X. C., and Mutter, M. (1996) Pseudo-prolines as a solubilizing, structure-disrupting protection technique in peptide synthesis, *J. Am. Chem. Soc. 118*, 9218-9227.
119. Marek, P., Woys, A. M., Sutton, K., Zanni, M. T., and Raleigh, D. P. (2010) Efficient microwave-assisted synthesis of human islet amyloid polypeptide designed to facilitate the specific incorporation of labeled amino acids, *Org. Lett. 12*, 4848-4851.
120. Palasek, S. A., Cox, Z. J., and Collins, J. M. (2007) Limiting racemization and aspartimide formation in microwave-enhanced Fmoc solid phase peptide synthesis, *J. Pept. Sci .13*, 143-148.
121. Bacsa, B., Horvati, K., Bosze, S., Andreae, F., and Kappe, C. O. (2008) Solid-phase synthesis of difficult peptide sequences at elevated temperatures: A critical comparison of microwave and conventional heating technologies, *J. Org. Chem. 73*, 7532-7542.
122. Tam, J. P., Wu, C. R., Liu, W., and Zhang, J. W. (1991) Disulfide bond formation in peptides by dimethyl-sulfoxide - scope and applications, *J. Am. Chem. Soc. 113*, 6657-6662.
123. Abedini, A., Singh, G., and Raleigh, D. P. (2006) Recovery and purification of highly aggregation-prone disulfide-containing peptides: Application to islet amyloid polypeptide, *Anal. Biochem. 351*, 181-186.
124. http://molprobity.biochem.duke.edu/
125. Fauchere, J. L., Charton, M., Kier, L. B., Verloop, A., and Pliska, V. (1988) Amino acid side chain parameters for correlation studies in biology and pharmacology, *Int. J. Pep. Protein Res. 32*, 269-278.
126. Pettersen, E. F., Goddard, T. D., Huang, C. C., Couch, G. S., Greenblatt, D. M., Meng, E. C., and Ferrin, T. E. (2004) UCSF Chimera--a visualization system for exploratory research and analysis, *J. Comput. Chem. 25*, 1605-1612.
127. Serrano, L., Neira, J. L., Sancho, J., and Fersht, A. R. (1992) Effect of alanine versus glycine in alpha-helices on protein stability, *Nature 356*, 453-455.
128. Kleiger, G., Grothe, R., Mallick, P., and Eisenberg, D. (2002) GXXXG and AXXXA: common alpha-helical interaction motifs in proteins, particularly in extremophiles, *Biochemistry 41*, 5990-5997.
129. Liu, W., Crocker, E., Zhang, W., Elliott, J. I., Luy, B., Li, H., Aimoto, S., and Smith, S. O. (2005) Structural role of glycine in amyloid fibrils formed from transmembrane alpha-helices, *Biochemistry 44*, 3591-3597.